# FINAL SUMMARY REPORT

# ELECTRO-OPTICAL PROCESSING OF PHASED ARRAY DATA

Prepared for

George C. Marshall Space Flight Center
Marshall Space Flight Center, ALABAMA 35812

By

Dr. David Casasent
Carnegie-Mellon University
Department of Electrical Engineering
Pittsburgh, Pennsylvania 15213

Date: August 1, 1973

Contract No.: NAS8-28737
Project No.: DCN1-2-40-23115 (IF)

ABSTRACT

An on-line spatial light modulator developed at CMU suitable as the input transducer for a real-time optical data processing system is described (Chapter 1). 1000 x 1000 point resolution and on-line operation at TV frame rates is possible. The use of such a device in the analysis and processing of radar data in real time has been considered and initial results reported.

The fundamentals of signal processing for linear (Chapter 3) and planar (Chapter 4) phased array radar data as well as Pulsed Doppler and Linear-Step FM system (Chapter 7) using this input modulator have been developed. Time and space multiplexing input formats, full and thinned aperture processing, and amplitude and phase modulation schemes using the system are developed, analyzed and compared.

An interface from the optical processor to a control-digital computer has been designed, constructed, and tested. The ability to digitize the entire Fourier transform plane or the correlation plane of an optical processor in real time and input the resultant data to a digital computer for storage or for use in controlling the entire optical processor has been demonstrated. The cell resolution and size and the gray scale levels in the backplane are variable under program control.

Real-time processing of linear phased array under data has been performed for the first time by other than an acousto-optic modulator. The Pockels tube modulator offers advantages in fabrication, angular coverage and resolution, in the larger array size it is now possible to handle and in-depth of modulation etc.

The input transducer, optical system, and computer interface have all been operated in real-time with real-time radar data with the input data returns recorded on the input crystal, processed by the optical system and the output

plane pattern digitized, thresholded and outputted to a display and storage in the computer memory all in real-time synchronized to TV frame rates.

No other input modulator offers the real-time operating characteristics of the Pockels tube. Its ability to process radar data in real-time has been demonstrated. The correlation with theory and experimental results have been most encouraging. Recommended directions for future research in the area of optical processing of radar data in real-time are sketched in Chapter 7 and the proposal.

# CHAPTER 1

# OPTICAL PROCESSOR

## 1.1 Introduction

This contract involved a one man year effort to investigate the feasibility of applying optical data processing techniques to the analysis of radar data. A theoretical analysis of the required data processing is included; input formats compatible with an electron beam addressed input modulator are analyzed and presented; an interface from the optical processor to a general purpose minicomputer was constructed and is described; a phased array simulator was designed and built to serve as an input data source and finally experimental results of real-time radar data processed electro-optically and interfaced to a control minicomputer were obtained and are also included along with recommendations for future work in the area of real-time processing of radar data using optical techniques. Radar Data Processing in real-time was shown to be possible using C-MU's (Carnegie-Mellon University's) hybrid Pockels tube real-time spatial light modulator (See Section 1.2).

As outlined in the proposal, the scope of the project included six areas:

A. Formal extension of the theory of two-dimensional phased array radar processing with an electron-beam addressed light modulator.

B. Determination of the ideal system configuration by means of evaluating simulations of various data formats.

C. Automation of the necessary preprocessing of the electrical signals from a phased array antenna, and the post processing of the resultant diffraction pattern.

D. Design of the input logic network which interfaces to the video input of the electron gun.

E. Investigation of feedback control loops to control the input plane format by sampling, analysis, and processing of output plane data.

F. Construction of peripheral electronics which convert investigators optical data processor to the task of a radar data processor.

## 1.2 ON-LINE INPUT TRANSDUCER

Optical data processing in real-time is nearing reality. One of the major obstacles in the implementation of such a system has been a two-dimensional electrical-to-optical input transducer from the real world to the optical processor. This device must be capable of creating a two dimensional image of an input electrical signal. A raster scan format and an input video signal are the easiest situation to envision. In this case a transparent version of the transmitted video image is formed. The material on which this image is formed must be capable of spatially modulating the amplitude and/or phase a collimated input laser beam.

Figure 1.1.1 shows a block diagram of the input transducer used. The input electrical signal, assumed for simplicity to be of TV raster scan video format, modulates the cathode and hence the beam current of an off-axis electron gun. The deflection of the electron beam is synchronized to horizontal and vertical sync pulses. The target is not a phosphor, but rather an electro-optic target crystal, on which the modulated electron beam deposits a variable charge pattern. A transparent conducting layer on the back surface of the crystal serves as the system's ground reference.

The mechanism by which this target material modulates light has been well documented. The locally varying voltage across the crystal at any point is a controllable function of position. The electric field produced at every point causes a retardation between components of the light beam incident at that point. By the linear longitudinal electro-optic or Pockels effect, this controlled voltage can be used to modulate the phase of the incident coherent light beam at each point on the crystal's surface.

When placed between crossed polarizers this phase modulation can be converted to amplitude modulation. The input and exit windows allow the light beam to pass through the target in a transmission mode.

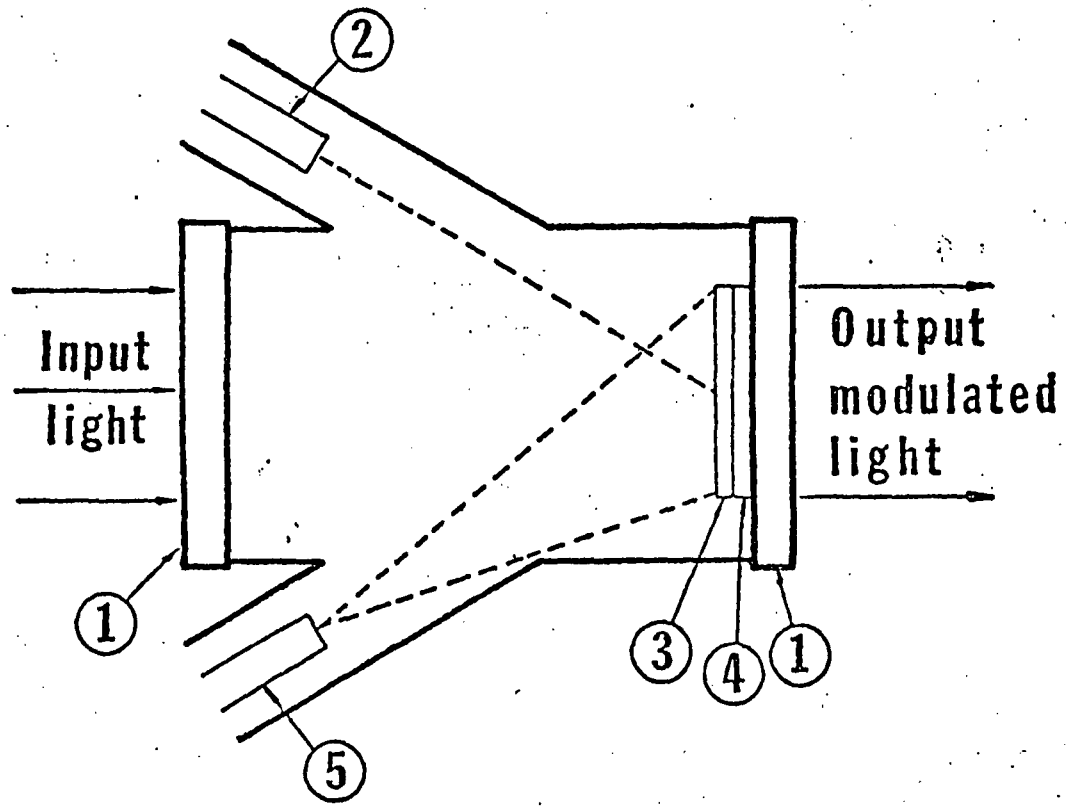


Fig. 1.1.1 Block Diagram of Input Transducer (Pockels Tube)
Code: 1 = optical window, 2 = write electron gun,
3 = target crystal ($KD_2P$),
4 = Conducting transparent grounded electrode,
5 = Erase Gun

Electron beam technology limits the obtainable spot size at the required beam currents to about 1 mil. Most data and signal processing applications require 1000 line resolution. 1000 x 1000 point resolution is possible by Curie point operation of the target crystal. This high resolution is purchased at the price of storage of the charge on the crystal's surface. Real time operation necessitates the use of an erase gun which emits a defocussed spray of electrons toward the target at a low accelerating potential such that the crystal's secondary emission ratio is greater than 1.

The detailed variation of the physical parameters of the target crystal with temperature and additional advantages of Curie Point operation of a Pockels tube are contained in Reference (2). Reference (3) explains the system more fully. The tube has been rather extensively documented elsewhere, References (1)-(6), and thus only a brief explanation is included here for completeness.

## 1.3 ELECTRO-OPTIC EFFECT

The electro-optic effect is well known (7). Figure 1.3.1 shows the geometry of the electro-optic system. A 0° Z-cut thin basal plane of KDP of thickness L is shown with a voltage V applied in the direction of the optic axis z. The x and y axes are the crystallographic axes while the x' and y' axes are the electrically induced principle dielectric axes in the crystal due to an electric field $E_z$ applied in the z direction.

### 1.3.1 AMPLITUDE MODULATION

In crystals exhibiting the linear electro-optic effect, the indices of refraction for light polarized in the x' and y' directions are changed by an amount $\Delta n$ in the presence of a longitudinal electric field

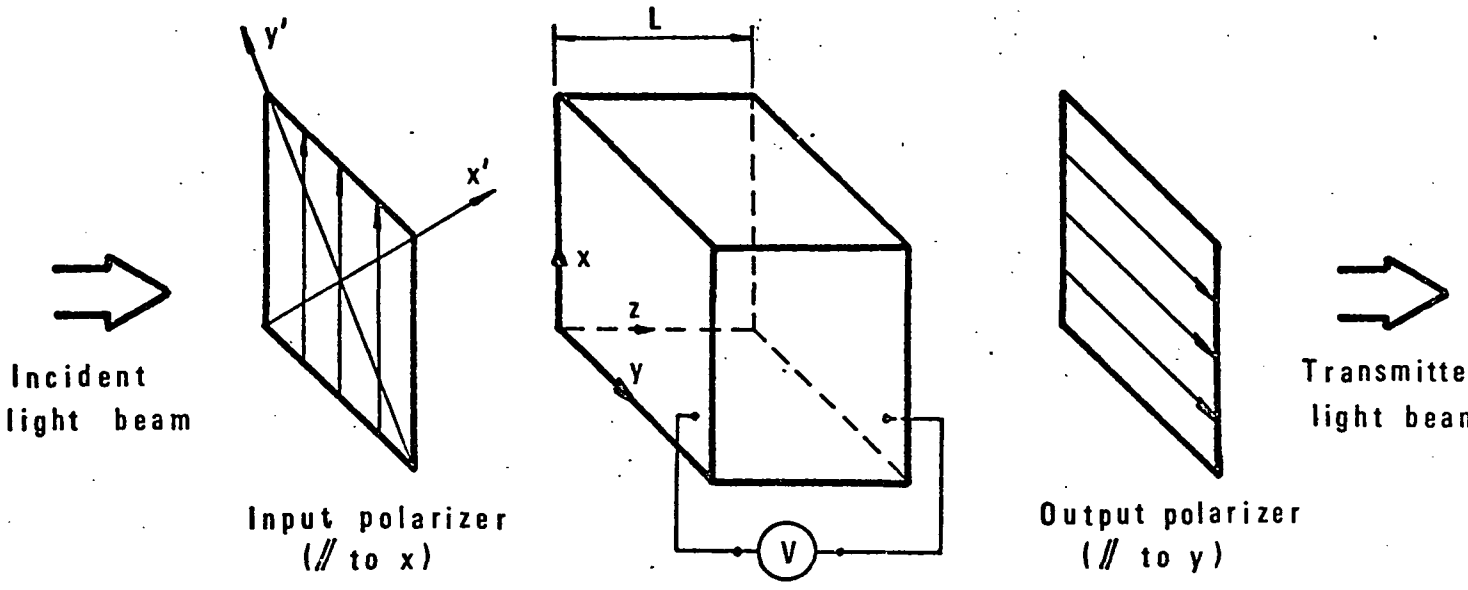


Fig. 1.3.1 Amplitude Modulation Using the Pockels Effect.

$$n_x' = n_o - \Delta n$$

$$n_y' = n_o + \Delta n$$

where $n_o$ is the ordinary index refraction and $n_x'$ and $n_y'$ are the indices of refraction along the x' and y' axes in the presence of an electric field. KDP and its isomorphs are biaxial in the absence of an applied voltage with $n_x = n_y = n_o$. The change in index of refraction is linearly related to the electric field $E_z = V/L$ by

$$\Delta n = n_o^3 r_{63} E_z / 2$$

where $r_{63}$ is a tensor component of the index ellipsoid.

This induced birefringence results in a differential phase delay or retardation between the components of an incident laser beam along the two induced axes given by

$$\Gamma = \frac{2\pi n_o^3 r_{63} E_z L}{\lambda} = \pi \frac{V}{V_\pi}$$

The phase retardation increases linearly with the voltage applied across the

crystal until at $V = V_\pi$ the phase retardation between component waves is $\pi$ and destructive interference can occur.

The transmission through the polarizer /crystal/ analyzer system of Fig.1.3.1 vs. the voltage applied across the crystal can now be evaluated. By combining the projections along the crystallographic axes when the polarization of the input beam is oriented along one of the crystallographic axes at 45° to the induced electro optic axes. The amplitude transmission is then

$$A = \sin\delta$$

where $\delta = \Gamma/2$. The intensity transmitted at each point is

$$I = I_0 \sin^2\delta$$

where $I_0$ is the incident intensity and $\delta$ is the modulation which is linearly proportional to the applied voltage.

## 1.3.2. PHASE MODULATION

The electro-optic crystal can also be used to phase modulate the incident light beam point-by-point. Figure 1.3 .2 shows the polarization setup required for this scheme. The incident light is now linearly polarized along one of the induced electro-optic axes rather than along the crystallographic axes as in the amplitude modulation scheme of Fig. 1.2.

The phase retardation along the $x'$ axis is related to the electric field $E_z = V/L$ by

$$\Delta\phi_{x'} = -\frac{\pi n_o^3}{\lambda_o} r_{63} E_z L$$

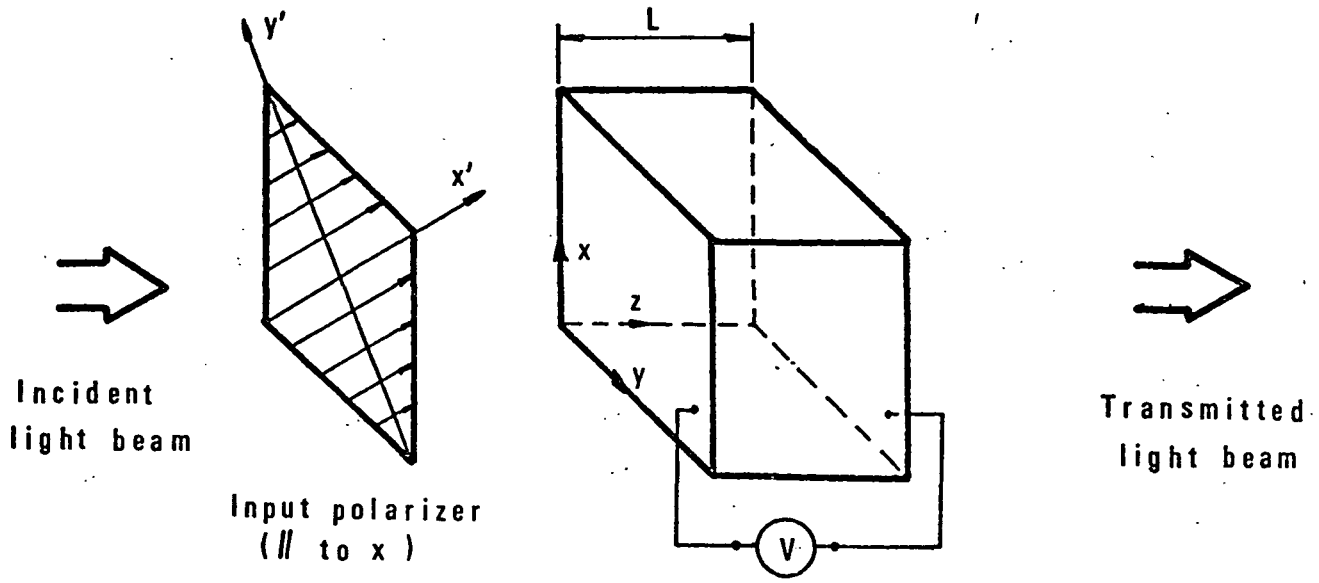


Fig. 1.3 .2 Phase Modulation Using the Pockels Effect.

where the terms are as previously defined. In Chapters 3 and 6 these two modulation schemes, amplitude modulation and phase modulation will be evaluated as they apply to optical processing of radar data.

## 1.4 Extent of Research Performed

The lack of any available radar data, phased array or other, from NASA severely limited the scope of the work and the impact of the results obtained. Any preprocessing needed would depend greatly on the specific radar used. Tradeoffs exist between the data availble to us, the format in which data could be obtained given complete access to a specific radar system, and the time and cost involved in constructing a hardware preprocessor. This preprocessor might be both special purpose (often for one radar system that might not be of adequate interest) and would in essence amount to converting data from one form (e.g. paper tape) back into its original form (e.g. an electrical signal vs. time). These factors and the interest of NASA in phased array radar processing specifically clearly indicated that no preprocessor be constructed. Rather a linear

phased-array waveform generator/simulator (Section 6.2) was designed, constructed, and used as the input data source.

Only in this way could actual real time radar data processing be demonstrated. No contract renewal was indicated and hence all work was organized to present a unified treatment of the theory of 1-D and 2-D phased array radar processing, an evaluation of various input data formats for an electron beam addressed spatial light modulator, an extension showing the possibilities of such processing, and an actual demonstration of real time on-line radar processing using optical processing.

Chapter 2 provides the theory of beam steering, the optical generation of such systems, and the analogy between beam steering and beam forming. Chapter 3 extends this treatment to the processing of linear phased array antenna data. Various input formats, modulation schemes, and the expected output data formats are theoretically treated. In Chapter 4, the theory for a 2-D phased array is developed. Treatments of various input formats, optical configurations, and output patterns are again included. Various new theories such as a scheme for simultaneously obtaining azimuth and doppler data are included. The digital computer to optical computer interface is described in Chapter 5. In Chapter 6, various phase and amplitude modulation schemes are included. On-line real time linear phased-array radar processing results are shown, performed optically for the first time by other than acousto-optic techniques. The interaction in real time of the output optical/digital interface is also shown by showing images of the on-line digitized versions of the output patterns as stored and digested by the computer.

Possible extensions of this work were submitted separately to Reginald Inman and Joe Kerr of MSFC as an informal proposal for continued

real-time optical processing of radar data. Topics proposed include:

1. Pulsed doppler radar processing in real time by optical techniques
2. Linear FM stepped radar processing in real time by optical techniques
3. Analysis of computer interface requirements
4. Spatial filter study for real time correlation in radar processing
5. Multiplexing 1-D transforms for radar processing
6. Automatic real time range gating by optical correlation
7. Real time fine range resolution by optical correlation
8. Improved S/N ratio schemes using optical correlation
9. Real time CW dopper processing using optical techniques
10. Simultaneous azimuth and doppler data from one processing frame
11. Alternate electron optic scanning scheme, optimized for radar processing

We now have access to chirp and doppler data and would hope to see these proposed efforts, all of which are proposed and currently possible in real-time, pursued since we are standing on the edge of major demonstrations in this area.

CHAPTER 2

# BEAM STEERING IN PHASED ARRAY ANTENNAS AND OPTICAL BEAM STEERING

## 2.1 Array Antenna Characteristics

Essentially, array antennas consist of a number of individual radiating antenna elements, spaced in accordance with some given pattern. The characteristics of such antennas are determined by the geommetric position of the radiators. The amplitude and phase of the excitation are modulated by controlling the individual elements to give beams that are scanned electronically. Three different methods for scanning are possible: phase shift, frequency shift and time delay. We shall concentrate our attention on phase shift scanning and show the analogy between such beam steering and optical beam steering using "optical" antennas. This analogy is the basis for the optical processing of signals received at phased array antennas, or beam forming, via the reciprocity theorem.

Linear as well as two-dimensional antennas will be considered.

For a uniform linear phased array of N radiating isotropic elements, let the transmitted signal at the nth array element be of the form

$$v_n(t,\phi) = p_T(t)\cos 2\pi[f_c t - n\phi_o]$$

where

$$p_T(t) = \begin{cases} 1, & |t| \leq T/2 \\ 0, & \text{otherwise} \end{cases}$$ where T is the transmitted pulse width

$f_c$ = RF carrier frequency

$\phi_o$ = differential phase delay in RF cycles applied per element

The entire signal transmitted by the array is thus a waveform whose equiphase front forms an angle $\theta_o$ with the normal to the array--or boresight direction--where

$$\sin\theta_o = \frac{\phi_o \lambda_c}{d}$$

$\lambda_c$ = free space wavelength of RF carrier

d = equidistance spacing between array elements.

Fig. 2.1.1 describes the scanned array configuration. For convenience in the computation, the signals $v_n(t)$ will be taken in its analytic form

$$V_n(t,\phi_o) = p_T(t)e^{j2\pi[f_c t - n\phi_o]}$$

with

$$v_n(t,\phi_o) = \mathrm{Re}\{V_n(t,\phi_o)\}$$

Application of the Fresnel-Kirchoff scalar diffraction theory to the antenna shows that, in its far field (this is for space points at a distance greater than $2N^2d^2/\lambda_c$), the signal received by a point located on a direction forming an angle $\theta$ with the boresight axis is

$$V(t,\phi,\phi_o) = \sum_{n=0}^{N-1} p_T(t - t_R)e^{j2\pi[f_c(t - t_R) - n\phi_o + n\phi]}$$

$$= p_T(t - t_R)e^{j2\pi f_c(t - t_R)} \sum_{n=0}^{N-1} e^{-j2\pi n(\phi_o - \phi)}$$

where $\phi = (d/\lambda_c)\sin\theta$, and $t_R$ is the one-way target range delay

By adjusting the phase terms relative to the center of the aperture, we obtain

$$V(t,\phi,\phi_o) = \psi(t)E_a(\theta,\theta_o)$$

where $\psi(t) = p_T(t - t_R)e^{j2\pi f_c(t - t_R)}$

and

$$E_a(\theta,\theta_o) = \sum_{-\frac{N-1}{2}}^{\frac{N-1}{2}} e^{-j2\pi n(\phi_o - \phi)} = \frac{-\sin N\pi(\phi_o - \phi)}{-\sin\pi(\phi_o - \phi)} =$$

$$= \frac{\sin[N\pi(d/\lambda_c)(\sin\theta - \sin\theta_o)]}{\sin[\pi(d/\lambda_c)(\sin\theta - \sin\theta_o)]}$$

For $\theta_o = 0$, the expression

$$E_a(\theta) = \frac{\sin[N\pi(d/\lambda_c)\sin\theta]}{\sin[\pi(d/\lambda_c)\sin\theta]}$$

is known as the array factor for isotropic radiators. When the radiating elements are not isotropic but have a radiation pattern $E_e(\theta)$, the antenna radiation pattern is given by

$$E(\theta) = E_e(\theta)E_a(\theta) = E_e(\theta)\frac{\sin[N\pi(d/\lambda_c)\sin\theta]}{\sin[\pi(d/\lambda_c)\sin\theta]}$$

Examination of the array factor shows the following points:

1) $E_a(\theta)$ is repetitive, with grating lobes spaced at values of $\theta$ for which $\pi(d/\lambda_c)\sin\theta = n\pi$, $n = 1, 2, 3, \ldots$
2) The half-power (3 dB) lobe width has the value $\frac{1}{N(d/\lambda_c)}$ thus application of the Rayleigh resolution criterion yields N resolvable main lobe positions corresponding to N values of $\sin\theta$ for $\theta$ between 0 and $\pi$ radians.

Fig. 2.1.2 illustrates the former results. An approximation to the array factor for small values of $\theta$ is given by

$$E(\theta) = \frac{\sin[\pi N(d/\lambda_c)\sin\theta]}{\pi N(d/\lambda_c)\sin\theta}$$

which corresponds to the Fourier transform of the illumination across the continuous aperture. This approximation holds when the array aperture is larger than several wavelengths. For larger values of $\theta$ the obliquity factor must be included so that

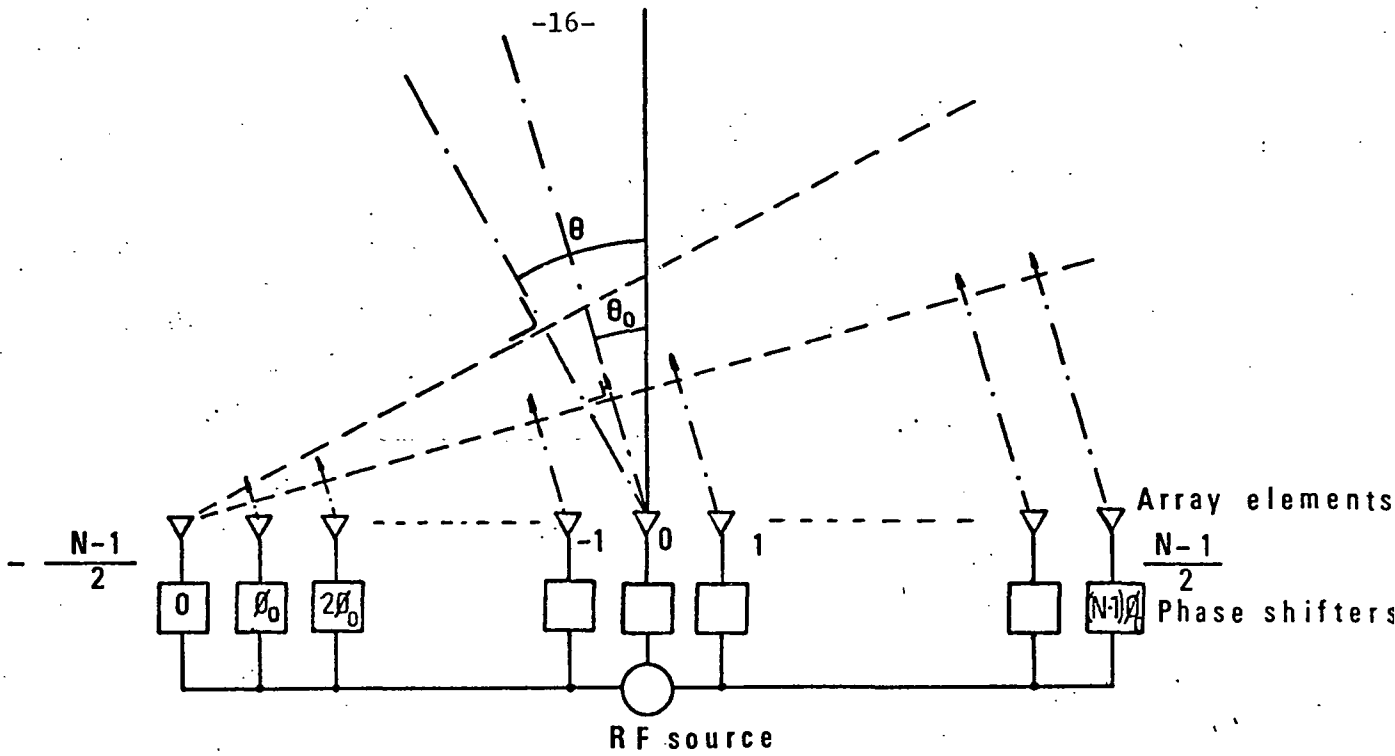


Fig. 2.1.1 Linear Phase-scanned array geometry

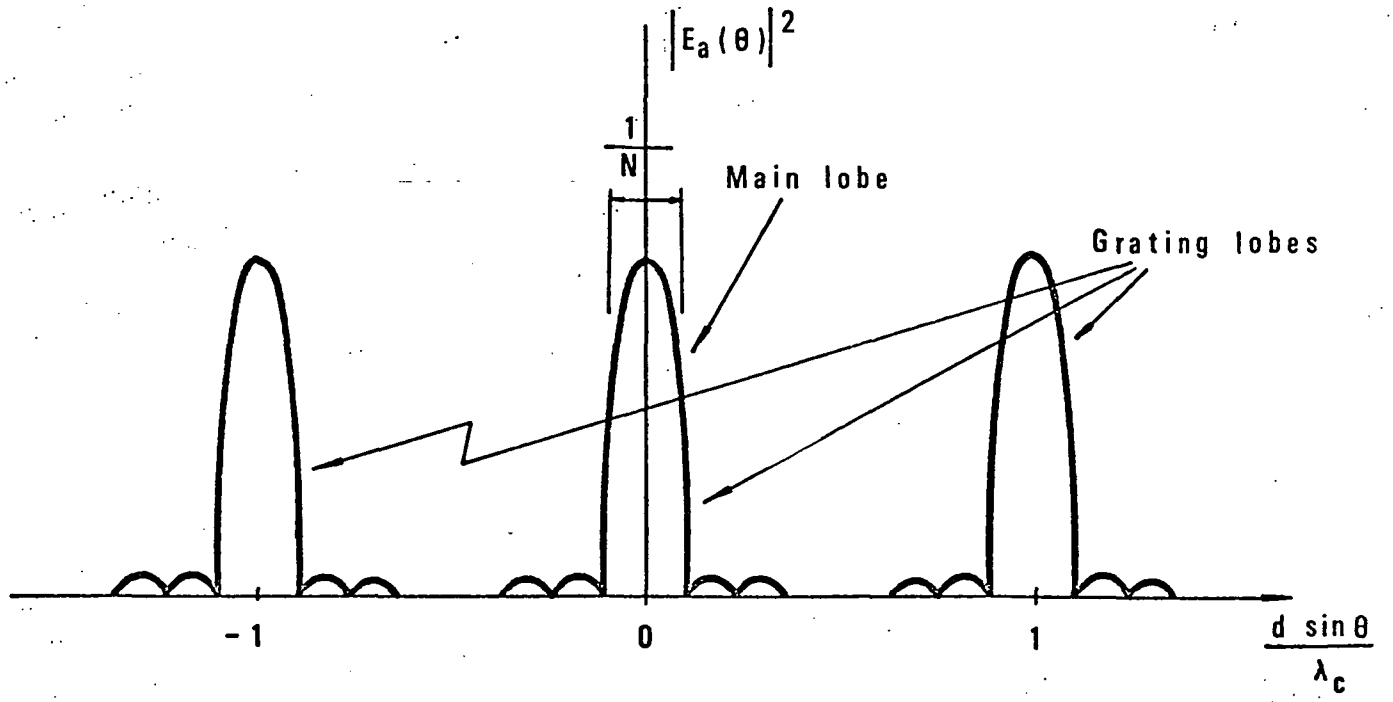


Fig. 2.1.2 Array factor for isotropic readiators

$$E(\theta) = \left( \frac{1 + \cos\theta}{2} \right) \frac{\sin[\pi N (d/\lambda_c) \sin\theta]}{\pi N (d/\lambda_c) \sin\theta}$$

For the scanned array system, the array pattern was shown to be

$$E_a(\theta) = \frac{\sin[N\pi (d/\lambda_c)(\sin\theta - \sin\theta_o)]}{\sin[\pi (d/\lambda_c)(\sin\theta - \sin\theta_o)]}$$

whose grating lobe maxima repeat at values of $\theta$ such that

$$\pi \frac{d}{\lambda_c}(\sin\theta - \sin\theta_o) = n\pi, \quad n = 1, 2, 3, \ldots$$

The 3 dB antenna beam width is again $\frac{1}{Nd/\lambda_c}$. A total of N values of $\sin\theta_o$ can thus be resolved between two consecutive grating lobes of the array pattern. Fig. 2.1.3 shows this result.

Again, the antenna pattern can be approximated by the Fourier transform of the illumination across the continuous aperture multiplied by the obliquity factor

$$E(\theta) \approx \left( \frac{1 + \cos\theta}{2} \right) \frac{\sin[\pi N (d/\lambda_c)(\sin\theta - \sin\theta_o)]}{\pi N (d/\lambda_c)(\sin\theta - \sin\theta_o)}$$

and the power associated with this pattern is

$$|E(\theta)|^2 = \left( \frac{1 + \cos\theta}{2} \right)^2 \frac{\sin^2[\pi N (d/\lambda_c)(\sin\theta - \sin\theta_o)]}{\pi^2 N^2 (d/\lambda_c)^2 (\sin\theta - \sin\theta_o)^2}$$

For $\theta \leq 30°$, however, the term $\left( \frac{1 + \cos\theta}{2} \right)$ has a maximum value of 1 at $\theta = 0^o$ and decreases smoothly to 0.93 for $\theta = 30°$ at which $\left( \frac{1 + \cos 30°}{2} \right)^2 = 0.87$. The power pattern for near-to-boresight directions is thus approximately

$$|E_a(\theta)|^2 = \frac{\sin^2[N\pi (d/\lambda_c)(\sin\theta - \sin\theta_o)]}{[\pi N (d/\lambda_c)(\sin\theta - \sin\theta_o)]^2}$$

where we recall that $\theta_o$ corresponds to the steered direction of the antenna and $\theta$ to the angle with the boresight axis as shown in Fig. 2.1.1

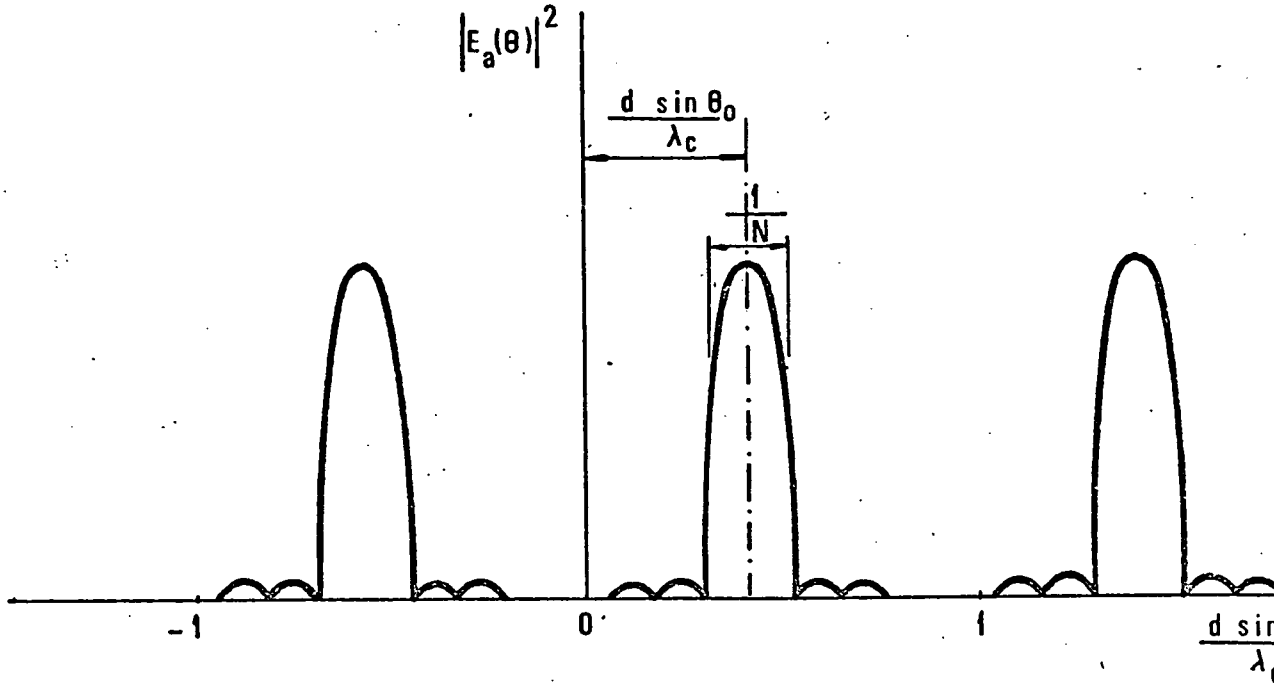


Fig. 2.1.3 Array factor for Phase -scanned Array

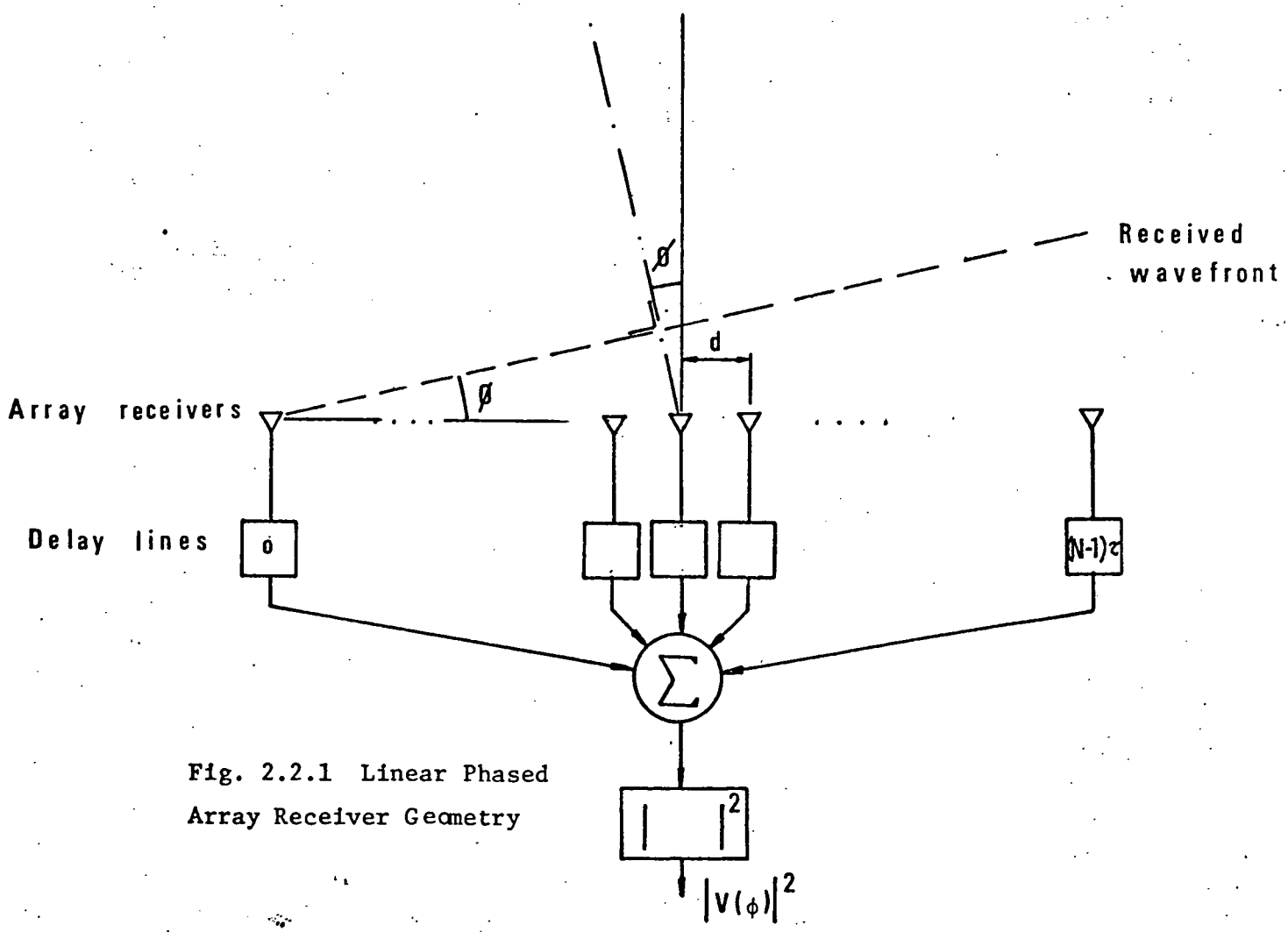


Fig. 2.2.1 Linear Phased Array Receiver Geometry

From this analysis it is clear that the ideal number of resolvable beam positions in the far field on the antenna is related to the array factor which in turn is determined by the antenna geometry. This array factor is thus a measure of the maximum angular resolution from an ideal processor. Once this spacing d between elements and the carrier wavelength $\lambda_c$ are chosen the maximum sector scanning angle $\theta$ for non ambiguous positions is defined by $(d/\lambda_c) \sin \theta \leq \pi$. Within $\pm \theta$ the number of resolvable beam positions is N, the length of the array; e.g. for $d/\lambda_c < 0.53$ N beam positions can be resolved between $\theta = \pm 60^\circ$, while for $d/\lambda_c < 0.5$ yields N resolvable positions for sin $\theta$ with $\theta = \pm 90^\circ$. It will be assumed from now on that the relation $d/\lambda_c = 0.5$ holds for all arrays considered.

## 2.2 Signal Processing Requirements

Phased array radar antennas present the advantage over conventional antennas, of rapid beam steering, this being achieved by varying the relative phases of the excitation applied to the different elements in a precise manner; no inertia, friction or moving parts are source of problems with this mode of operation.

With the capability of rapidly and accurately positioning phased array antennas, it has become possible to develop radars that perform multiple functions interlaced in time. Sequential scanning in azimuth and elevation can produce the scene in front of the antenna as well as range and velocity information.

Another mode of operation is also possible with a phased array that can only be realized with this type of antenna. The whole solid angle of space to be explored can be illuminated at once by using a broadbeam antenna as transmitter, and the desired information about targets in the searched volume can be extracted by processing the signals received at every element of the array. Elevation angle can be obtained for linear arrays, and elevation and azimuth angles for planar arrays. The requirements placed on the processor are, however, quite formidable: real time operation for a broad class of targets require parallel processing of all array elements as well as multitarget capability.

Essentially, the function to be performed by the processor, for every range bin of interest, (a linear array is considered), consists of combining the signals received at every element of the array to obtain an output signal $V(\theta)$ such that for any angle $\theta_i$ at which a target is present the output presents a maximum and for all other values $\theta \neq \theta_i$ it varies in proportion to the antenna radiation pattern associated with the mode of

operation of the antenna, (pulsed RF carrier in most cases). The processor thus must correlate the phase slope present at the returned signals with all possible linear phase slopes and determine, for every peak of the correlation function, the value of the elevation angle of the target. This can be accomplished by

1) Quantizing the angle coverage in N discrete values $\theta_1 \cdots \theta_N$
2) For every such value $\theta_i$, delaying each of the RF signals by an amount such that the nth signal is delayed by an amount $n\tau$, where $\tau = (d/\lambda_c) \sin \theta_i$
3) Sum the resulting ensemble of N signals which are now of the same phase
4) Coherently integrate the summed signal for the entire signal duration.

It can be seen that the processor must perform the aforementioned operations for all values of $\tau$ of interest, i.e. for all values of the angle variable $\theta$.

In Section 2.1 the resolution capability of a phased array was derived and its relationship to the array geometry demonstrated using the array factor. This process is beam steering. We now consider the analysis required on the signals received at the detector array from a point target. This processing is beam forming since the required analysis involves shifting, delaying, and summing all returns to form all possible beam directions in which targets may exist. There clearly exists a duality between beam forming at the detector array and beam steering at the transmitting antenna array. This reciprocity will become apparent from a detailed discussion of an ideal phased array processor.

To describe the process more fully let the line antenna of length D

consisting of N elements spaced at distances d, with illumination function

$$I(x)\ e^{j2\pi\chi\ (x)}$$

where I(x) accounts for the possibility of weighting the signals received at every antenna element and $\chi(x)$ is the phase delay (in RF cycles) introduced at the receiver. The variable x quantized at discrete values corresponding to the locations of the N elements

$x_i = id,\ i = 0, \pm \ldots \pm \frac{N-1}{2}$

Let the antenna receive a plane wave impinging under the angle $\emptyset$, as depicted in Fig. 2.2.1. The processor output signal is the sum of all contributions, weighted by the illumination function and delayed by amounts depending on the path length differences. The differential delay for each

element is

$$\tau = \frac{d}{c} \sin \phi$$

In the general case of a narrow band signal with complex envelope $\mu(t)$, the signal received at a particular point on the antenna has the form $\mu(t-\tau)e^{j2\pi f_c(t-\tau)}$. The processor output signal is then

$$V(t,\phi) = \sum_{n=-\frac{N-1}{2}}^{\frac{N-1}{2}} \mu(t-\frac{nd}{c} \sin \phi)\ e^{j2\pi(f_c t - \frac{nd}{\lambda_c} \sin \phi)} I(nd) e^{j2\pi\ \chi(nd)}$$

For waveforms with small percentage bandwidth, the complex envelope distortion is negligible across the array elements. This allows us to write

$$V(t,\phi,\ \phi_o) = \mu(t)\ e^{j2\pi f_c t}\ E_e(\theta) \sum_{n=-\frac{N-1}{2}}^{\frac{N-1}{2}} e^{\ j2\pi n\frac{d}{\lambda_c}\ [\sin \phi_o - \sin \phi]}$$

where the element pattern has been included to take into account the directivity of each receiving element, and where the following assumptions have been made:

1) $I(nd) = 1$ for all n: that is, uniform amplitude illumination across the entire array.

2) $\chi(nd) = n\frac{d}{\lambda_c} \sin \phi_o$: that is, the incoming signal is correlated against a linear phase slope corresponding to an assumed incidence angle $\phi_o$.

The summation term in $V(t, \phi, \phi_o)$ reduces to

$$\frac{\sin[N\pi(\frac{d}{\lambda_c})(\sin \phi - \sin \phi_o)]}{\sin[\pi(\frac{d}{\lambda_c})(\sin \phi - \sin \phi_o)]}$$

which corresponds exactly to the scanned array pattern derived in section 2.1. This part of the output of the ideal processor has thus been shown to correspond to the scanned array pattern of the receiving antenna. The

Fourier transform relationship between the approximate array pattern and the aperture illumination function of the antenna shall be conveniently exploited in the implementation of the optical processor. The same conclusion can be arrived at by writing $V(t,\phi,\phi_o)$ as

$$V(t,\emptyset,\emptyset_o) = \mu(t)e^{j2\pi f_c t}\left(\frac{1+\cos\emptyset}{2}\right)\int_{-\frac{N-1}{2}d}^{\frac{N-1}{2}d} I(x)e^{j2\pi\chi(x)}\ e^{-j2\pi x\ \sin\emptyset}\ dx$$

where $x = \frac{\ell}{\lambda_c} = \left(\frac{\ell}{c}\right)f_c$, $\ell$ = distance across the array, the summation over a discrete set of points has been approximated by an integral and the element pattern equal to the obliquity factor $\frac{1+\cos\emptyset}{2}$. The antenna pattern is then

$$E\ \ (\emptyset,\ \emptyset_o) = \left(\frac{1+\cos\emptyset}{2}\right)\int_{-\infty}^{\infty} I(x)e^{j2\pi\chi(x)}\ e^{-j2\pi x\ \sin\emptyset}\ dx$$

which, for $I(x) = \begin{cases}1, |x| \leq \frac{D}{2}\\ 0, \text{otherwise}\end{cases}$ and $\chi(x) = \frac{\ell\sin\emptyset_o}{\lambda_c} = x\sin\emptyset_o$ (where $D = (N-1)d$) reduces to:

$$E\ \ (\emptyset,\emptyset_o) = \left(\frac{1+\cos\emptyset}{2}\right)\ \ \int_{-\infty}^{\infty} P_D(x)\ e^{j2\pi x(\sin\emptyset_o\ -\ \sin\ \emptyset)}\ dx$$

and thus,

$$V(t,\emptyset,\ \emptyset_o) = \mu(t)\ e^{j2\pi f_c t}\ E\ \ (\emptyset,\ \emptyset_o)$$

where a Fourier transform relationship holds between $E\ \ (\emptyset,\ \emptyset_o)$, the approximate scanned array pattern, and the illumination function of the antenna.

The approximation of the element pattern $E_e$ (equal to $\sqrt{\cos \phi}$ for a well-designed array) by the obiquity factor $\frac{1 + \cos \phi}{2}$ is valid for values of $\phi$ up to 60° or 70°.

The Fourier transform relationship which was just proven to exist between the illuminating function $I(x)e^{j2\pi\chi(x)}$ and the antenna pattern $E(\phi,\phi_o)$ is the basis for optical beam steering which we will now consider. The analogy between beam forming and optical beam steering will then be apparent.

## 2.3 Optical Beam Steering

It is well known that optically a lens forms in its back focal plane a light distribution--in amplitude and phase-which equals the Fourier transform of the light distribution existing in its front focal plane, when monochromatic coherent light is used. In the physical situation, if a collimated plane light wave is modulated with the one dimensional phase distribution corresponding to the linear phase slope of a RF waveform impinging over a linear array antenna and then an one-dimensional Fourier transform is taken, the output plane presents a light amplitude distribution which corresponds to the continuous aperture antenna pattern (for appropriate scaling factors) and which presents a maximum at a location corresponding to the angle of incidence on the array of such waveform. Fig. 2.3.1 depicts this situation.

Also, for a planar phased array, if the two-dimensional phase distribution of a plane waveform impinging on the array at angles $\theta$ and $\psi$, as described in Fig. 2.3.2 is used to modulate the phase of a plane collimated light wave by using a convenient transducer, the Fourier transform of such light distribution is again the continuous aperture antenna pattern which presents a maximum at a location corresponding to such incidence angles $\theta$ and $\psi$ as shown in Fig. 2.3.3.

Optical beam steering based on such principles has been successfully performed with devices such as the Membrane Light Modulator at A.P.L. (Johns Hopkins University). (The reader is referred to Report TG 1193A for further details). This mode of operation requires, however, knowledge of the phase of the RF signal received at every array element prior to the operation of beam forming. For an array with N elements, a total of N phase detectors and D/A converters are required for parallel operation, and there is no provision for optical waveform processing, since the input transducer is a pure phase

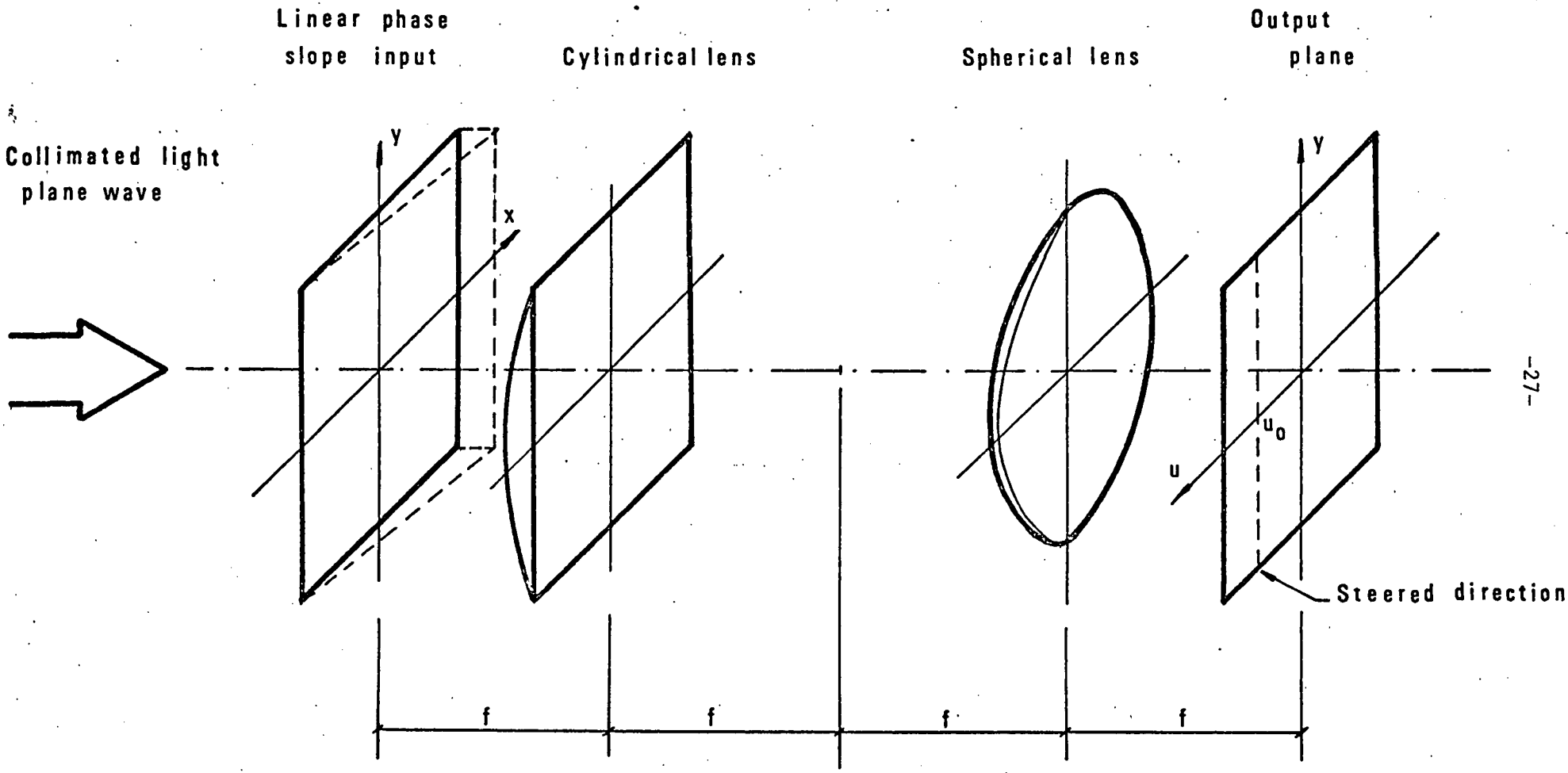


Fig. 2.3.1 Optical Beam Steering for a Linear Phased Array Antenna

modulator. It seems thus advantageous to build a processor which operates on the received waveforms themselves rather than on the RF phase. Most of the pre-processing hardware is eliminated and the required operations of amplitude weighting and filtering are much simpler.

With the availability of the Pockels light modulator, the possibility of such processing exists. This has been the center of much of our recent research effort.

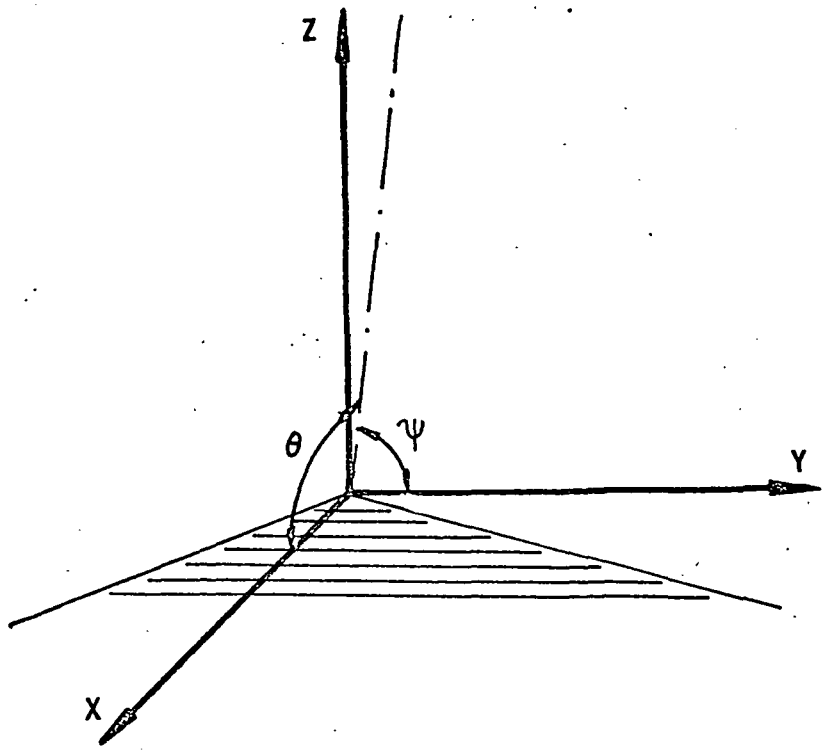


Fig. 2.3.2 Characterization of a Plane Waveform Impinging on 2-D Phased Array

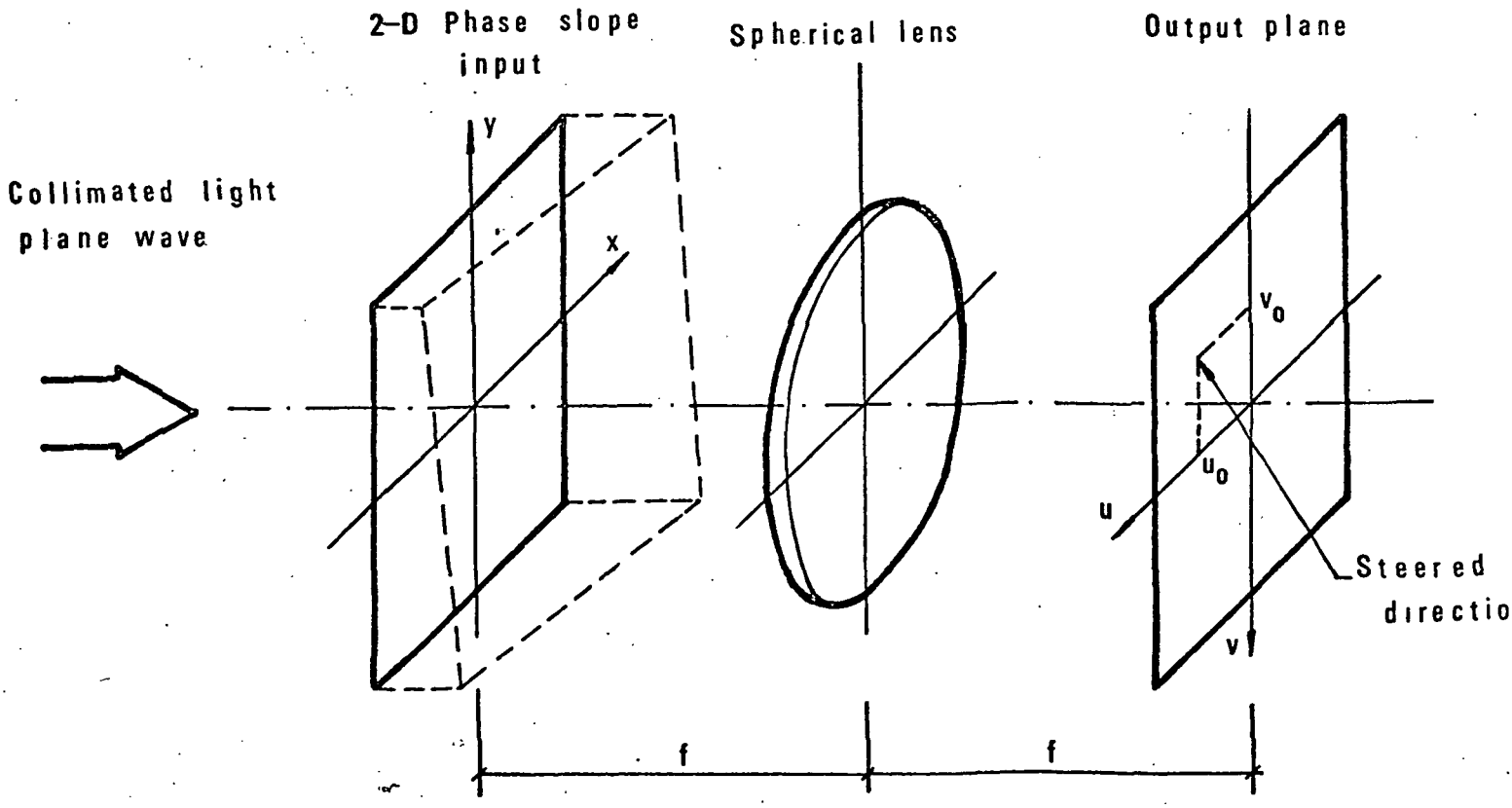


Fig. 2.3.3 Optical Beam Steering for a Planar Phased Array

# CHAPTER 3

# ELECTROOPTICAL PROCESSING OF LINEAR PHASED ARRAY ANTENNA SIGNALS

## 3.0. Introduction

In Chapter 2, the Fourier transform relation between the continuous aperture antenna illuminating function and the far-field antenna pattern in beam steering was shown to be the reciprocal of the relation between the array illumination function of the receiving antenna and the processor output in beam forming. One possible processing format which related beam forming and optical beam steering was also presented. In this chapter, beam forming by an optical processor is shown to result when the returned electrical signals, converted to optical signals by means of an appropriate transducer, are used in optical beam steering. It will be shown that such optical beam steering yields an output corresponding to that of the ideal processor defined in Chapter 2. The optical system, several possible input formats to be used with the input transducer described in Section 1.2, and derivations of the format the optical output pattern are also included.

## 3.1 Signal Preprocessing

The simplest configuration for a linear receiving array was shown in Fig. 2.2.1. The RF signal reflected from an assumed point target located at a direction forming an angle $\phi$ with the boresight axis at a range R is represented by a plane waveform impinging on the linear array. The elements of the array are equi-spaced by distance sd. The ideal processor described in Chapter 2 is shown on the same diagram; it consists of N delay lines, a summer and a coherent integrator yielding the processor output $V(\phi)$.

Modern radars transmit RF signals of frequencies in the S, C and X bands. With the limited input plane resolution available and the present electron gun scan at video rates, it is impossible to directly record the returned RF signals. The approach usually taken is to first amplify the RF returns in a radio-frequency amplifier, then heterodyne down such signals with a local oscillator; the resultant IF signals are range gated before processing to extract angular information. Fig. 3.1.1 shows a block diagram of such a system.

## 3.2 Input Format

The most feasible input format is now described, with alternate configurations to be discussed later. To process linear phased array antenna data, the time history of each detector/receiver element after amplifying and heterodying is recorded along each horizontal line in the input plane. With a total of N detector elements, N horizontal lines are used on the input plane electrooptic crystal. The spacing between these lines is proportional

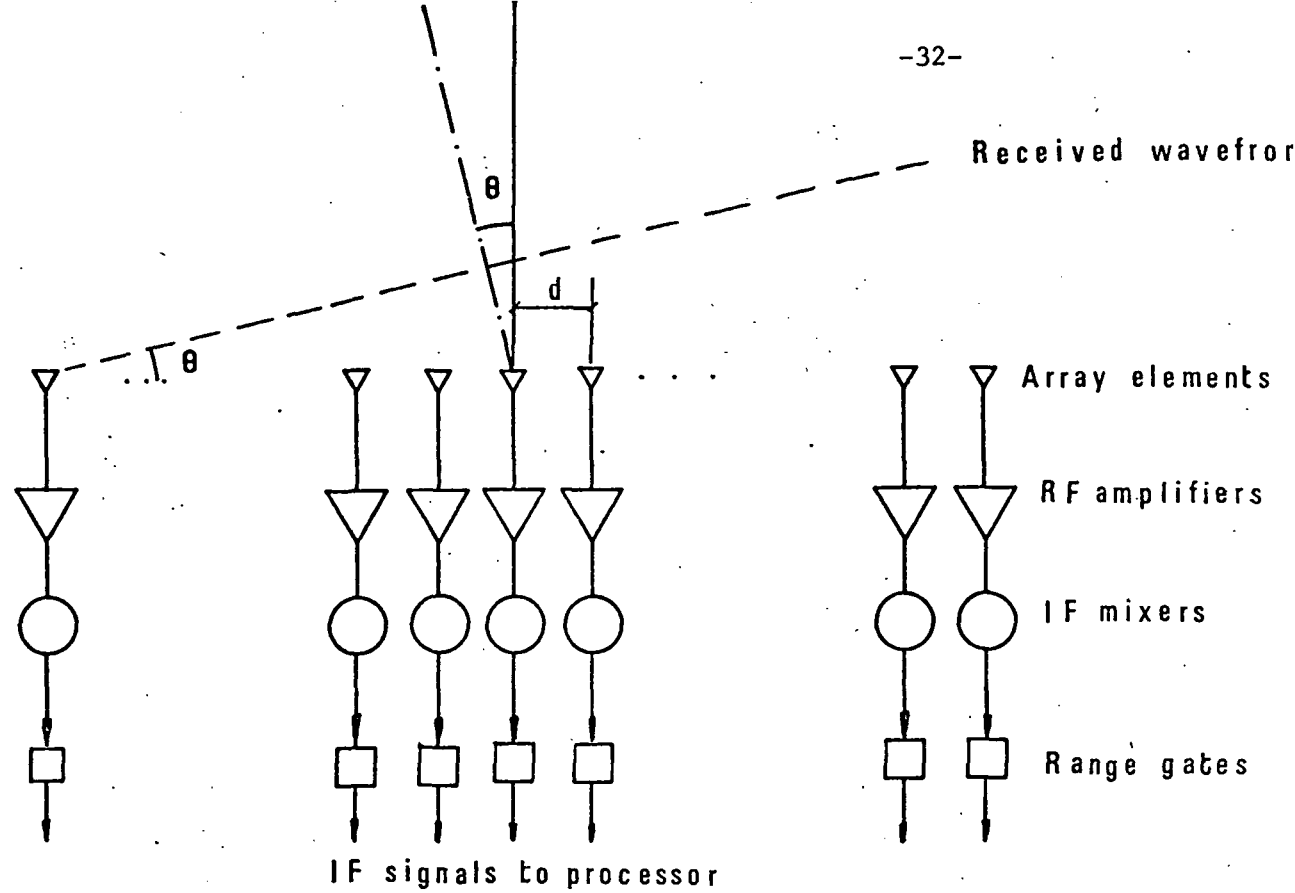


Fig. 3.1.1 Linear Phased Array Radar Preprocessing

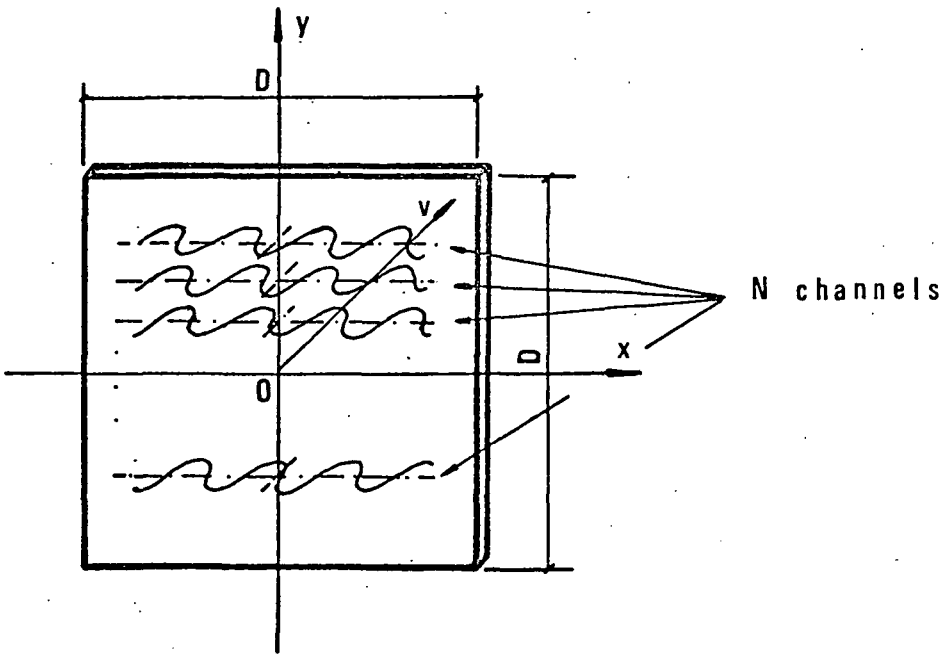


Fig. 3.2.1 Input Format for Optical Processing of Linear Phased Array Radar Data

to the spacing of the detector elements in the detector array. Such an input format is depicted in Fig. 3.2.1.

Let us now consider this processing and the resulting output plane pattern in detail. Recall that the input electrical signals from the detector elements will be used to modulate the beam current in an off-axis electron gun. This gun then deposits a charge pattern on the electro-optic target crystal which results in a voltage being developed across the crystal and hence an electric field all of which are controllable functions, point-by-point, of the input electrical signal. By the linear longitudinal electro-optic effect, this charge distribution then modulates the amplitude and/or phase of a collimated input laser beam, as described in Section 1.3.

For an array consisting of N identical elements, the optical image placed on line n of the crystal should be a representation of the (heterodyned) signal received by the nth antenna element $v_{in}(t)$ over the integration time $T_i$ for the range delay $\tau_R$ of interest. The integration time $T_i$ is defined as

$$T_i = T_1 - T_2$$

where

$T_1$ = time at which recording of returned signals begins

$T_2$ = time at which recording of returned signals ends.

With the electron gun scanning the electrooptic crystal at horizontal TV rates, $T_i$ is approximately 50 μsec. Fig. 3.2.2 shows the pulse width $T_p$, range delay $\tau_R$, and integration time $T_i$ for one detector element and their inter-relations. The value of $T_i$ is set by the range gates following the IF mixers in Fig. 3.1.1.

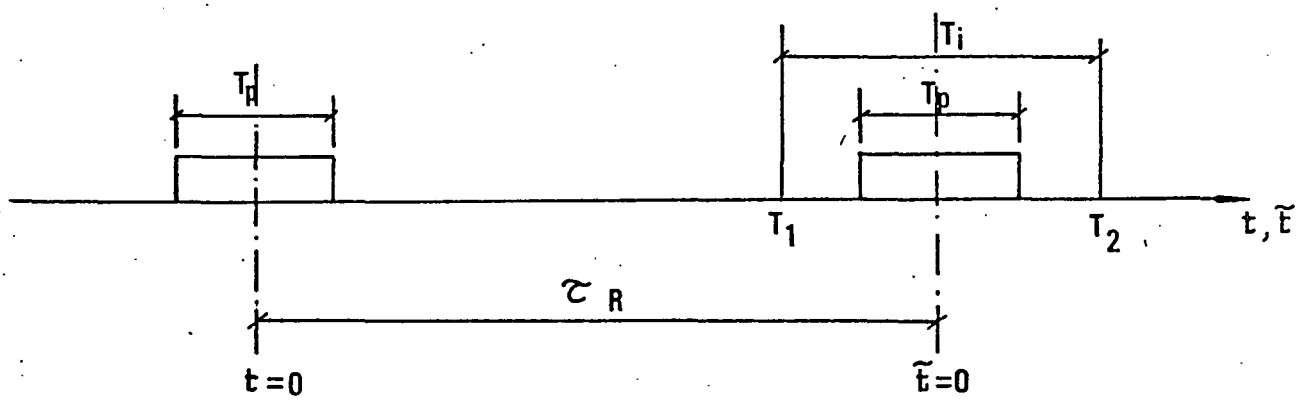


Fig. 3.2.2 Relationships Between Integration Time $T_i$, Range Delay $\tau_R$ and Transmitted Pulse Width $T_p$.

Let the signal transmitted by the antenna be an RF pulse of the form

$$v_T(t) = p_{T_p}(t)\cos(2\pi f_c t)$$

where

$$p_{T_p}(t) = \begin{matrix} 1, |t| < T_p/2 \\ 0, |t| > T_p/2 \end{matrix}$$

After being reflected by a target at a range R, the received signal at the nth element of the array is given by

$$v_n(t) = p_{T_p}(t - \tau_R - n\tau)\{\cos[2\pi f_r(t - \tau_R - n\tau)]\}$$

where

$\tau = \frac{d\sin\theta_o}{c}$ = differential time delay between 2 consecutive array elements

$\tau_R = \frac{2R}{c}$ = round trip time to target; $f_r$ = received frequency

For a static target, the received frequency $f_r$ equals the transmitted frequency $f_c$. However for a target moving at a radial rate $\frac{dR}{dt}$, the carrier frequency will be modified by the Doppler effect and

$$f_r = f_c \pm 2\frac{dR}{dt}\frac{f_c}{c} = f_c + f_d$$

where the sign depends on the sense of the radial movement of the target.

Very high carrier frequencies are used. To process these, the received signals are heterodyned down in frequency. The signal received at the nth element of the array after heterodying then has the form

$$v_{in}(\tilde{t}) = p_{T_p}(\tilde{t} - n\tau)\cos[2\pi(f_{if} + f_d)\tilde{t} - 2\pi(f_c + f_d)n\tau]$$

where the time origin is now taken at $t = \tau_R$, $f_d$ is the Doppler frequency and $f_{if}$ is the intermediate frequency of heterodyning.

If the maximum delay in the received signal across all of the detector elements is small in comparison with the pulse width, and if the doppler frequency shift is small in comparison with the carrier frequency (these are reasonable assumptions for real targets and existing arrays) that is if

$$n\tau << T_p \quad \text{for} \quad \text{all n. and}$$

$$f_d << f_c$$

then the approximate heterodyne signal at the nth array element can be written as

$$v_{in}(\tilde{t}) = p_{T_p}(\tilde{t})\cos[2\pi(f_{if} + f_d)\tilde{t} - 2\pi n\alpha]$$

where

$$\alpha = \tau(f_c + f_d) \simeq \frac{d}{\lambda_c}\sin\theta_o$$

and

$\lambda_c$ = free-space wavelength of transmitted carrier.

If the range of interest corresponds to a range delay $\tau_R$, only those signals, reflected by targets whose range delays satisfy

$$\tau_R - \frac{(T_i - T_p)}{2} \leq \frac{2R_i}{C} \leq \tau_R + \frac{(T_i - T_p)}{2}$$

will be completely processed where $T_i$ is the integration time for the processor and $T_p$ is the pulse width.

With the electron gun scanning in a raster format, the input electronic signals can be arranged in the proper sequence to be compatible with the raster scan format by using N delay lines and an electronic switch.

For now we will assume that the input data in the format of Fig. 3.2.1 exists. Since only negative signal polarities can be formed by the electron beam, the most faithful optical transmission obtainable is

$$T(x,y) = \sum_{n=-\frac{N-1}{2}}^{+\frac{N-1}{2}} \delta(y - n\ell)[1 + \mu v_{in}(x)]P_D(x)$$

Where $P_D(x) = \begin{matrix} 1, |x| \leq D/2 \\ 0, \text{ otherwise.} \end{matrix}$

The distance x across the crystal is related to time $\tilde{t}$ by

$$x = \frac{D}{T_i}\tilde{t}$$

$T_i$ is the integration time, $\ell$ is the vertical separation between scan lines in the input, D is the crystal aperture along the x direction, and $\mu$ is the modulation index $0 \leq \mu \leq 1$. $T(x,y)$ is the ratio of transmitted/incident light amplitude.

This image, and consequently the output data also, will remain on the crystal until it is electrically erased or until it decays through leakage currents (see Chapter 1). Delay line modulators may use similar input data image formats for data processing, but the output is available only during the short time that the signals fill the delay medium.

## 3.3 Electro-Optic Processor

The optical system used is shown in Fig. 3.3.1. A choice must be made between the two possible light modulation schemes, amplitude modulation and phase modulation, described in Section 1.3. For reasons to be explained later, amplitude modulation of light is preferable. The electro-optic crystal transducer is then placed between crossed polarizers. A general analysis of the signals and processing involved will now be presented.

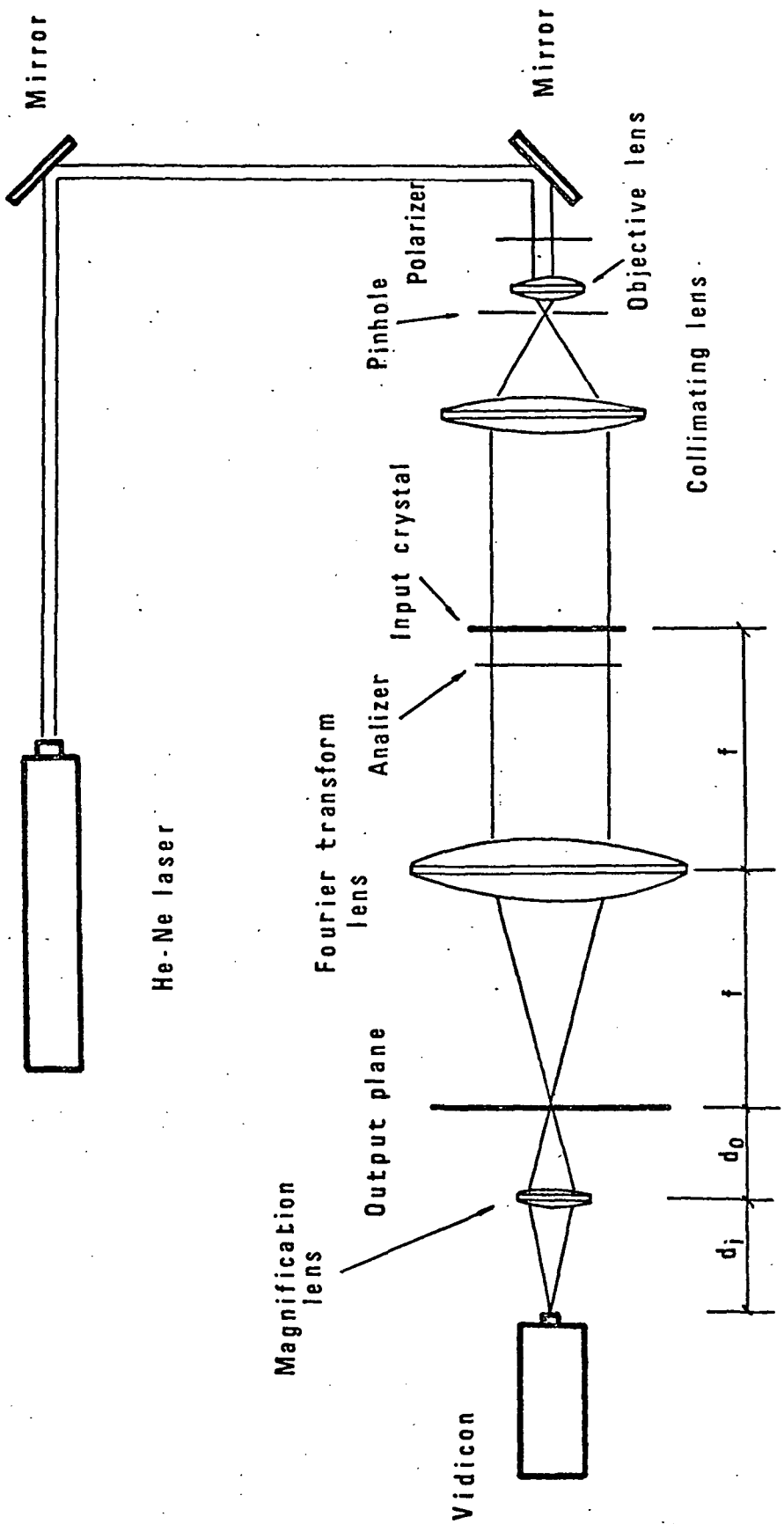


Fig. 3.3.1 Optical System for Radar Processing

The ideal optical processor illuminates the input (x,y) plane in Fig. 3.3.1 with a collimated coherent light beam and passes the image formed through the integrating or Fourier transform lens in Fig. 3.3.1. The back focal plane of this lens contains the Fourier transform F(u,v) of T(x,y)

$$F(u,v) = E \int_{-\infty}^{\infty} T(x,y) e^{-2\pi j(ux + vy)} dxdy$$

where

$$u = \frac{x'}{\lambda_L f} \quad \text{and} \quad v = \frac{y'}{\lambda_L f}$$

(u,v) = back focal plane spatial frequency coordinates

(x',y') = back focal plane geometrical coordinates

$\lambda_L$ = light wavelength

f = focal length of transform lens

E = constant dependent on optical system

F(u,v) = back focal plane light amplitude distribution

With a crystal transmissivity

$$T(x,y) = \sum_{n=-\frac{N-1}{2}}^{\frac{N-1}{2}} \delta(y - n\ell)[1 + \mu v_{in}(x)]P_D(x)$$

and an input IF modulated signal

$$v_{in}(x) = p_{T_p}(x\tfrac{T_i}{D})\cos[2\pi(f_{if} + f_d)x\,\tfrac{T_i}{D} - 2\pi n\alpha]$$

where

$$\alpha = \tau(f_c + f_d) \simeq \frac{d}{\lambda_c}\sin\theta_o$$

Substituting T(x,y) into F(u,v) the output plane pattern is found to be

$$F(u,v) = E \int_{-\infty}^{\infty} \sum_{n=-\frac{N-1}{2}}^{\frac{N-1}{2}} \delta(y - n\ell)[1 + \mu v_{in}(\,x\,)]P_D(x)e^{-2\pi j(ux + vy)} dxdy =$$

substituting $V_{in}(x)\ F(u,v)$ becomes

$$= E\int_{-\infty}^{\infty}\sum \delta(y - n\ell)[1 + P_{T_p}(x\frac{T_i}{D})\cos\{2\Pi(f_{if} + f_d)x\frac{T_i}{D} - 2\pi n\alpha\}]P_D(x)e^{-2\pi j(ux+v\,y)}dxdy$$

$$= E\int_{-\infty}^{\infty}\sum \delta(y - n\ell)P_D(x)e^{-2\pi j(ux + vy)}dxdy \qquad (1)$$

$$+ E\int_{-\infty}^{\infty}\sum \delta(y - n\ell)P_{X_p}(x)\cos[2\pi(f_{if} + f_d)x\frac{T_i}{D} - 2\pi n\alpha]e^{-2\pi j(ux + vy)}dxdy \qquad (2)$$

where

$$X_p = \frac{T_p}{T_i}D \leq D \quad \text{and} \quad P_{X_p}(x) = \begin{cases} 1 \text{ for } |x| \leq X_p/2 \\ 0 \text{ otherwise} \end{cases}$$

The 1st term can be written as

$$(1) = \int_{-\infty}^{\infty}\sum \delta(y - n\ell)e^{-2\pi j(ux + vy)}P_D(x)dxdy =$$

$$= (\sum\int_{-\infty}^{\infty}\delta(y - n\ell)e^{-2\pi jvy}dy)\int_{-\infty}^{\infty}P_D(x)e^{-2\pi jux}dx =$$

$$= \frac{\sin\pi Du}{\pi Du}\sum_{-\frac{N-1}{2}}^{\frac{N-1}{2}}e^{-2\pi jvn\ell} = \frac{\sin\pi Du}{\pi Du}(1 + 2\sum_{1}^{\frac{N-1}{2}}\cos 2\pi v\ell n)$$

$$= \frac{\sin\pi Du}{\pi Du}\left\{1 + 2\cos\left[\left(\frac{N+1}{2}\right)\pi v\ell\right]\frac{\sin\left[\left(\frac{N-1}{2}\right)\pi v\ell\right]}{\sin\pi v\ell}\right\}$$

$$= \frac{\sin\pi Du}{\pi Du}(1 + \frac{\sin N\pi v\ell}{\sin\pi v\ell} - \frac{\sin\pi v\ell}{\sin\pi v\ell}) = \frac{\sin\pi Du}{\pi Du}\frac{\sin N\pi v\ell}{\sin\pi v\ell}$$

while the second term can similarly be manipulated into the form

$$(2) = \int_{-\infty}^{\infty}\sum \delta(y - n\ell)P_{X_p}(x)\cos[2\pi(f_{if} + f_d)\frac{T_i}{D}x - 2\pi n\alpha]e^{-2\pi j(ux + vy)}dxdy$$

$$= \frac{1}{2}\int_{-\infty}^{\infty}\int \sum \delta(y - n\ell)P_{X_p}(x)[e^{2\pi j(f_{if} + f_d)\frac{T_i}{D}x - 2\pi jn\alpha} + e^{-2\pi j(f_{if} + f_d)\frac{T_i}{D}x + 2\pi jn\alpha}]e^{-2\pi j(ux + vy)}dxdy =$$

$$= \frac{1}{2}[\sum \int_{-\infty}^{\infty} \delta(y - n\ell)e^{-2\pi jn\alpha}e^{-2\pi jvy}dy \int_{-\infty}^{\infty} P_{X_p}(x)e^{2\pi j(f_{if} + f_d)\frac{T_i}{D}x}e^{-2\pi jux}dx] +$$

$$+ \frac{1}{2}[\sum \int_{-\infty}^{\infty} \delta(y - n\ell)e^{2\pi jn\alpha}e^{-2\pi jvy}dy \int_{-\infty}^{\infty} P_{X_p}(x)e^{-2\pi j(f_{if} + f_d)\frac{T_i}{D}x}e^{-2\pi jux}dx] =$$

$$= \frac{1}{2}\left[\frac{\sin\pi X_p(u - \frac{1}{\lambda_x})}{\pi X_p(u - \frac{1}{\lambda_x})} \sum_{-\frac{N-1}{2}}^{\frac{N-1}{2}} e^{-2\pi jn(\alpha + v\ell)} + \frac{\sin\pi X_p(u + \frac{1}{\lambda_x})}{\pi X_p(u + \frac{1}{\lambda_x})} \sum_{-\frac{N-1}{2}}^{\frac{N-1}{2}} e^{-2\pi jn(\alpha - v\ell)}\right] =$$

$$= \frac{1}{2}\left[\frac{\sin\pi X_p(u - \frac{1}{\lambda_x})}{\pi X_p(u + \frac{1}{\lambda_x})}\{1 + 2\cos\frac{N+1}{2}\pi(\alpha + v\ell)\frac{\sin(\frac{N-1}{2})\pi(\alpha + v\ell)}{\sin\pi(\alpha + v\ell)}\} +\right.$$

$$\left. + \frac{\sin\pi X_p(u + \frac{1}{\lambda_x})}{\pi X_p(u + \frac{1}{\lambda_x})}\{1 + 2\cos\frac{N+1}{2}\pi(\alpha + v\ell)\frac{\sin(\frac{N-1}{2})\pi(\alpha - v\ell)}{\sin\pi(\alpha - v\ell)}\}\right] =$$

$$= \frac{1}{2}\left[\frac{\sin\pi X_p(u + \frac{1}{\lambda_x})}{X_p(u - \frac{1}{\lambda_x})}\frac{\sin N\pi(\alpha + v\ell)}{\sin\pi(\alpha + v\ell)} + \frac{\sin\pi X_p(u + \frac{1}{\lambda_x})}{\pi X_p(u + \frac{1}{\lambda_x})}\frac{\sin N\pi(\alpha - v\ell)}{\sin\pi(\alpha - v\ell)}\right]$$

where

$$\lambda_x = \frac{D}{T_i(f_{if} + f_d)}\ ,\ \alpha \simeq \frac{d}{\lambda_c}\sin\theta_o$$

Combining these expressions, we find

$$F(u,v) = (1) + (2) = E\frac{\sin\pi Du}{\pi Du}\frac{\sin N\pi v\ell}{\sin\pi v\ell} +$$

$$+ \frac{E}{2}\frac{\sin\pi X_p(u - \frac{1}{\lambda_x})}{\pi X_p(u - \frac{1}{\lambda_x})}\frac{\sin N\pi(\alpha + v\ell)}{\sin\pi(\alpha + v\ell)} \qquad (*)$$

$$+ \frac{E}{2} \frac{\sin\pi X_p (u + \frac{1}{\lambda_x})}{\pi X_p (u + \frac{1}{\lambda_x})} \frac{\sin N\pi(\alpha - v\ell)}{\sin\pi(\alpha - v\ell)}$$

Fig. 3.3.2 shows this output pattern.

With the variable change $v\ell = -\frac{d}{\lambda_c} \sin\theta$, we obtain

$$F(u,\theta) = E \frac{\sin\pi Du}{\pi Du} \frac{\sin(N\pi\frac{d}{\lambda_c}\sin\theta)}{\sin(\pi\frac{d}{\lambda_c}\sin\theta)}$$

$$+ \frac{E}{2} \frac{\sin\pi X_p (u - \frac{1}{\lambda_x})}{\pi X_p (u - \frac{1}{\lambda_x})} \frac{\sin[N\pi\frac{d}{\lambda_c}(\sin\theta - \sin\theta_o)]}{\sin[\pi\frac{d}{\lambda_c}(\sin\theta - \sin\theta_o)]}$$

$$+ \frac{E}{2} \frac{\sin\pi X_p (u + \frac{1}{\lambda_x})}{\pi X_p (u + \frac{1}{\lambda_x})} \frac{\sin[N\pi\frac{d}{\lambda_c}(\sin\theta + \sin\theta_o)]}{\sin(\pi\frac{d}{\lambda_c}(\sin\theta + \sin\theta_o)]}$$

where the dependence on $\theta_o$ has been emphasized.

In this derivation, we have assumed that $T_i >> T_p$ or $D >> X_p$ which is the case for real time processing of radar signals at horizontal TV scan rates. The first term in the $F(u,v)$ expression is the zero-order pattern resulting from the constant in the $1 + v$ form of $T(x,y)$. This term yields no useful information.

The second term (*) is the positive first order fringe; the position of its lowest order maximum is at

$$u_1 = \frac{1}{\lambda_x} = \frac{T_i}{D} (f_{if} + f_d)$$

$$v_1 = -\frac{\alpha}{\ell} = \frac{-d}{\ell\lambda_c} \sin\theta_o$$

As shown in Fig. 3.3.2, $f_{if}$ is assumed to be greater than $f_d$ in absolute value so that there is no indetermination in deciding which first order spot to choose, the one corresponding to the positive u axis is chosen

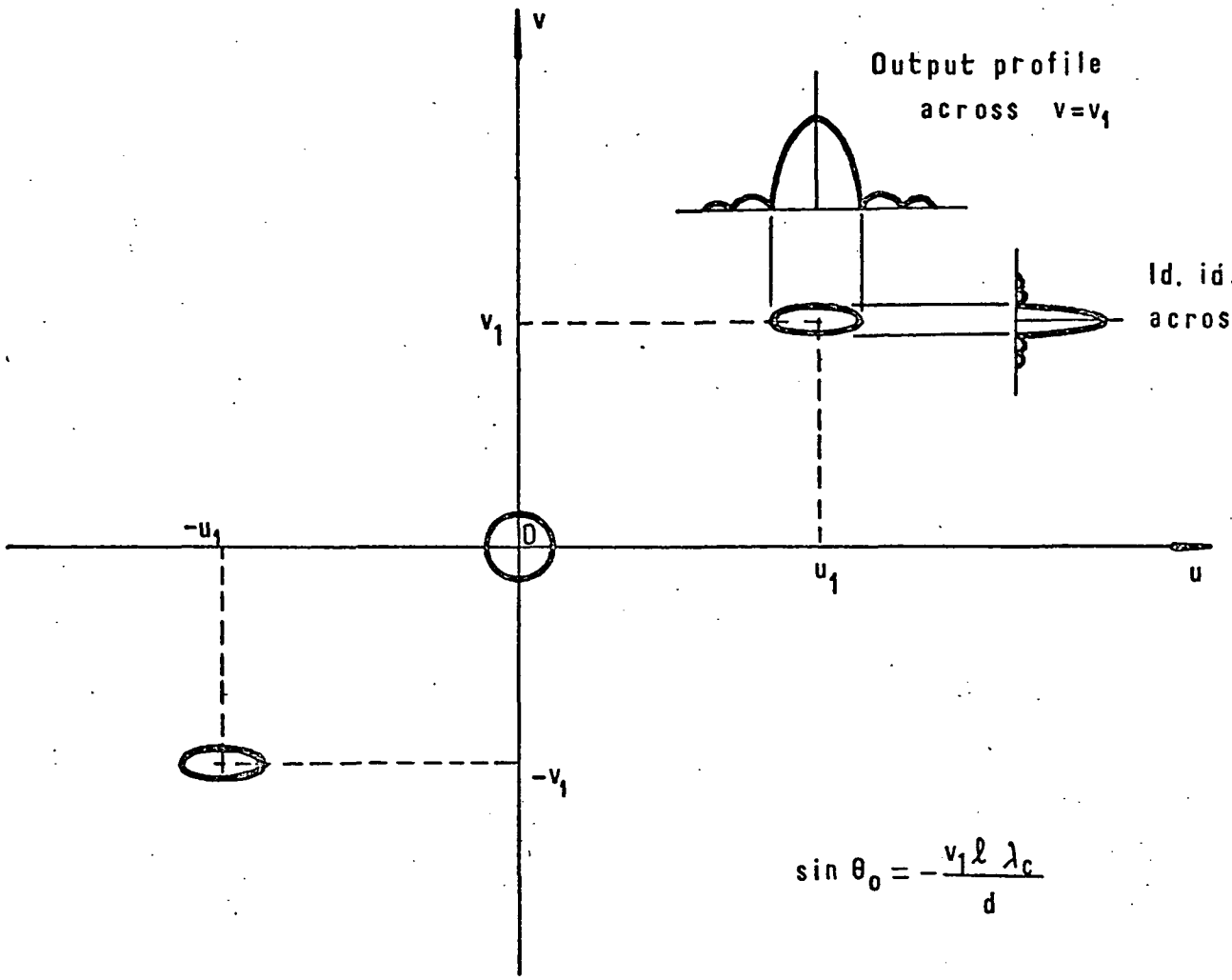


Fig. 3.3.2 Output Transform Plane Pattern for the Optical Processor of Fig. 3.3.1 with the Input Format of Fig. 3.2.1

From these expressions and Fig. 3.3.2, we see that we can obtain both range rate and angle information about the target from the position of this output plane maximum. The linearity of the system allows multi-target processing capability also.

Furthermore, the amplitude profile of this first order maximum will be the same as the amplitude profile of the antenna beam itself.(Ref 9)

$$\left|F(u = \frac{1}{\lambda_x},\ \theta)\right|^2 \cong \left|V(\theta)\right|^2 = K(\theta)\ \frac{\sin^2[\pi N \frac{d}{\lambda_c}(\sin\theta - \sin\theta_o)]}{\sin^2[\pi\frac{d}{\lambda_c}(\sin\theta - \sin\theta_o)]}$$

where $K(\theta)$ represents the radiation pattern of an individual element in the array; $K(\theta)$ usually varies only slightly from unity for the values of $\theta$ of interest, as shown in Chapter 2. This proves that the output of the optical processor corresponds to the output of the ideal processor defined in Chapter 2. The Doppler resolution obtained is the same as that of an ideal processor with integration time $T_i$.

The result just obtained, indicating that the angular and frequency resolutions of the processed signal are the same as the ideal output resolutions, depends on the implicit assumptions that the optical system is diffraction limited and that the pattern on the input crystal is a faithful representation of the idealized IF radar signal. For the second assumption to be valid, the crystal resolution must be sufficient to reproduce the $T_i(f_{if} + f_d)$ cycles of signal along each line in the x direction in proper relative phase to the signals along the other lines. For processing of an N element linear array, this condition requires a crystal resolution of at least N lines in the y direction. These minimal values must be weighted against the attainable resolution of the target crystal.

Pockels tubes operated at the Curie temperature exhibit resolutions of 1000 lines in 5 cm square crystals. This means that intermediate frequencies up

to

$$f_{if\ max} = \frac{1000/2}{50x10^{-6}} = 10\ MHz$$

can be faithfully represented on the crystal. The restriction in N allows us to process returns for arrays of up to 500 elements, by far larger than any existing linear array.

Another remark about T(x,y) must be made. The delta functions $\delta(y-n\ell)$ account for the fact that the time history from each detector element is written at discrete vertical locations $y = n\ell$ on the crystal, where n = 0...N and $\ell$ is the separation between vertical channels on the input crystal. This approach simplifies the summations and computations involved.

However, if we consider the finite size of the spot (1 mil) and assume the cross-section transmission of a horizontal line to be given by

$$g(y) = P_{y_s}(y) = \begin{cases} 1, 0 \leq |y| \leq \frac{s}{2} \\ 0 \text{ otherwise} \end{cases}$$

where s is the spot size, the value of F(u,v) formerly derived must be modified to

$$F(u,v) = E \frac{\sin \pi Du}{\pi Du} G(v) \frac{\sin N\ \pi v\ell}{\sin \pi v\ell}$$

$$+ \frac{E}{2} \frac{\sin \pi X_p (u - \frac{1}{\lambda_x})}{\pi X_p (u - \frac{1}{\lambda_x})} G(v) \frac{\sin N\ \pi(\alpha + v\ell)}{\sin \pi(\alpha + v\ell)}$$

$$+ \frac{E}{2} \frac{\sin \pi X_p (u + \frac{1}{\lambda_x})}{\pi X_p (u + \frac{1}{\lambda_x})} G(v) \frac{\sin N\ \pi(\alpha - v\ell)}{\sin \pi(\alpha - v\ell)}$$

where $G(v) = \int_{-\infty}^{\infty} g(y)\ e^{-j2\pi vy} dy$ is the Fourier transform of g(y).

A numerical example will be most instructive here. The 3 dB width of G(v) is given by

$$\Delta G_{3dB} = \frac{1}{s} = \frac{1}{25 \times 10^{-6}} = 4 \times 10^{4}\ m^{-1}$$

while the beamforming area for $\theta = \pm 90°$, considering $\frac{d}{\lambda_c} = 0.5$, is given by

$$v_{max} = \pm \frac{1}{2\ell} = \pm \frac{1}{2 \times 10^{-4}} = 5 \times 10^{3}\ m^{-1}$$

from which we find that G(v) is almost constant along the beam forming area for $\theta$. The approximation of g(y) by $\delta(y)$ is then valid.

### 3.4 Data Format Considerations

Two methods have been considered for producing the format depicted in Fig. 3.2.1 and we now devote some attention to the advantages of each scheme.

#### 3.4.1 Time-Delay Multiplexing

In this implementation, the time stories of the range gated IF signals for every element are delayed an amount of time which is a multiple of the horizontal scan time $T_h$ of the electron gun prior to being written on the crystal sequentially element by element. Fig. 3.4.1 shows this situation.

This method requires N delay lines, an electronic switch and support electronic equipment. The pulse repetition rate of the transmitting antenna has to be lower or equal to the 30 frames per second video rate.

#### 3.4.2 Time Sampling

Another implementation consists of sampling the IF signal present across every array element during the total video frame time. Fig. 3.4.2 and 3.4.3 illustrate this input format. This procedure is similar to time multiplexing but in this case the electronic switch will sample each of the N elements of the detector array at the rate of 1 sample per element every 50 μs. The electron gun now scans vertically at the normal horizontal scan rate of TV.

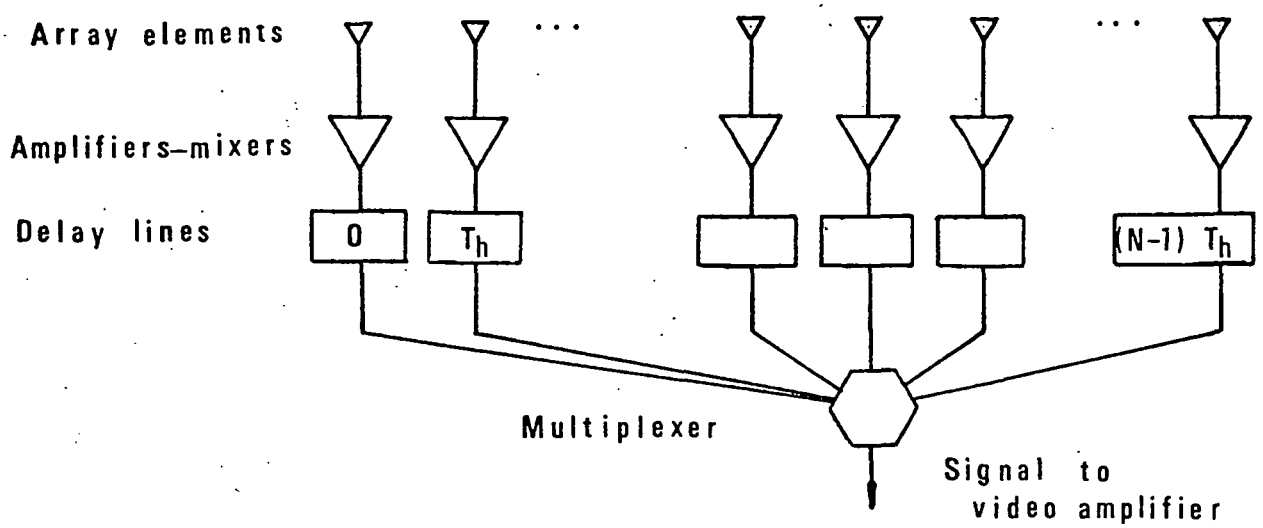


Fig. 3.4.1 Realization of Time-Delay Multiplex Input Data Format

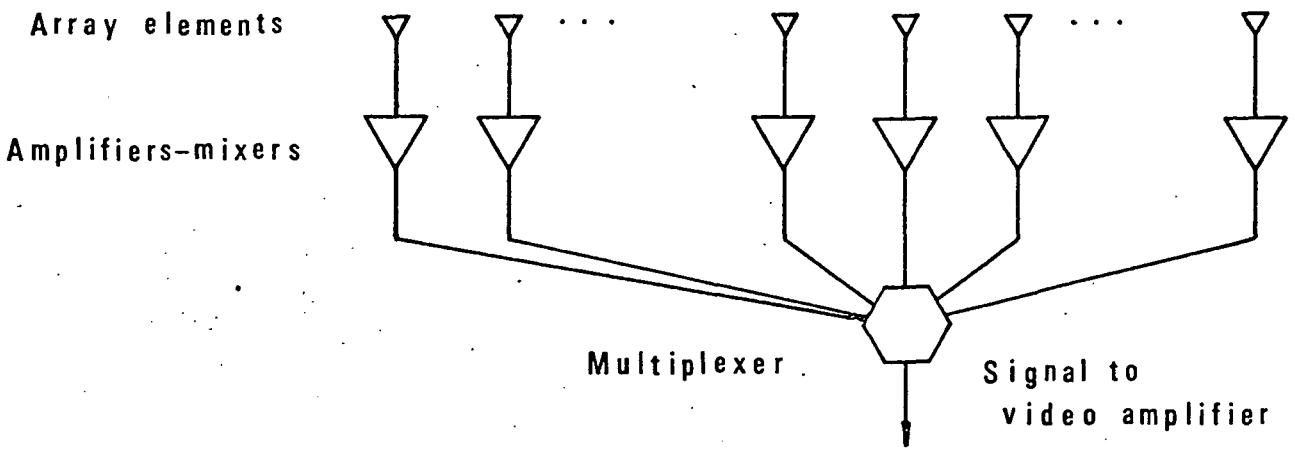


Fig. 3.4.2 Realization of Time Sampling Input Data Format

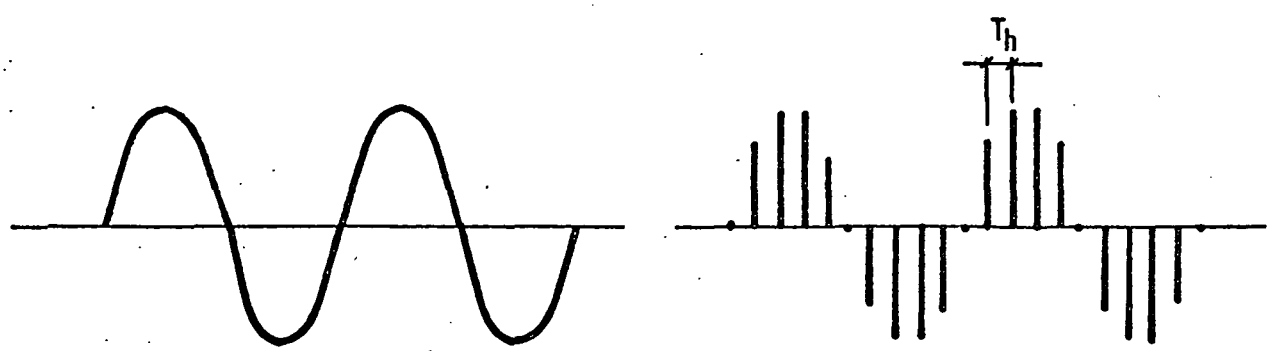


a. Input Signal b. Sampled Input Signal

Fig. 3.4.3 Input Waveforms for Time Sampled Input Data Format

Fig. 3.4.3 shows the actual detector signal and the result after sampling. For the sampled signal to accurately represent the real signal, the frequency and pulse width of the signal are severely constrained. For TV writing rates, $f_{max} = \frac{1}{2 \times 50\ \mu s} = 10^4$ Hz is the maximum frequency which can be accurately represented on the crystal, this corresponds to two samples per cycle. The pulse width transmitted by the antenna must now be larger than 100 μs, if a one cycle cosinusoidal signal at the maximum frequency is to be written.

It must be remembered that now the electron gun is scanning the crystal vertically, at the rate of 1 vertical line every 50 μs. This scheme again requires the least support electronics. Its disadvantage in radar systems is the large pulse width required. This scheme can be shown to be quite applicable and practical with sonar data however.

## 3.5 Amplitude versus Phase Modulation of Light

Amplitude modulation and phase modulation of light present both advantages and disadvantages. Phase modulation of light presents a higher diffraction efficiency than amplitude modulation; furthermore, the phase modulation is linearly related to the voltage applied across the crystal (as shown in Section 1.3.2). While the amplitude transmittance varies as a sinusoidal function of such voltage (Section 1.3.1), being approximately linear for $\delta \leq 30^\circ$ with error less than 10%.

Phase modulation of light requires a larger optical system bandwidth than amplitude modulation, for the same amount of distortion. Furthermore, it introduces greater noise consequently reducing the signal-to-noise ratio at the output plane, and it is more sensitive to irregularities in the crystal and windows surfaces. Based on these facts and observations performed for both modulation types using the same input patterns, the choice to use

amplitude modulation for this particular kind of processing was made.

CHAPTER 4

# ELECTROOPTIC PROCESSING OF TWO-DIMENSIONAL PHASED ARRAY ANTENNA SIGNALS

## 4.1 Introduction

Two dimensional phased array signal processing consists essentially of correlating the phase slope corresponding to the planar waveform impinging on the array proceeding from a reflecting point target at a range R at a direction given by two angles refered to a coordinate system consisting of the array itself and the boresight direction. All that was said about the linear array applies here, with the added requirement that the output of the ideal processor must now yield information on two angles at a time. Two input formats will be considered, their requirements compared and their on-line implementation discussed.

## 4.2 Full Array Processing

We consider the receiving array depicted in Fig. 4.2.1 where the received waveform has a plane equiphase front whose normal is defined by the two angles $\phi_X, \phi_Y$. An array consisting of a uniform rectangular grid of M elements spaced at a distance $\Delta X$ in the X direction and N elements spaced at a distance $\Delta Y$ in the Y direction. The input format used consists of dividing each of N lines in the electrooptic crystal into M sections or cells. The mth cell of the nth line contains the representation of the signal received at element (m,n) of the array after amplifying and heterodyning during the integration time $T_i$.

Let this i.f. signal be represented as

$$v_{i_{nm}}(t) = p_{T_p}(t - \tau_{nm})\cos[2\pi(f_{if} + f_d)t - 2\pi(f_c + f_d)\tau_{nm}]$$

where

$\tau_{nm}$ = differential delay per element
$= \frac{d_{nm}}{c}$

$d_{nm}$ = distance from antenna element (n,m) to the impinging plane wavefront

$f_c$ = RF carrier frequency

$f_{if}$ = IF frequency

$f_d$ = Doppler frequency shift ($f_d \ll f_c$ and $f_d \ll f_{if}$)

When $\tau_{nm} \ll T_p$ for all m, n which is a reasonable approximation in most cases we have,

$$v_{inm}(t) \simeq p_{T_p}(t)\cos[2\pi(f_{if} + f_d)t - 2\pi(f_c + f_d)\tau_{nm}]$$

where

$$\tau_{mn} = \frac{d_{nm}}{c} = \frac{m\Delta X \cos\phi_X + n\Delta Y \cos\phi_Y}{c}$$

follows from the geometry of Fig. 4.2.1, and

$$(f_c + f_d)\tau_{mn} \simeq f_c\tau_{mn} = \frac{m\Delta X}{\lambda_c}\cos\phi_X + \frac{n\Delta Y}{\lambda_c}\cos\phi_Y$$

$$= \frac{m\Delta X}{\lambda_c}\sin\theta_X + \frac{n\Delta Y}{\lambda_c}\sin\theta_Y$$

$\phi_x$ and $\phi_y$ are related by

$$\theta_X = 90° - \phi_X$$

$$\theta_Y = 90° - \phi_Y$$

if we define two $\alpha$ parameters

$$\alpha_X = \frac{\Delta X}{\lambda_c}\sin\theta_X$$

$$\alpha_Y = \frac{\Delta Y}{\lambda_c}\sin\theta_Y$$

we can rewrite $v_{i_{nm}}$ as

$$v_{i_{nm}}(t) = p_{T_p}(t)\cos[2\pi(f_{if} + f_d)t - 2\pi(m\alpha_X + n\alpha_Y)]$$

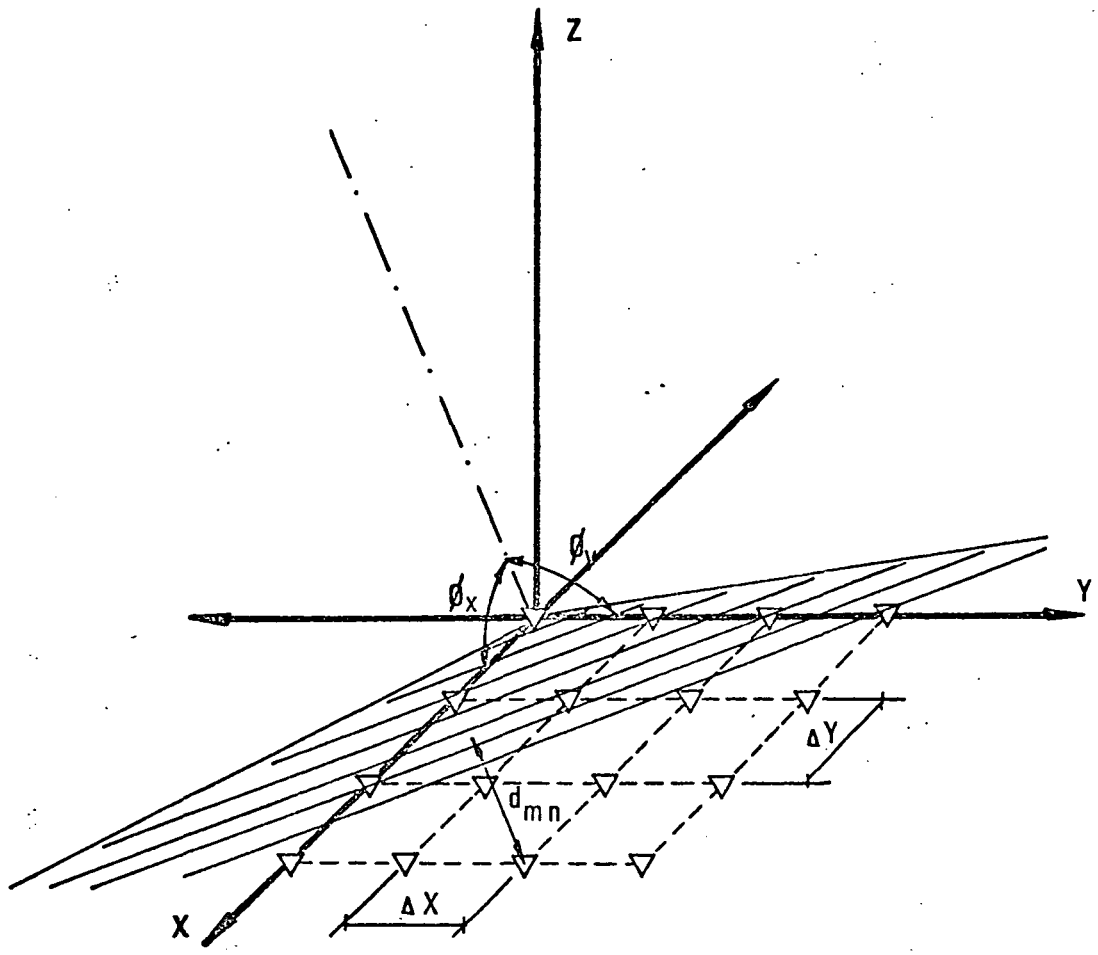


Fig. 4.2.1 Geometry for a Planar Phased Array Antenna.

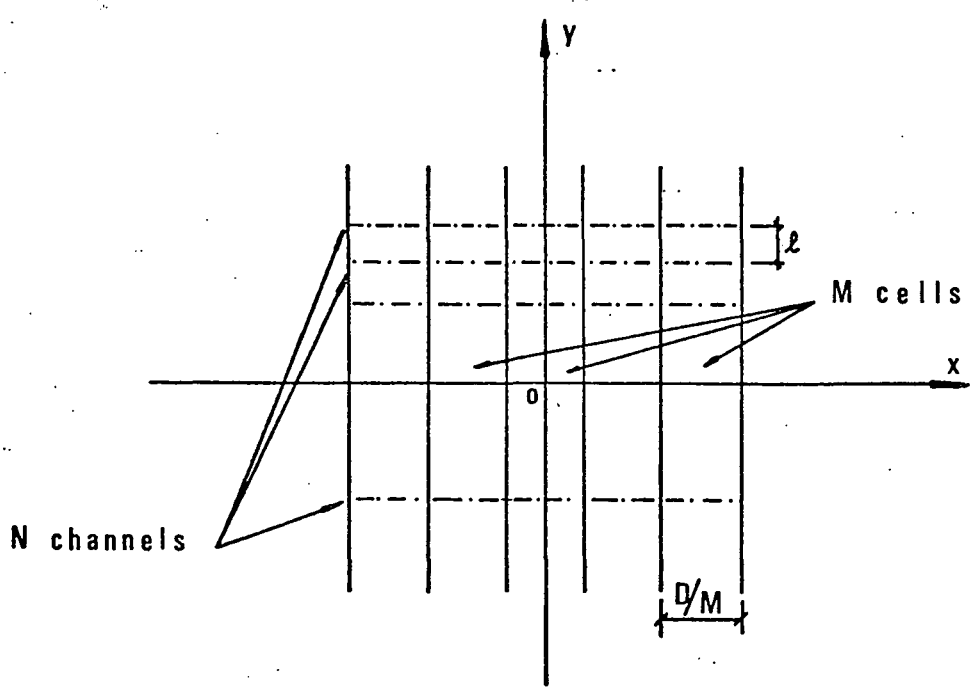


Fig. 4.2.2 Input Format for Full Array Processing of a Planar Phased Array Antenna.

With the input format depicted in Fig. 4.2.2 the optical transmission function is given by

$$T(x,y) = \sum_{n=-\frac{N-1}{2}}^{\frac{N-1}{2}} \delta(y - y_n) P_D(x) \left[1 + \mu \sum_{m=-\frac{M-1}{2}}^{\frac{M-1}{2}} P_{D/M}(x - x_n) v_{i_{nm}} \left( \frac{x - x_n}{D/M} T_i \right)\right]$$

where X and Y are the geometrical coordinates of the array (Fig. 4.2.1) and x and y are the geometrical coordinates in the input crystal plane (Fig. 4.2.2) $y_n$ and $x_m$ are related to $X_{mn}$, $Y_{mn}$ by two scaling factors $k_x$ and $k_y$

$$x_m = \frac{Xmn}{k_x} = \frac{m\Delta X}{k_x} = m \frac{D}{M}$$

$$y_n = \frac{Ymn}{k_y} = \frac{m\Delta Y}{k_y} = n \ell$$

As shown in Fig. 4.2.2, M is the number of channels, $\ell$ is the vertical spacing between them $P_{D/M}(x) = \begin{matrix} 1, & |x| \leq D/2M \\ 0, & \text{otherwise} \end{matrix}$ and

D is the crystal dimension across the x axis. Using the optical system shown in Fig. 3.3.1 a two dimensional Fourier transform of this input plane amplitude distribution is taken.

The output plane pattern is given by

$$F(u,v) = E\int_{-\infty}^{\infty} T(x,y) e^{-2\pi j(ux + vy)} dxdy$$

$$= E\int_{-\infty}^{\infty} \sum_{n=-\frac{N-1}{2}}^{\frac{N-1}{2}} \delta(y - n\ell) P_D(x) \{1 + \mu \sum_{m=-\frac{M-1}{2}}^{\frac{M-1}{2}} P_{D/M}(x - m\frac{D}{M})$$

$$P_{X_p}(x \frac{T_i M}{D} - mT_i) \cos\{2\pi[(f_{if} + f_d)(\frac{xT_i M}{D} - mT_i) - (m\alpha_X + n\alpha_Y)]\}$$

$$e^{-2\pi j(ux + vy)} dxdy$$

where

$$X_p = \frac{D}{M} \frac{T_p}{T_i}$$

With $T_i \leq T_p$, the $P_{X_p}$ pulse is absorbed into the $P_{D/M}$. Thus we obtain, decomposing the cosine term into the sum of two imaginary terms,

$$F(u,v) = E\int_{-\infty}^{\infty}\int \sum_{-\frac{N-1}{2}}^{\frac{N-1}{2}} \delta(y - n\ell)e^{-2\pi j(ux + vy)}\,dx\,dy$$

$$+ \mu E \left\{\int_{-\infty}^{\infty} e^{-2\pi jvy} \sum_{-\frac{N-1}{2}}^{\frac{N-1}{2}} \delta(y - n\ell)e^{-2\pi jn\alpha_Y}\,dy\right\}$$

$$\left\{\int_{-\infty}^{\infty} P_D(x)e^{-2\pi jx}\left[u - (f_{if} + f_d)\frac{T_i M}{D}\right]\right\}$$

$$\left\{\sum_{-\frac{M-1}{2}}^{\frac{M-1}{2}} P_{D/M}(x - m\frac{D}{M})e^{-2\pi jm(\alpha_X + T_i(f_{if} + f_d))}\right\}$$

$$+ \mu E \left\{\int_{-\infty}^{\infty} e^{-2\pi jvy} \sum_{-\frac{N-1}{2}}^{\frac{N-1}{2}} \delta(y - n\ell)e^{2\pi jn\alpha_Y}\,dy\right\}$$

$$\left\{\int_{-\infty}^{\infty} P_D(x)e^{-2\pi jx}\left[u + (f_{if} + f_d)\frac{T_i M}{D}\right]\right\}$$

$$\left\{\sum_{-\frac{M-1}{2}}^{\frac{M-1}{2}} P_{D/M}(x - m\frac{D}{M}) \sum_{-\frac{N-1}{2}}^{\frac{N-1}{2}} \delta(y - n\ell)e^{-2\pi jn\alpha_Y}\,dy\right\}$$

Expression which reduces to

$$F(u,v) = K_o \frac{\sin N\pi\ell v}{\sin\pi\ell v}\frac{\sin\pi Du}{\pi Du} +$$

$$+ K_1 \frac{\sin\pi N(\alpha_X + \ell v)}{\sin\pi(\alpha_X + \ell v)} \frac{\sin\pi\frac{D}{M}(u - \frac{1}{\lambda_X})}{\pi\frac{D}{M}(u - \frac{1}{\lambda_X})} \frac{\sin M\pi[\alpha_X + \frac{D}{M}u]}{\sin\pi[\alpha_X + \frac{D}{M}u]}$$

$$+ K_1 \frac{\sin\pi N(\alpha_X - \ell v)}{\sin\pi(\alpha_X - \ell v)} \frac{\sin\pi\frac{D}{M}(u + \frac{1}{\lambda_x})}{\pi\frac{D}{M}(u + \frac{1}{\lambda_x})} \frac{\sin M\pi[\alpha_X - \frac{D}{M} u]}{\sin\pi[\alpha_X - \frac{D}{M} u]}$$

where

$$\lambda_x = \frac{D}{MT_i} \frac{1}{(f_{if} + f_d)}$$

The second term in F(u,v) corresponds to the first order positive fringe of interest. This distribution is shown in Fig. 4.2.3

It can be seen that this term corresponds to the antenna pattern in the v direction, with grating lobes occuring at

$$v_1 = - \frac{\alpha_Y}{\ell} + \frac{n}{\ell}, \quad n = 0, \pm 1, \pm 2, \ldots$$

In the u direction, two terms in u appear. The term $\frac{\sin\pi\frac{D}{M}(u - \frac{1}{\lambda_x})}{\pi\frac{D}{M}(u - \frac{1}{\lambda_x})}$ corresponds to the Fourier transform of the input cell in the x direction, is non-repetitive, presents a maximum at $u = \frac{1}{\lambda_x}$ and varies smoothly over its half power width which is given by $\Delta u = \frac{M}{D}$. The term $\frac{\sin M\pi[\alpha_X + \frac{D}{M}u]}{\sin\pi[\alpha_X + \frac{D}{M}u]}$ corresponds to the antenna pattern on the x direction, is repetitive and presents main grating lobes spaced at values of u given by

$$u_m = - \frac{M}{D} \alpha_X + \frac{M}{D} m, \quad m = 0, \pm 1, \pm 2, \ldots$$

It can be seen that there are N resolvable beams in the v direction and M in the u direction. The angular information corresponding to $\theta_Y$ can be extracted from the position of the zero order grating lobe in the v direction

$$v_1 = - \frac{\alpha_Y}{\ell}$$

$$\therefore \text{thus } \sin\theta_Y = \frac{\alpha_Y \lambda_c}{\Delta Y} = - \frac{\ell\lambda_c}{\Delta Y} v_1$$

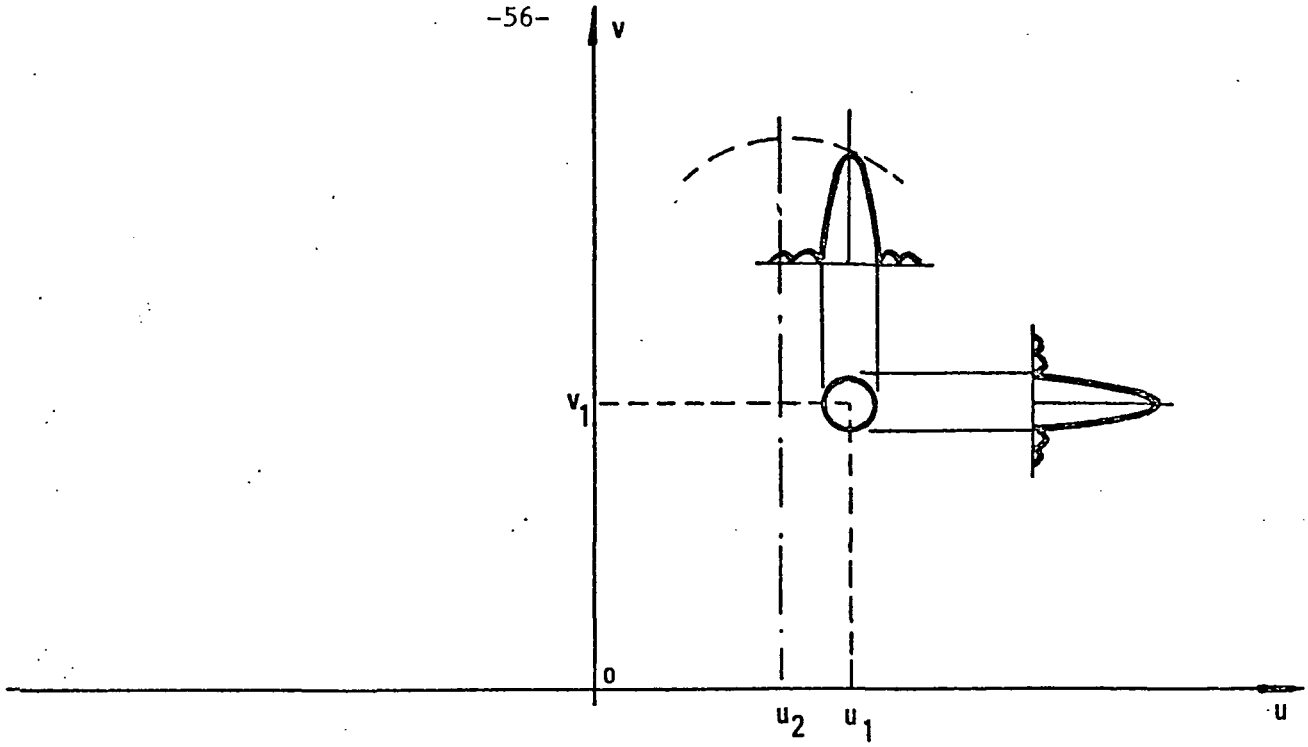


Fig. 4.2.3 Output Plane Pattern for the Full Array Input Format of Fig. 4.2.2

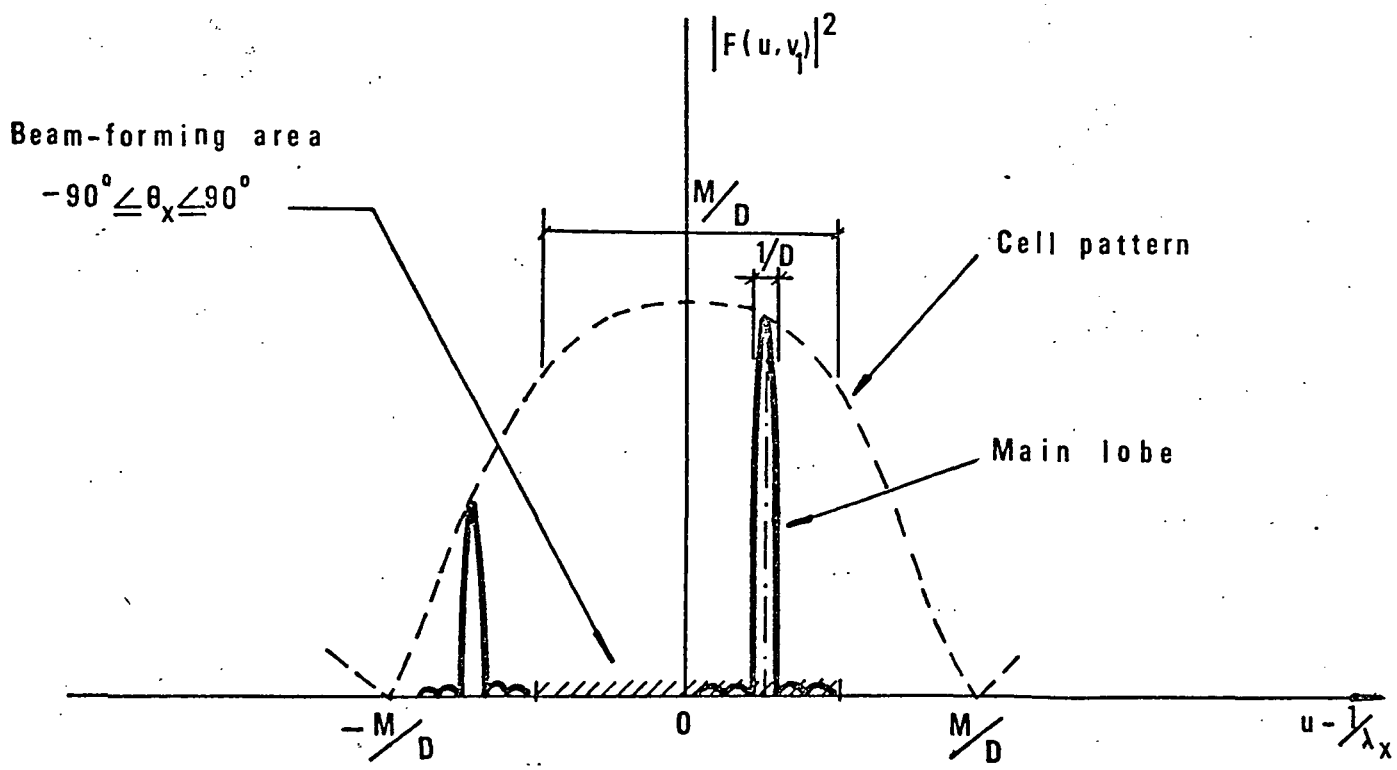


Fig. 4.2.4 Cross-section of the Output Pattern across $v=v_1$ showing the cell pattern and the sampling term.

To obtain the information corresponding to $\theta_X$ we observe that the zero order grating lobe of the sampling term in the u direction should fall inside the 3 dB width of the term corresponding to the input cell, for all values of $\theta_X$ of interest. This can be achieved by selecting $f_{if}T_i$ to be an integer $n_i$. The position of the $n_i$th order grating lobe of the sampling term now occurs at

$$u_1 = (n_i - \alpha_X)\frac{M}{D}$$

and the maximum of the cell term occurs at

$$u_2 = \frac{1}{\lambda_x} = \frac{M}{D} f_{if}T_i = n_i \frac{M}{D}$$

Figure 4.2.4 shows these peaks in an output plane cross-section
The angular data corresponding to $\theta_X$ is thus contained in the position of $n_i$th order grating lobe of the sampling term

$$u_i = (f_{if}T_i - \alpha_X)\frac{M}{D}$$

from which

$$\sin\theta_X = \frac{\alpha_X \lambda_c}{\Delta X} = -\frac{\frac{D}{M}(u_1 - f_{if}T_i)\lambda_c}{\Delta X}$$

It has been shown that the optical processor with the input format described functions as the ideal processor for two-dimensional phased array, presenting a resolution of M cells in the u direction (corresponding to $\theta_X$) and N cells in the v direction (corresponding to $\theta_Y$), in accordance with the Rayleigh resolution criterion. However the input plane requirements are very severe, independently of real time operation for the full array format to be implemented with the current crystal resolution. Indeed, $N \simeq 100$ lines across the vertical dimension are easily accomodated; in the horizontal direction, however we must accommodate $M \simeq 100$ time

histories. For $f_{if}$ = 5 MHz and $T_p$ = 1 μsec, this corresponds roughly to the full crystal resolution, using only two signal samples per cycle and we recall that we must also maintain the relative phase of each cell accurate to one part in N.

Real time processing of the full array would always require at least M x N delay lines, amplifiers and heterodyners.

Even with the low degree of feasibility of this format, its study is of interest because modifications of it will lead to a far more feasible input format.

## 4.3 Thinned Array Processing

### 4.3.1 Input Format

The input resolution requirements for a full array processing can be relaxed by processing only the returns corresponding to some of the array elements, that is, by taking a thinned array. Again in this case the time histories of various detector elements are recorded in separate channels along the crystal. However, only one element in each row and column of the receiving array is considered, i.e., a total of N elements assuming a square planar array of N x N elements. Fig. 4.3.1 shows the thinned array geommetry.

In the input plane format, the y coordinate of each channel, $y_i^g$, is directly proportional to the $Y_i^g$ geometrical displacement of the ith sensor from the center of the array. Similarly, the center of the ith received waveform is displaced by an amount $x_i^g$ from the optic axis corresponding to the $X_i^g$ displacement of the sensor from the center of the array. Figure 4.3.2 shows this input format. With the appropriate scaling, time and x displacements are comparable. If we represent a length D of crystal as a

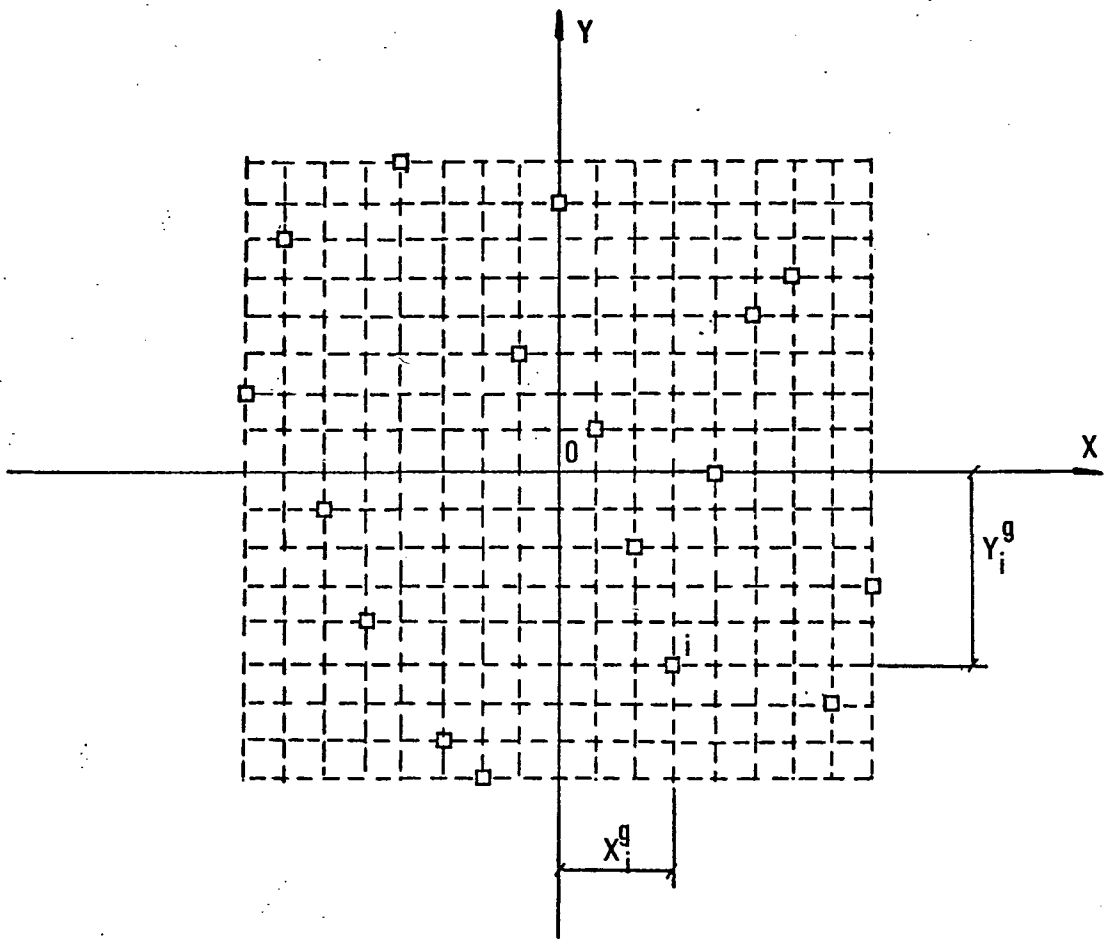


Fig. 4.3.1 Sampling and Notation for the Thinned Array Input Format

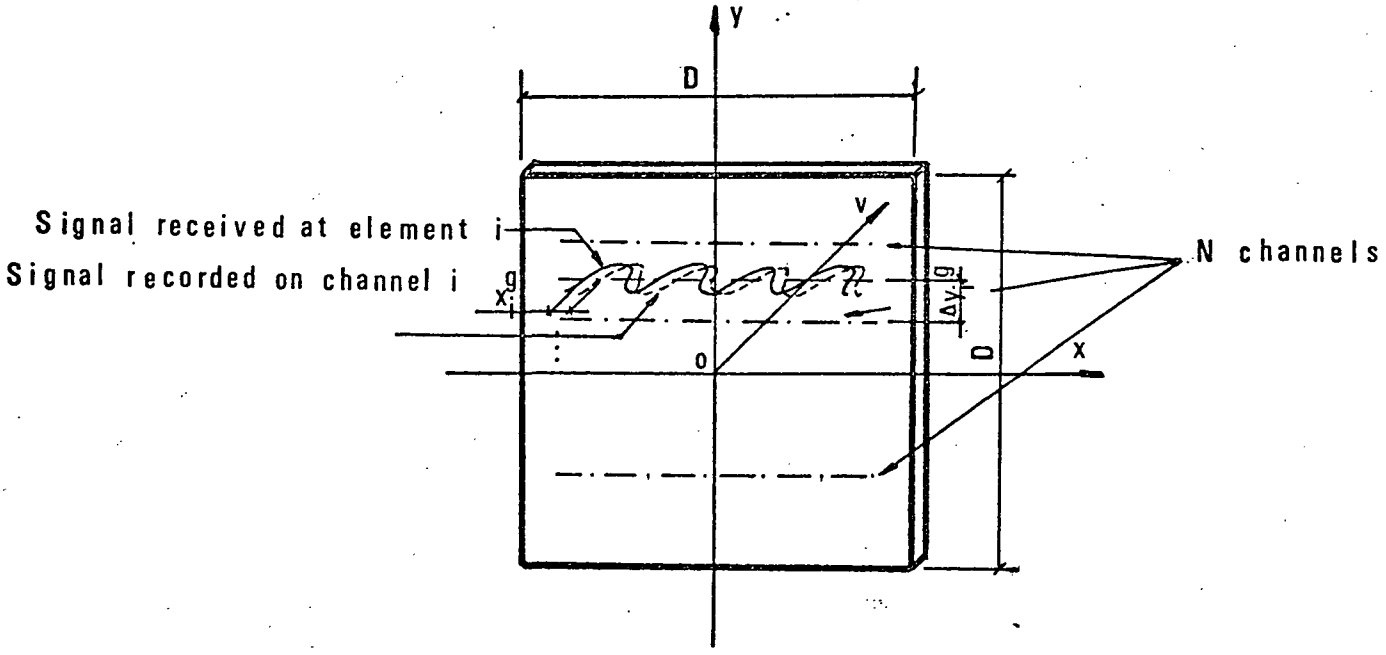


Fig. 4.3.2 Input Format for a Thinned Array Planar Phased Array Processor

time T, time and displacement in the input plane are compatible and for the spatial signal the relations are

$$t = x\frac{T}{D} \; ; \; x = \frac{D}{T}t$$

To avoid retaining additional unnecessary terms in the computation, the complex signal $V_i(t)$ corresponding to the real signal $v_i(t)$ is considered. This will result in fewer terms in the output plane which correspond exactly to the terms of interest to determine angular information. The complex form of the received signal at element i of the receiver array prior to heterodyning is

$$V_i(t) = s_{T_p}(t - \tau_i)\exp[2\pi j(f_c + f_d)t - 2\pi j(f_c + f_d)\tau_i]$$

where $s_{T_p}(t)$ is the signal envelope, assumed of temporal duration $T_p$ (Requirements on s(t) will be considered later. After heterodyning and assuming $\tau_i << T_p$,

$$V_i(t) \simeq s_{T_p}(t)\exp[2\pi j(f_{if} + f_d)t - 2\pi j(f_c + f_d)\tau_i]$$

The spatial signal is given by

$$V_i(x) = s_{X_p}(x)\exp[2\pi j(f_{if} + f_d)\frac{T}{D}x - 2\pi j(f_c + f_d)\tau_i]$$

where $X_p = \frac{D}{T}T_p$. Figure 4.3.2 shows this input format. The time delay $\tau_i$ for element i, of geommetrical coordinates $X_i^g, Y_i^g$ in the real array is

$$\tau_i = \frac{d_i}{c} = \frac{X_i^g\cos\phi_X + Y_i^g\cos\phi_Y}{c} = x_i^g\frac{k_x\sin\theta_X}{c} + y_i^g\frac{k_y\sin\theta_Y}{c}$$

where $\phi_X$, $\phi_Y$, $\theta_X$ and $\theta_Y$ were defined in paragraph 4.2 and

$k_x = \frac{X_i^g}{x_i^g}$ and $k_y = \frac{Y_i^g}{y_i^g}$ are scaling factors which relate the geometries of the receiving array and the input plane. $V_i$ can thus be written as

$$V_i(x) = s_{X_p}(x)\exp[2\pi j f'_{if} x - 2\pi j f_c (x_i^g \frac{k_x \sin\theta_X}{C} + y_i^g \frac{k_y \sin\theta_Y}{C})]$$

where we have assumed

$$f_c >> f_{if} >> f_d$$

and where

$$f'_{if} = f_{if}\frac{T}{D} \simeq (f_{if} + f_d)\frac{T}{D}$$

After being delayed by an amount $x_i^g$ corresponding to its coordinate $X_i^g$ on the array such that

$$x_i^g = \frac{X_i^g}{k_x}$$

the form of the signal written on the crystal for the ith element is

$$V_i(x) = s_{X_p}(x - x_i^g)\exp[2\pi j f'_{if}(x - x_i^g) - 2\pi j(\alpha_x x_i^g + \alpha_y y_i^g)]$$

where

$$\alpha_x = \frac{f_c k_x \sin\theta_X}{c} = \frac{k_x \sin\theta_X}{\lambda_c}$$

$$\alpha_y = \frac{f_c k_y \sin\theta_Y}{c} = \frac{k_y \sin\theta_Y}{\lambda_c}$$

The optical transmission function will again be of the form

$$T(x,y) = E \sum_{i=-\frac{N-1}{2}}^{\frac{N-1}{2}} [1 + \mu V_i(x)]\delta(y - y_i^g)$$

The Fourier transform of this amplitude distribution is taken by the optical system described in Fig. 3.3.1.

The first order fringe of interest in the output plane is given by

$$F_1(u,v) = E \int_{-\infty}^{\infty}\int_{-\infty}^{\infty} \sum_{i=-\frac{N-1}{2}}^{\frac{N-1}{2}} \delta(y - y_i^g) e^{2\pi j[f'_{if}(x - x_i^g) - \alpha_x x_i^g - \alpha_y y_i^g]} e^{-2\pi j(ux + vy)} dxdy$$

$$= \mu E \sum_{-\frac{N-1}{2}}^{\frac{N-1}{2}} \{ \int_{-\infty}^{\infty} \delta(y - y_i^g) e^{-2\pi jvy} e^{-2\pi jy_i^g \alpha_y} \}$$

$$\{ \int_{-\infty}^{\infty} s_{X_p}(x - x_i^g) e^{2\pi j[f'_{if}(x - x_i^g) - \alpha_x x_i^g]} e^{-2\pi jxu} dx \} =$$

$$= \mu E \sum_{-\frac{N-1}{2}}^{\frac{N-1}{2}} \{ \int_{-\infty}^{\infty} \delta(y - y_i^g) e^{-2\pi jv(y - y_i^g)} e^{-2\pi jy_i^g(v + \alpha_y)} dy \}$$

$$\{ \int_{-\infty}^{\infty} s_{X_p}(x - x_i^g) e^{2\pi j[f'_{if}(x - x_i^g) - (\alpha_x + u)x_i^g]} e^{-2\pi ju(x - x_i^g)} dx \} =$$

$$= \mu E \sum_{-\frac{N-1}{2}}^{\frac{N-1}{2}} \{ e^{-2\pi jy_1^g(v + \alpha_y)} \} \{ S(u - f'_{if}) e^{-2\pi j(u + \alpha_x)x_i^g} \} =$$

$$= \mu E \sum_{-\frac{N-1}{2}}^{\frac{N-1}{2}} \{ e^{-2\pi jy_i^g(v + \alpha_y)} \} S(w) \{ e^{-2\pi j(w + f'_{if} + \alpha_x)x_i^g} \}$$

$$= \mu E\, S(w) \sum_{-\frac{N-1}{2}}^{\frac{N-1}{2}} e^{-2\pi jy_i^g(v + \alpha_y)} e^{-2\pi jx_i^g(w + f'_{if} + \alpha_x)}$$

where u and v were defined in Chapter 2, and w is given by

$$w = u - f'_{if}$$

and

$$S(w) = \int_{-\infty}^{\infty} s_{X_p}(x) e^{-j2\pi xw} dx$$

is the Fourier transform of the transmitted signal envelope s(t).

The grating lobes of $F_1(u,v)$ occur at points (u,v) in the output plane which satisfy

$$2\pi\{[y_i{}^g(v + \alpha_y)] + [x_i{}^g(w + f'_{if} + \alpha_x)]\} = m2\pi,$$

where m is an integer. The desired angular information ($\theta_X$ and $\theta_Y$) can be obtained by considering those points in the (u,v) plane for which

$$y_i{}^g(v + \alpha_y) = n_i{}^y, \text{ an integer}$$

$$x_i{}^g(w + \alpha_x + f'_{if}) = m_i{}^x, \text{ an integer} \qquad i = -\frac{N-1}{2}, \ldots 0, \ldots \frac{N-1}{2}$$

By choosing $f'_{if} x_i{}^g$ to be an integer for all i, these equations reduce to

$$y_i{}^g(v + \alpha_y) = n_i{}^y$$

$$x_i{}^g(u + \alpha_x) = n_i{}^x \qquad \text{for all i.}$$

The zero order grating lobe is obtained for $n_i{}^y = n_i{}^x = 0$, yielding the coordinates

$$v_1 = -\alpha_y = -\frac{k_y \sin\theta_Y}{\lambda_c}$$

$$u_1 = -\alpha_x = -\frac{k_x \sin\theta_X}{\lambda_c}$$

thus

$$\sin\theta_Y = -\frac{\lambda_c}{k_y} v_1$$

$$\sin\theta_X = -\frac{\lambda_c}{k_x} u_1$$

Two requirements for this processing to be valid are:

1) The half power width of the transmitted signal spectrum S(w) must be large enough to accomodate all possible beams for $\theta_X$ within the beam forming cone.

2) It must be proved that grating lobes of $F_1(w,v)$ occur only at the points for which

$$y_i^g(v + \alpha_y) = n_i^y$$

$$x_i^g(u + \alpha_x) = n_i^x \qquad \text{for all i.}$$

The design parameters must be thus chosen so that both of these conditions are satisfied. It is also a design objective to keep the sidelobe level of $F_1(u,v)$ as near as possible to the sidelobe level corresponding to the full array aperture.

The crystal resolution must now be able to accomodate only $(f_{if} + f_d)T_p$ cycles of IF signal across the x direction, which is a factor of N improvement over the full array requirement.

4.3.2 Choice of Design Parameters

The following parameters are considered

Carrier frequency $f_c$ = 5 GHz

Carrier wavelength $\lambda_c = 6 \times 10^{-2}$ m

Spacing across array elements $\Delta X_i^g = \Delta Y_i^g = L = 3 \times 10^{-2}$ m.

Scaling factors $k_y = k_x = 100$

Intermediate frequency $f_{if} = 3.\overline{333}$ MHz

Transmitted envelope s(t) = 13-bit Barker coded signal with $T_p = 13$ μsec.

Number of array elements = 4900; N = 70

Cone of beam forming $\theta_X \leq 30°$

$\theta_Y \leq 30°$

The following points will prove the feasibility of the processing:

a) $f_{if}$ is large enough so that the quantizing of $x_i^g$ in units of $1/f'_{if}$ leads to negligible errors. Indeed:

$$f'_{if} = f_{if} \frac{T_i}{D} = 3.3 \times 10^6 \times \frac{50 \times 10^{-6}}{5 \times 10^{-2}} = 3.3 \times 10^3$$

$$1/f'_{if} = 3 \times 10^{-4}$$

$$x_{i\,min}^g = \frac{3 \times 10^{-2}}{100} = 3 \times 10^{-4}$$

thus the quantization is exact even for the smallest $x_i^g$.

b) The maximum value of $x_i^g$ is much less than the aperture width of the crystal so that nearly complete waveform stories can be recorded there without significant loss from edge effects.

Indeed, $x_{i\,max}^g = \frac{70 \times 3 \times 10^{-2}}{100} = 2.1 \times 10^{-2}$ m.

With

$$X_p = \frac{D}{T_i} T_p = \frac{5 \times 10^{-2}}{5 \times 10^{-6}} 13 \times 10^{-6} = 1.3 \times 10^{-2} \text{ m.},$$

complete time histories can be recorded on the 5 cm ($5 \times 10^{-2}$ m) crystal aperture.

c) The angular resolution desired in beam forming and the scale factor relating $x_i^g$ and $y_i^g$ to the sensor locations in the array must be chosen so that adjacent beams are not more closely spaced in the

Fourier plane than the diffraction limit allows. The diffraction limit in the system is approximately

$$\frac{1}{D} = \frac{1}{5 \times 10^{-2}} = 20 \text{ m}^{-1}$$

The attainable resolution in beam forming corresponds to the half-power beam width of the main lobe in $F_1(u,v)$ which is

$$\frac{1}{N\Delta x_i^g} = \frac{1}{70 \times 3 \times 10^{-2}/100} = \frac{100}{2.1} \simeq 47 \text{ m}^{-1}$$

The required resolution in $\alpha_X$, $\alpha_Y$ thus exceeds the diffraction limit of the optical system.

d) The spectrum of the transmitted signal must be broad enough to accomodate all beam positions within the beam forming cone for $\theta_X \leq 30°$. For $\theta_X = 30°$, the value of $\alpha_X$ is

$$\alpha_{X\ max} = \frac{100 \times 1/2}{6 \times 10^{-2}} = \frac{10^4}{12} = 830 \text{ m}^{-1}$$

The choice of signal s(t) must take this fact into account as well as simplicity of implementation when simulations in real time must be run. Such conditions are met by envelope coded signals such as Barker coded signals. Plots of the spectrum S(w) for 7, 11 and 13 bit Barker coded signals are shown and the choice was made of the 13 bit coded envelope with a duration of 13 μsec which affords the smoothest variation in the area $|w| \leq 0.8 \times 10^6$ Hz corresponding to 800 $\text{m}^{-1}$. Fig. 4.3.3 shows such plots.

e) The choice of sensor distribution must be done in such a way that ambiguous beams do not appear in the output plane for values of (u,v)

other than those considered in 4.3.1. We shall now prove that such is the case when the choice of sensors over the array (one for each row and column) is randomly performed.

The equations to consider are

$$x_i^{g}(w + \alpha_x) = n_i^{x}$$

$$y_i^{g}(v + \alpha_y) = n_i^{y}$$

For a value $n_i^{x} \neq 0$, for instance, we have

$$x_i^{g}(w + \alpha_x) = n_i^{x}$$

this is $$x_i^{g}w + x_i^{g}\alpha_x = n_i^{x}$$

but since $$x_i^{g}f'_{if} = n_i, \text{ for all } i,$$

we have

$$\frac{n_i}{f'_{if}} w + \frac{n_i}{f'_{if}} \alpha_x = n_i^{x}$$

$$\frac{n_i}{f'_{if}} (w + \alpha_x) = n_i^{x}$$

yielding $w = -\alpha_x + \frac{n_i^{x}}{n_i} f'_{if}$ for the possible maxima of $F_1(w,v)$. Two cases now arise:

I) The ratio of $n_i^{x}$ and $n_i$ depends on i. In this case, the minimum variability in the value of w is given when $n_i^{x} = 1$ and

$$n_i = n_{i\,max} = x_{i\,max}^{g} \times f'_{if} =$$

$$= \frac{1.05}{10^2} \times 3.3 \times 10^3$$

$$= 35$$

thus $\Delta w_{min} = \frac{1}{35} \times 3.3 \times 10^3 = \frac{100}{1.05} = 95\ m^{-1}$

Thus even the smallest variability possible for $\Delta w$ exceeds the output plane resolution of 20 $m^{-1}$ and in-phase contributions from all or even several of the sensors is not possible within a single resolution interval in the Fourier plane.

II) The ratio of $n_i^x$ and $n_i$ is constant and independent of i. In this case, since $x_i^g f'_{if} = n_i$, we have

$$\frac{n_i}{f'_{if}} (w + \alpha_x) = n_i^x$$

which implies

$$\frac{w + \alpha_x}{f'_{if}} = n, \text{ an integer}$$

and thus

$$w = -\alpha_x + nf'_{if}, \quad n = \pm 1, \pm 2....$$

are the positions of the grating lobes other than the zero order lobe (similar reasoning can be applied along the v direction).

With $f'_{if} = 3.\hat{3} \times 10^3 m^{-1}$, no ambiguous grating lobes occur within the beam forming angle of $|\theta| \leq 30°$.

It remains to be proved that no maxima of $F_1(w,v)$ occur for these directions $\frac{v}{w}$ for which

$$y_i^g(v + \alpha_y) + x_i^g(w + \alpha_x) = n_i, \text{ an integer.}$$

In such a case, we have

$$y_i^g(v + \alpha_y) = n_i - x_i^g(w + \alpha_x)$$

$$v + \alpha_y = \frac{n_i}{y_i^g} - \frac{x_i^g}{y_i^g} (w + \alpha_x)$$

this is

$$v = -\alpha_y - \frac{x_i^g}{y_i^g}\alpha_x + \frac{n_i}{y_i^g} - \frac{x_i^g}{y_i^g}w.$$

Three cases arise now:

I) $n_i = 0$

Then the set of straight lines

$$v = -\alpha_y + \frac{n_i}{y_i^g} - \frac{x_i^g}{y_i^g}(w + \alpha_x)$$

reduces to

$$v = -\alpha_y - \frac{x_i^g}{y_i^g}(w + \alpha_x)$$

which, for randomly chosen sensors across the array, this is, $\frac{x_i^g}{y_i^g} = f(i)$, interset only at the point

$$v_1 = -\alpha_y$$

$$w_1 = -\alpha_x$$

thus in phase contributions for all of the array elements are possible only on the zero order lobe.

II) $\frac{n_i}{y_i^g} = R$, constant

Then we have

$$v = -\alpha_y + R - \frac{x_i^g}{y_i^g}(w + \alpha_x)$$

which, for $\frac{x_i^g}{y_i^g} = f(i)$, represents a set of straight lines intersecting at the point

$$w = -\alpha_x$$

$$v = -\alpha_y + R$$

It remains to be proved that R can take on only the values $\pm m\frac{1}{\ell}$ where $\ell = \frac{L}{k_y}$ and $m = \pm 1, \pm 2 \ldots$

and since $y_i^g$ is quantized in units of $\ell$, it turns out that the product $y_i^g \frac{1}{\ell}$ is an integer. $\frac{1}{\ell}$ plays here the role of $f'_{if}$ when ambiguities across the u direction were considered and thus this problem reduces to one already solved.

III) $\frac{n_i}{y_i^g} = R_i$, some function of i.

In this case we have

$$v = -\alpha_y + R_i - \frac{x_i^g}{y_i^g}(\alpha_x + w)$$

which is a set of straight lines that cannot intersect at a single point on the (u,v) plane, what would require $R_i$ to be constant and independent of i in the case of sensors chosen randomly across the array. Thus in phase contributions from all or several sensors is not possible outside the grating lobes formerly considered and the proof is complete. As a conclusion, Fig. 4.3.4 shows the position of the grating lobes for $\theta_X = \theta_Y = 0°$.

4.3.3 Choice of Array Sensors

The criteria to be used for selecting the location of the elements in the thinned array are

1. The resolution in the transform pattern of the entire N x N array should be maintained
2. The sidelobe levels in the transform pattern should be as low as possible.

When $N^2$ elements of the array were used, the optical beam could be steered into $N^2$ resolvable positions. For the thinned array of N elements, in order to avoid the observation of false beam positions, it is necessary to minimize the peak power in lobes other than the main grating lobes. This problem has been the object of much research and up

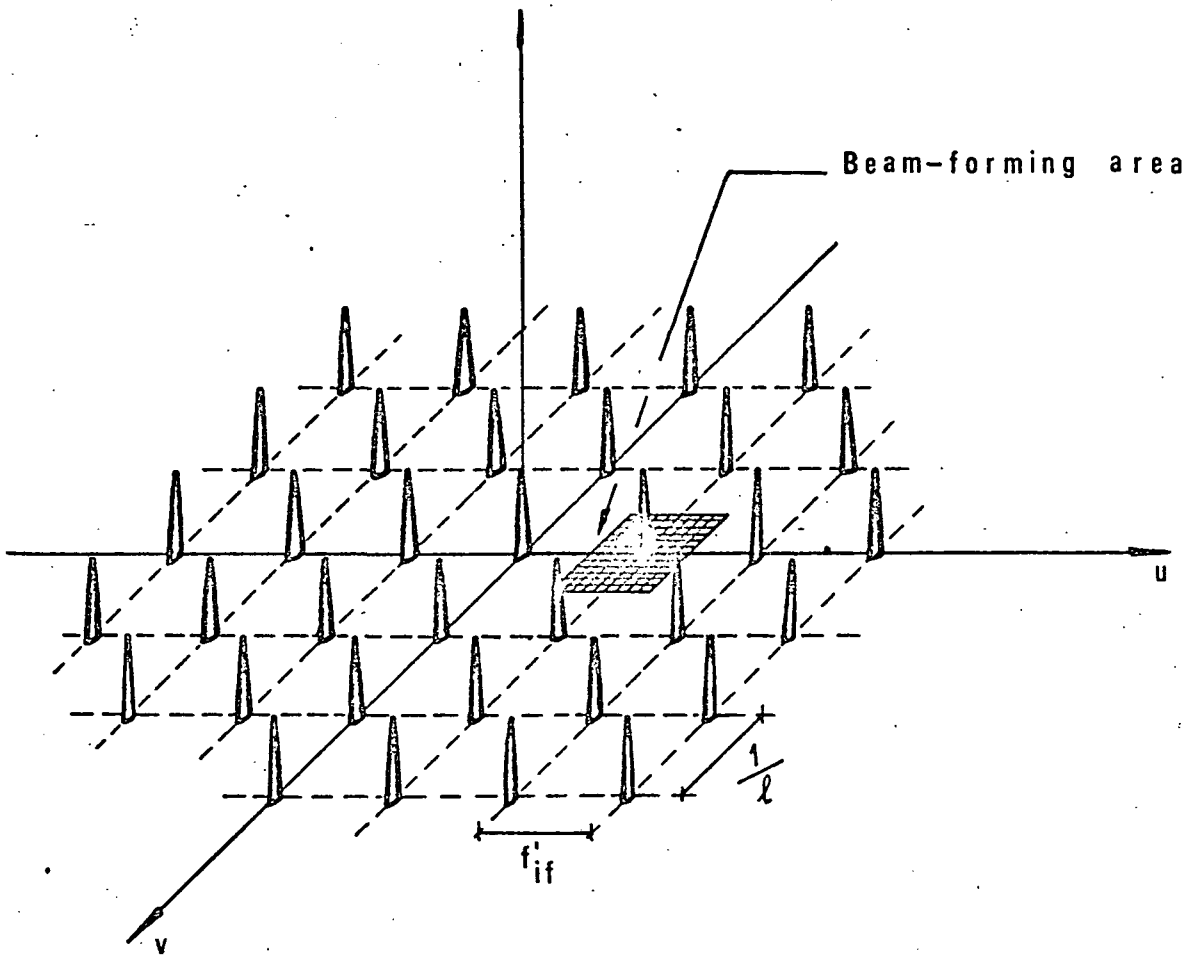


Fig. 4.3.4 Output pattern corresponding to thinned array processing showing the grating lobes and beam-forming area.

to date no better approach to solve the problem is known than a pseudo-random choice of the elements across the array (as proved by intensive computer research of this specific thinned array pattern by A.P.L, Reference 8 ) . Such pseudorandom choices have been proven to yield sidelobe levels 10 dB down from the main lobe peak power against the 13 dB attainable for the full array beam. (Ref. 8, 10, 11)

A computer program has been written that automatically selects the elements in a planar array in a pseudorandom mode so that several configurations can be evaluated and the best pattern orientation chosen.

# CHAPTER 5

# COMPUTER INTERFACE

## 5.0 Introduction

One of the major accomplishments in the project is the completion of the computer interface. This provides the connecting link from the optical processor to a digital computer. The resultant hybrid processor was first proposed in April 1972 at the Optical Computing Symposium in Darien, Conn. It extends the versatility and processing power of the system further beyond those of other optical computers. It enables one to utilize the optical processor for those operations for which it is best suited and the digital computer for those areas in which it performs best.

The interface is constructed from modular computer functional blocks, known as Register Transfer Modules, RTMs that were designed here at CMU. Reference 12 provides some of the design details of these computer modules. The forthcoming Sept. , 1973 issue of IEEE trans.on Computers contains a brief description of this interface, Ref. 6. A complete description of the work is one of the many papers that must be written this summer and submitted for publication.

The modules used were loaned from ARPA funds and should at some point be purchased. The PDP-11 to which the system is interfaced is also shared with the RTM program in the department. If free money ever appears, we should purchase our own since its workload increases monthly and we could move much faster with our own unit.

## 5.1 OUTPUT INTERFACE

An extensive discussion of this optical-digital interface is included, as it appears to offer considerable interest. The interface essentially digitizes each TV frame into a number of cells or picture elements, 4 x 4 to 128 x 128 cells at a rate of 33 frames/sec (standard TV rates). The intensity of each cell will be either a 1 or a 0. This decision being determined by whether the light intensity within each cell exceeds some programable threshold level. The resolution of each frame is under computer control. The prime use of the system is in locating points of light in the output correlation plane of a real time optical processor, this search being done automatically without the need for human intervention. Figure 5.1.1. illustrates sample results of this digitization process.

The block diagram of Fig. 5.1.2 shows the system with the interface enclosed by the dashed lines. A vidicon will be continually scanning the output correlation plane, and its composite output signal fed to a sync separator. For timing reasons, scanning the output correlation plane, and its vidicon is driven by an external sync generator central to the entire optical data processing system. The TV signal then enters the video thresholder which digitizes each horizontal scan line, according to programmed horizontal resolution information. Timing for the thresholder is provided by horizontal and vertical blanking pulses from the sync separator.

This data is then buffered and transferred to the digitized frame generator which, according to vertical resolution information, combines data from successive horizontal lines to form the final picture cells. The contents of these picture cells are then transferred to a PDP-11 which can analyze and display the data, and, conceivably control the entire optical process.

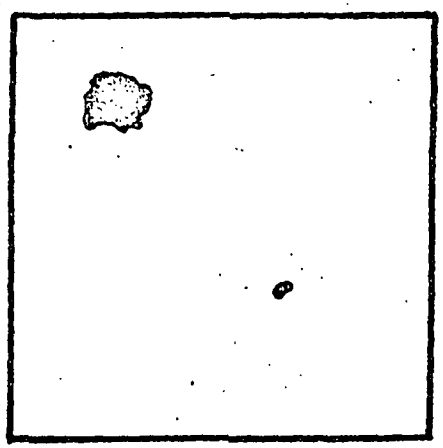

correlation output plane (contrast reversed- actually white on black).

| | | | |
|---|---|---|---|
| 1 | 1 | 0 | 0 |
| 1 | 1 | 0 | 0 |
| 0 | 0 | 1 | 0 |
| 0 | 0 | 0 | 0 |

digitized frame (4 x 4)

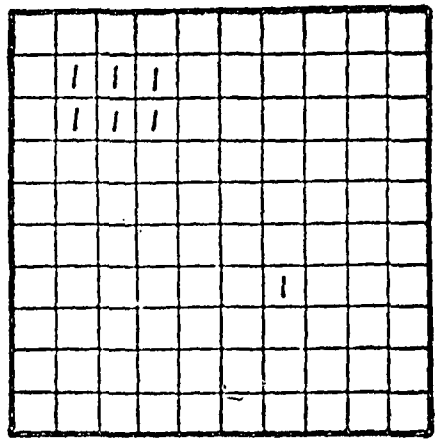

digitized frame (10 x 10)

Fig. 5.1.1 Illustration of TV frame digitizing process.

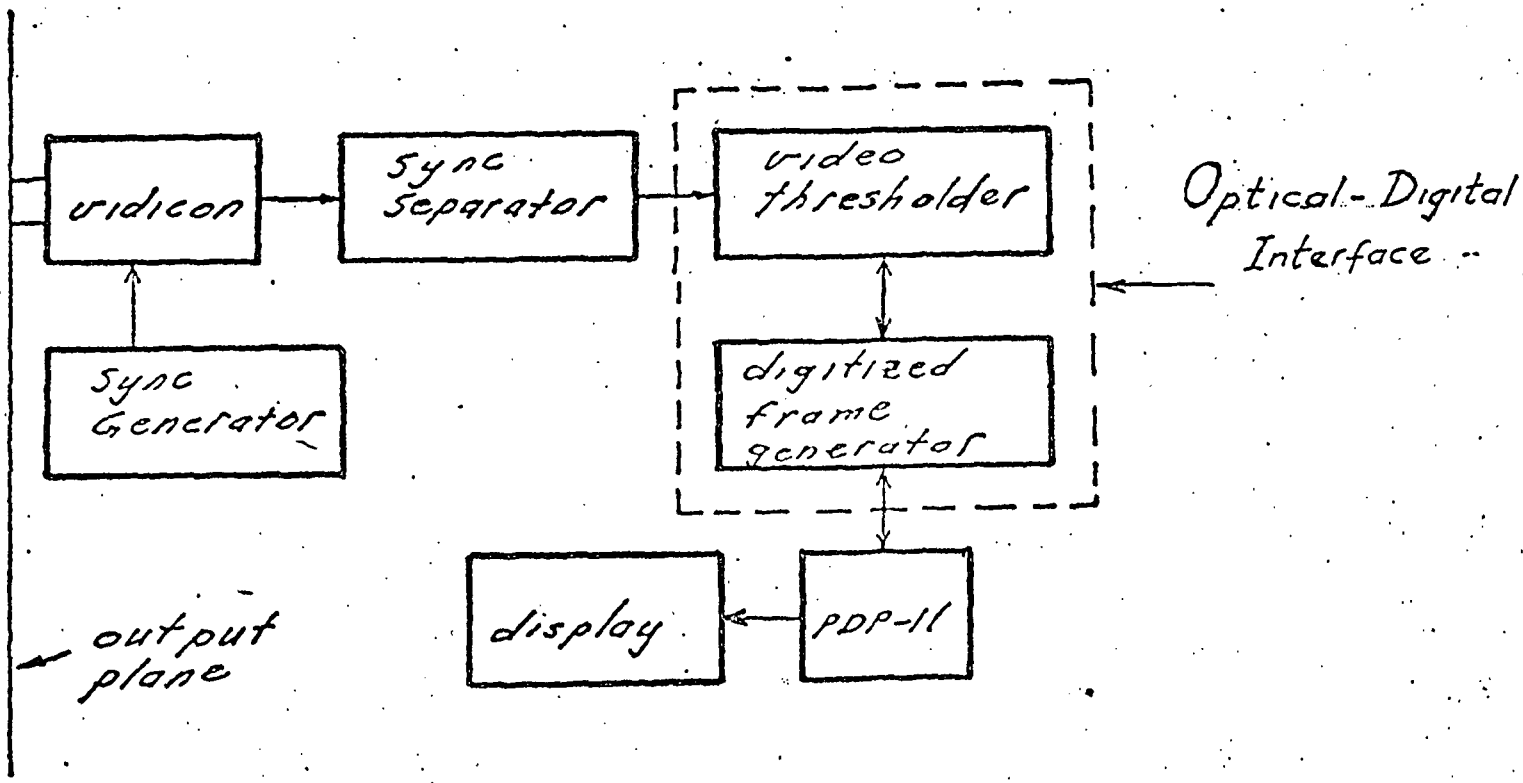


Fig. 5:1.2 Block diagram of system for processing information in an optical correlation output plane.

## 5.2 VIDEO THRESHOLDER

A block diagram of the thresholder is shown in Fig. 5.2.1 A portion of the horizontal scan line ($\tau_c$ seconds) is examined. This corresponds to one cell size. If the voltage level of the signal (corresponding to light intensity) exceeds the threshold $v_T$ during the time, a 1 is placed in the shift register shown. After 16 $\tau_c$ portions of the line have been examined, or the end of the horizontal line has been reached one 16-bit data word is transferred to the digitized frame generator.

The time $\tau_c$ is determined by the value of the frequency control word from the PDP-11. The threshold voltage is manually variable at present but a simple modification can place this under computer control also.

The horizontal and vertical blanking pulses reset all counters in the thresholder, and phase lock its master clock. The DATAIN flag shown in Fig. 5.2.1 is set to 1 whenever a data word is ready for transfer to the frame generator. DATAIN is reset to 0 by the frame generator upon receipt of the transferred data word. Only 15 TTL packages are required to implement this thresholder.

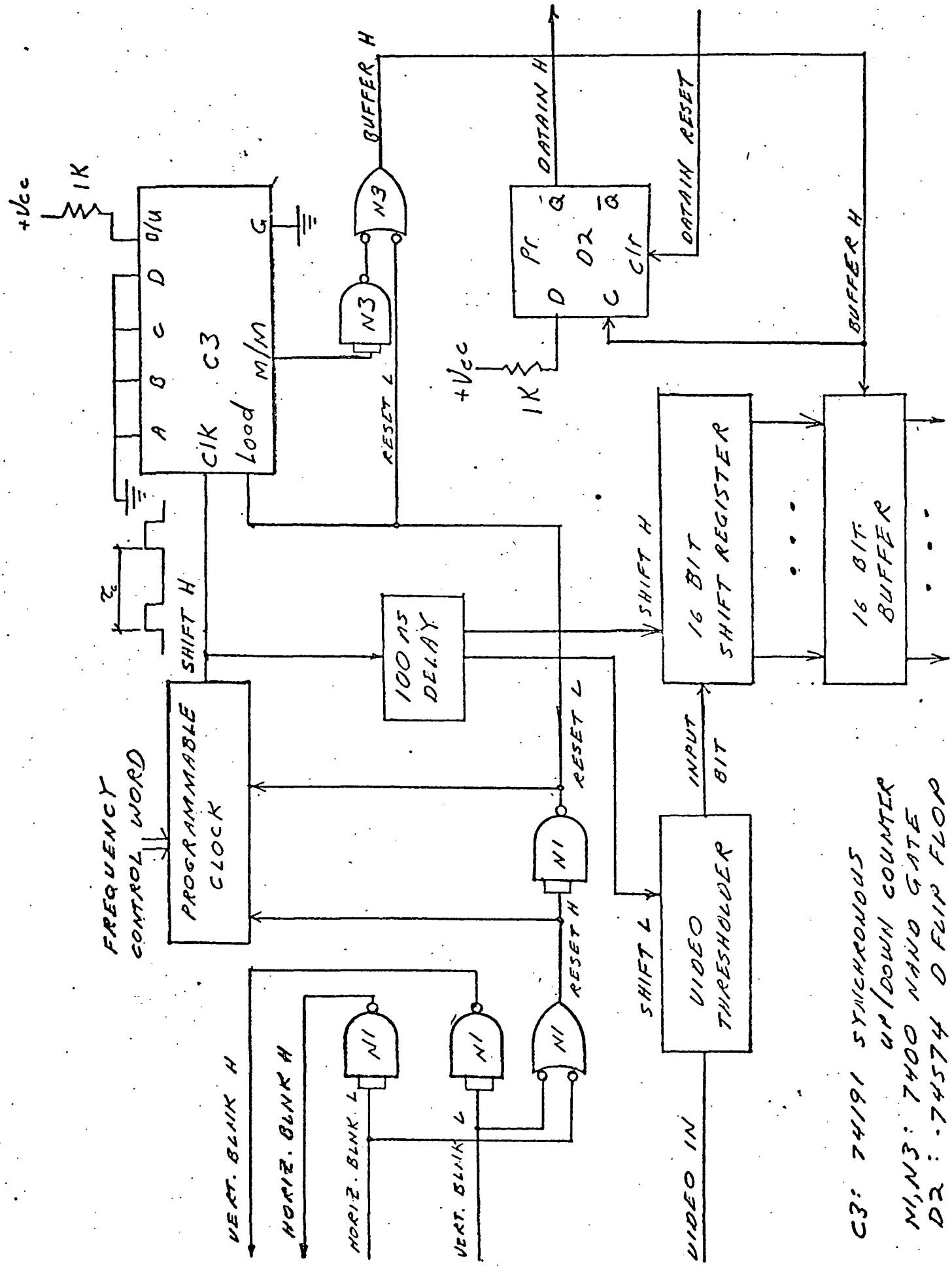


Figure 5.2.1 Diagram of Vidicon Interface

## 5.3 DIGITIZED FRAME GENERATOR

The digitized frame generator shown in Fig. 5.3.1 forms the final digital picture cells by combining data from successive horizontal scan lines as shown. Although 1 TV frame is made up of 2 fields (2:1 interlace) only 1 field is needed in this process since the field resolution is only 250 lines.

The control flow of the frame generator is shown in Fig. 5.3.2. Before entering the main control loop all resolution information is loaded from the PDP-11, and all counters are initialized. Within the control loop the generator processes

1. Data words from the video thresholder, forming the picture elements.
2. Control words from the PDP-11, and
3. All counters and flags during the horizontal blanking pulse.

The frame generator is constructed exclusively from Register Transfer Modules (RTMs). These modules allow hardware to be designed at the register transfer level; that is, the level at which data words (16 bits) are transferred between storage locations and operated upon. Table 1 lists the RTM data modules used to construct the frame generator. It also serves to define all registers and flags. Figure 5.3.3 shows the RTM implementation of the main control flow in Figure 5.3.2. Although Figure 5.3.3 resembles a software flowchart it has, in fact, been directly implemented in hardware via backplane wiring between the various RTM modules.

To provide some tutorial background on RTMs, the three types of modules used in RTM implementations are listed below with brief functional descriptions.

| | | | |
|---|---|---|---|
| Lights and Switches | | | displays bus transfers |
| Bus Control | reg: | BSR | controls bus use. |
| General Purpose Arithmetic Unit | reg: | A,B | performs arithmetic operations |
| 16 word scratch-pad memory | reg: | IN | picture element pointer |
| | | LINTOT | horizontal line counter |
| | | LINE | picture element line counter |
| | | LINEMAX | number of lines in picture element. |
| 1K scratch pad memory | reg: | MA | memory address |
| | | MB | memory buffer |
| 4 word read only memory | reg: | MASK | masks PDP-11 control word |
| | | $240_{10}$ | number of horizontal scan lines in 1 video field. |
| Boolean Flag Modules | flag: | inflag | PDP-11 control word ready |
| | | outflag | output word for PDP-11 ready |
| | | firstline | horizontal line is 1st line of picture element |
| | | start | starts/stops digitized frame generator. |
| | | skipline | set to skip 1st line of video field. |
| | | lastline | horizontal line is last line of picture element. |
| | | firstframe | used to skip every other video field. |
| | | linedone | disables counter updates during horizontal blank time. |
| Interface 1 | reg: | INREG1 | input from PDP-11 |
| | | OUTREG1 | output to PDP-11 |
| Interface 2 | reg: | INREG2 | input from video thresholder |
| | | OUTREG2 | output to video thresholder |
| Video Thresholder | flag: | SAMPLE | data word ready |
| | | NEWFRAME | positive vertical blanking pulse |
| | | NEWLINE | positive horizontal blanking pulse. |

**Table 1.** RTM Modules for Digitized Frame Generator.

1. Control modules - these evoke data operations in their proper sequence, and select paths through diverging control sequences on the basis of boolean flags.
2. Data modules - these perform typical data operations (addition, shifting, boolean logic) on data words.
3. Memory modules - these are used for data word storage.

As a further illustration of the RTM concept, the details of the Kmacro (SAMPLE) operation are shown in Fig.5.3.4.This portion of the control flow is executed when a data word from the video thresholder buffer is to be processed. The work is OR'ed with data from previous horizontal scan lines to form the picture cells.

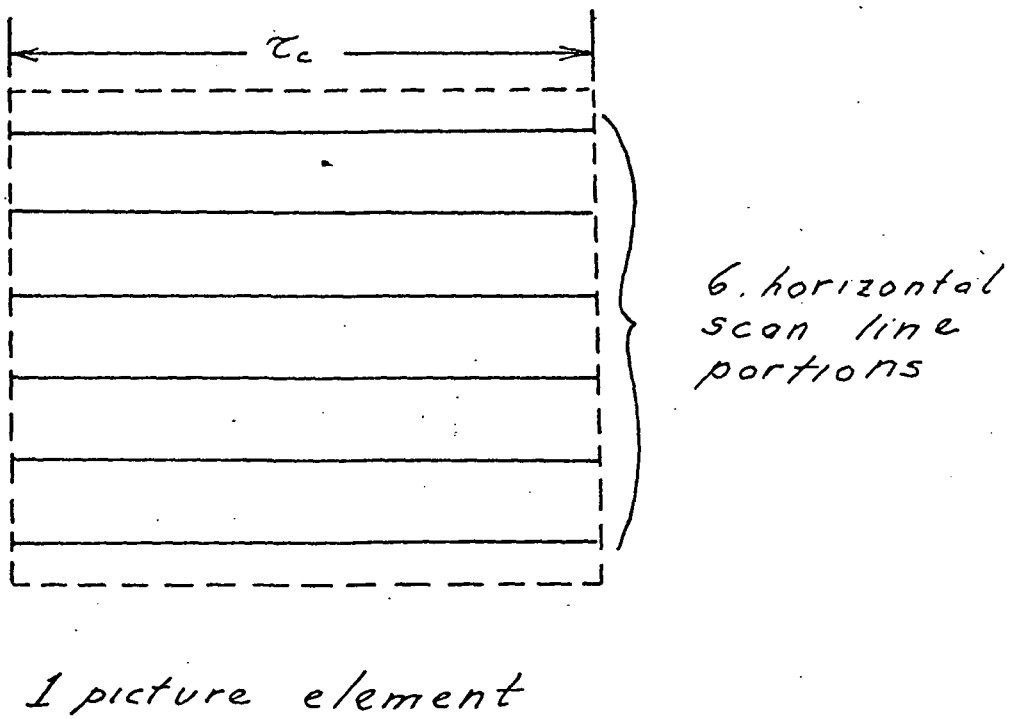


Fig. 5.3.1 Composition of 1 picture element.

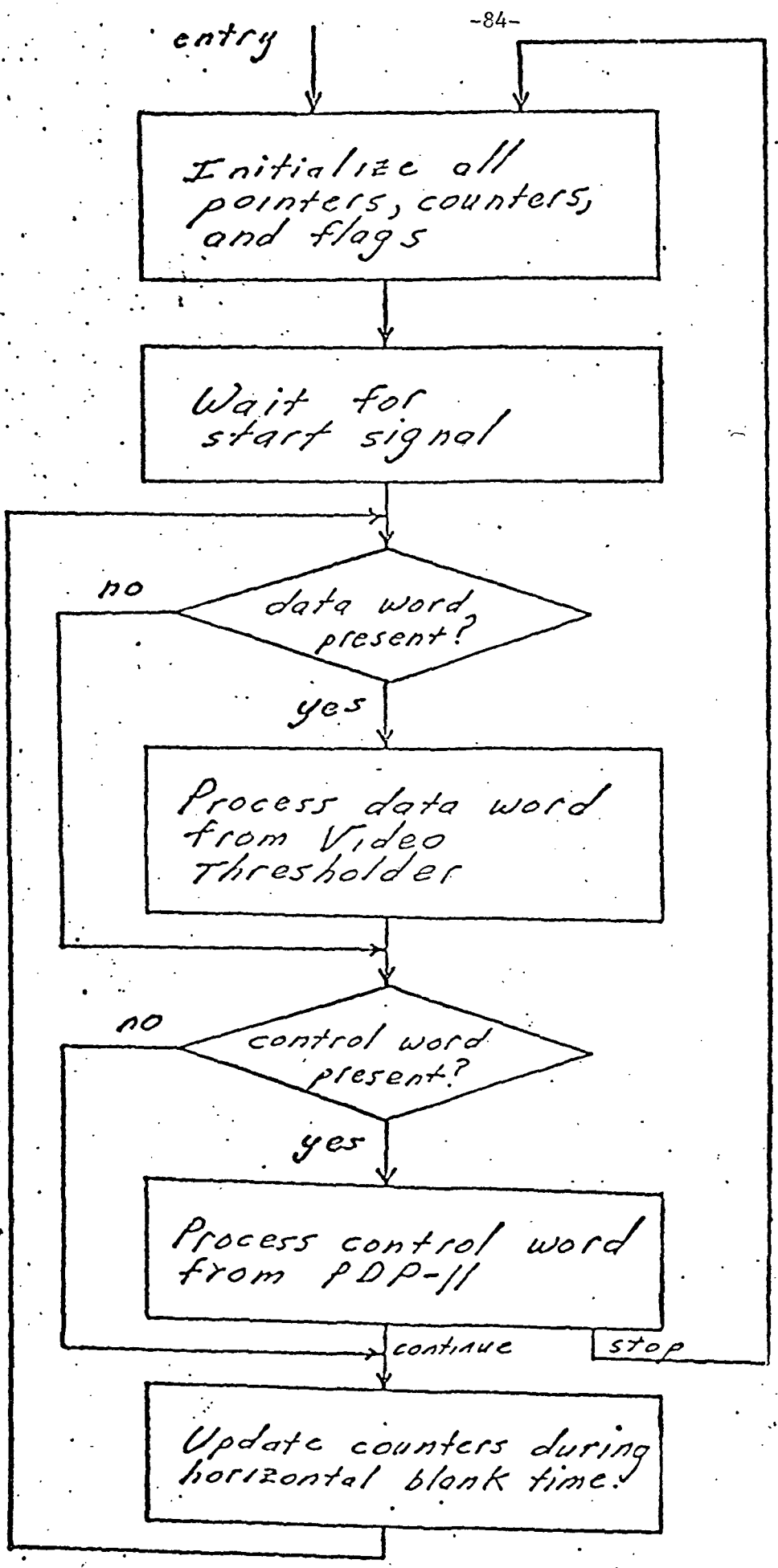


Fig.5:3.2 General control flow of digitized frame generator.

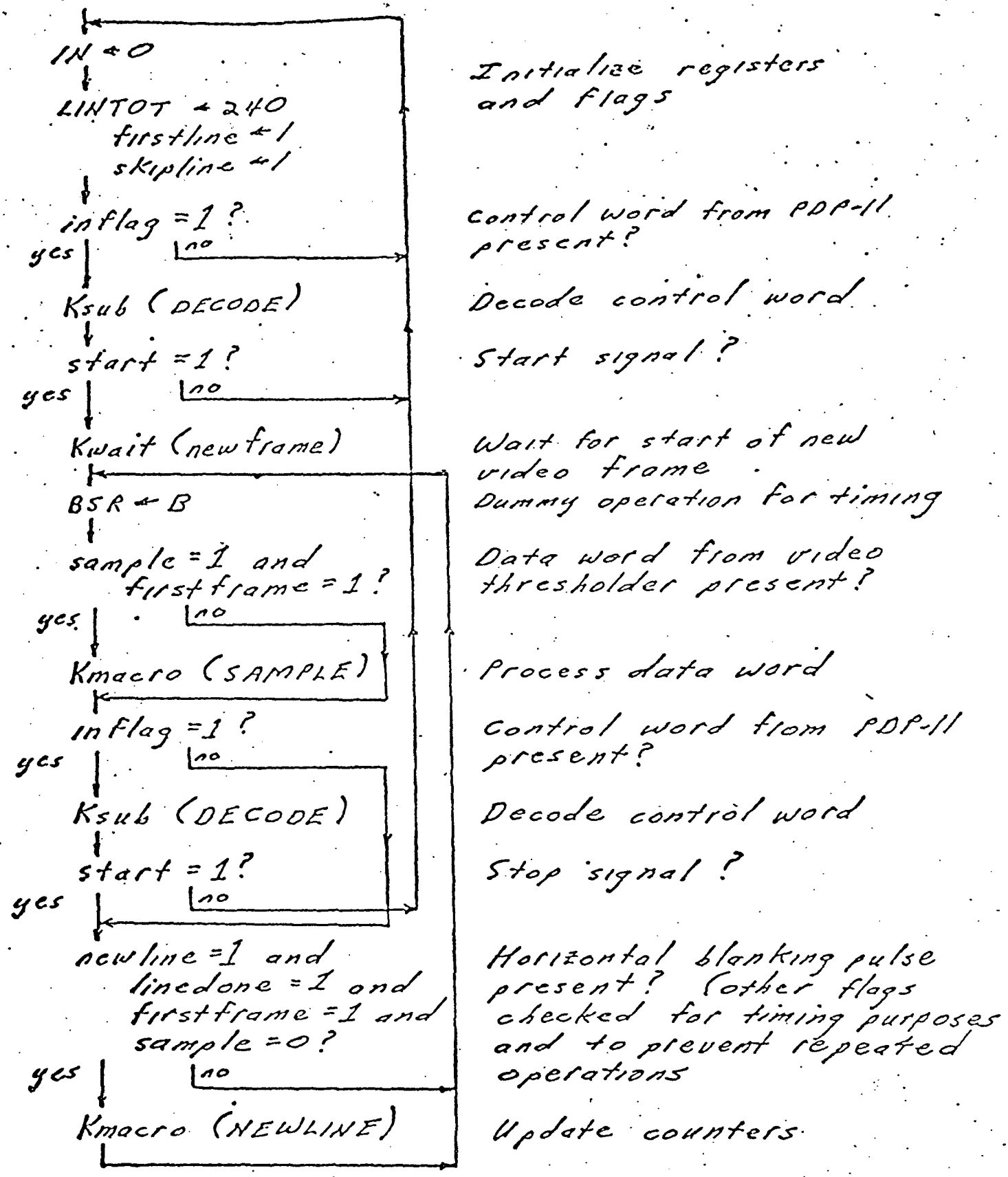


Fig. 5.3.3 RTM flowchart for main control of digitized frame generator.

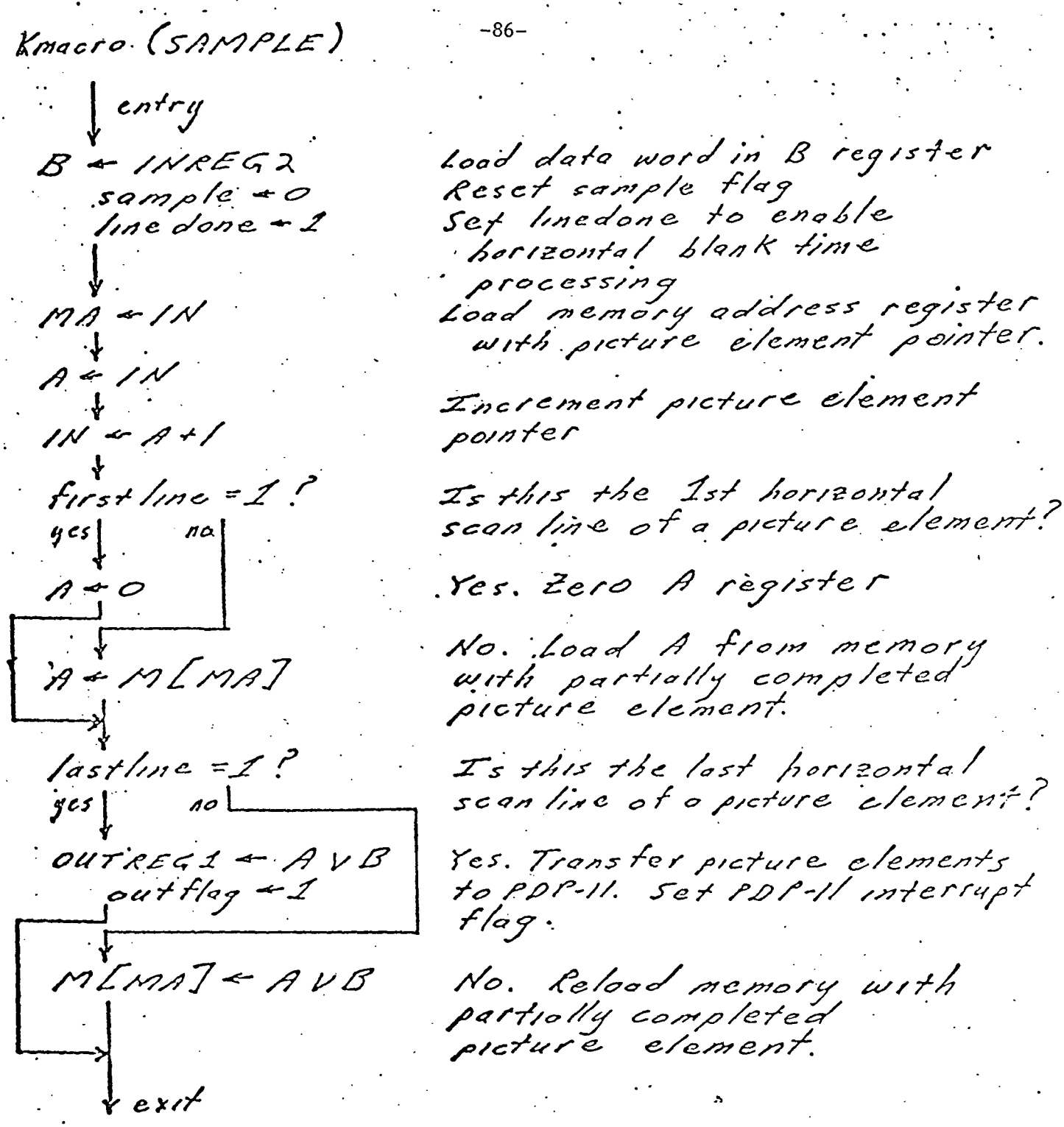


Fig. 5.3.4 RTM flowchart for Kmacro (SAMPLE).

## 5.4 PDP-11 PROCESSING

The PDP-11 minicomputer must be able to accept the picture cells from the digitized frame generator, search them for 1s (points of light) and record the location of these light intensity peaks. This data can be displayed directly on a teletype or graphics display terminal or in some statistical fashion. Eventually the PDP-11 will be used as a real-time controller for the optical system, with direct control of the input image, spatial filter, and digitized frame generator.

# CHAPTER 6

# EXPERIMENTAL RESULTS

## 6.0 Introduction

As has been pointed out earlier in this report, no real-time data from phased array antennas was made available to us for a variety of reasons. It was thus reluctantly decided to simulate the phased array data. To this end a special purpose function generator was constructed to produce simulated input plane patterns. This section describes the simulator and provides documentation on the real-time processing of radar data using the Pockels tube input modulator (Chapter 1), the input formats described (Chapters 3 and 4) and the computer interface (Chapter 5).

## 6.1 Linear Phased Array Simulator

We recall from paragraph 3.3 that the returned signal at the nth element of a linear array, after heterodyning, has the form

$$v_{in}(\tilde{t}) = P_{T_p}(\tilde{t}) \cos\left[2\pi(f_{if} + f_d)\,\tilde{t} - 2\pi n\alpha\right]$$

where the time origin t = o is taken at $T_R = 2\ R/C$, the round trip to the target, $f_{if}$ is the intermediate frequency of heterodyning, $f_d$ is the Doppler frequency shift, and $\alpha = \frac{d}{\lambda_c} \sin\theta$ is the differential delay per element in cycles of $f_c$ (carrier frequency) and d is the uniform spacing of the array elements, $\lambda_c$ is the RF carrier wavelength, $\theta$ is the target angle from ore-sight and $T_p$ is the pulse duration.

The radar simulator produces these waveforms as a train of square pulses at a frequency $(f_{if} + f_d)$ with a total duration $T_p$ and a linear phase shift per line. $T_p$ is adjustable in the range 0 to 50 $\mu$sec, while the frequency of the pulse train can vary from 20 KHz to 10 MHz. The radar simulator is phase-locked

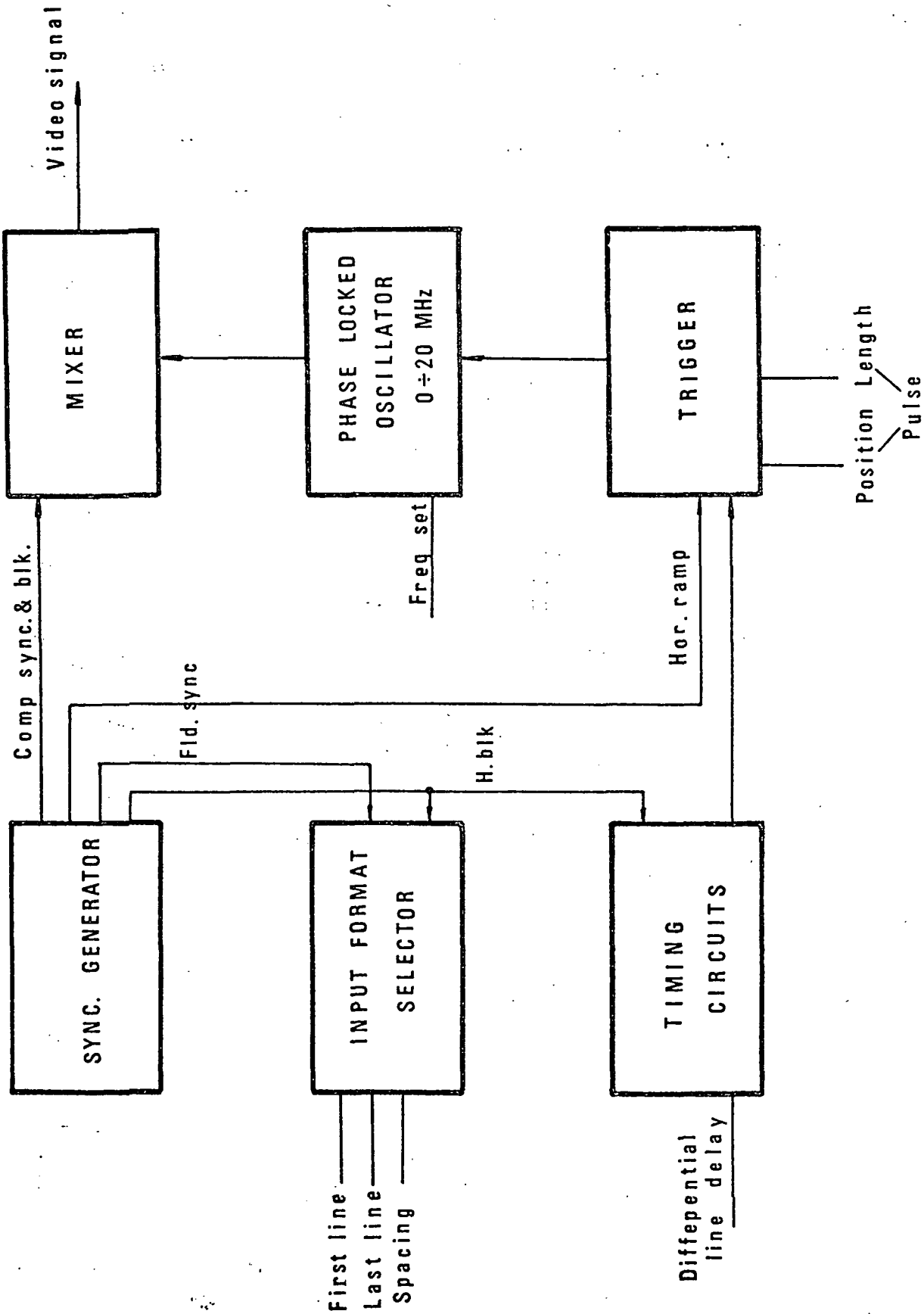


Fig. 6.1.1 Black Diagram of Linear Phased Array Simulator

to a timing signal to allow any variable delay per line $\Delta\tilde{t}$ to be introduced while maintaining the proper phase relationships between signals on different lines. (Recall that the signal written on each line of the electro-optic target crystal corresponds to one of the antenna array elements.)

Linear arrays of up to 256 receiving elements can be simulated (with extension to 500 elements possible); the number of elements and their spacing can be varied by control knobs on the front panel of the simulator. The position of the returned pulse signal in the horizantal time axis, as well as the pulse duration and the relative delay between consecutive array elements, can all be independently varied by control knobs.

The functional diagram of this phased array radar simulator is shown in Figure 6.1.1

## 6.2 Basic Optical System

Figure 6.2.1 shows the basic optical system used. To conserve table top space, a stand for the laser is suspended from the bottom of the table top. The laser, a focusing lens and aperture are mounted on this stand. The remaining optical system is on the table top. A periscope prism arrangement brings the beam to the table top. A fairly plane, uniform intensity beam over the 50 x 50 mm dimensions of the target crystal is needed for optical data processing. This 70 mm diameter ($50\sqrt{2}$) and the laser beams size to the 1/e points determines the collimating optics. A 20X AR coated microscope objective focuses the beam to a diffraction limited spot. A spatial filter pinhole was found to be essential if a uniform beam was to be obtained. A 10μm diameter pinhole works well to eliminate noise in the beam without loosing laser power. The incident beam diameter is 2 mm, the 20X objective and a 381 mm collimating lens provide a 75 mm collimating lens provide a 75 mm diameter beam which illuminates the crystal. An additional input polarizer is used to insure linearly polarized incident light. The output polarizer is crossed to provide no light out with

no voltage on the crystal.

The spatially modulated collimated laser beam is now Fourier transformed. The focal length of the transform lens is determined by matching the optical spatial bandwidth to that of the vidicon used for pick-up and detection. The spatial frequency n is related to the focal length f by

$$n = x/\lambda f$$

where x is the distance in the tramsform plane associated with the vidicon scan, $\lambda$ is the wavelength of the laser light (633 nm) and f is the focal length of the Fourier transform lens. The electro-optic crystal resolution is 20 lines/mm and the vidicon scan dimensions are 0.8 cm x 0.6 cm, from which the focal lengths needed are

$$f_{horiz} \leq 635 \text{ mm}$$

$$f_{vert} \leq 475 \text{ mm}$$

These limits insure an optical spatial bandwidth greater than or equal to the highest spatial frequency on the crystal. With the 495 mm focal length transform lens used and a 2.5 cm diameter vidicon, a resolution of

$$n_{horiz} = 25.6 \text{ lines/mm}$$

$$n_{vert} = 19.2 \text{ lines/mm}$$

can be resolved in the spatial frequency plane. These values are comparable with the vidicon and crystal specifications.

The Fourier Transform plane can be reviewed directly on the vidicon or first magnified and then viewed on the vidicon (in the case where the maximum spatial frequencies contained on the input pattern are lower than the maximum spatial bandwidth allowed by the crystal). In the second case, a scanning microscope is used which can also drive an X-Y platter for beam recording. With

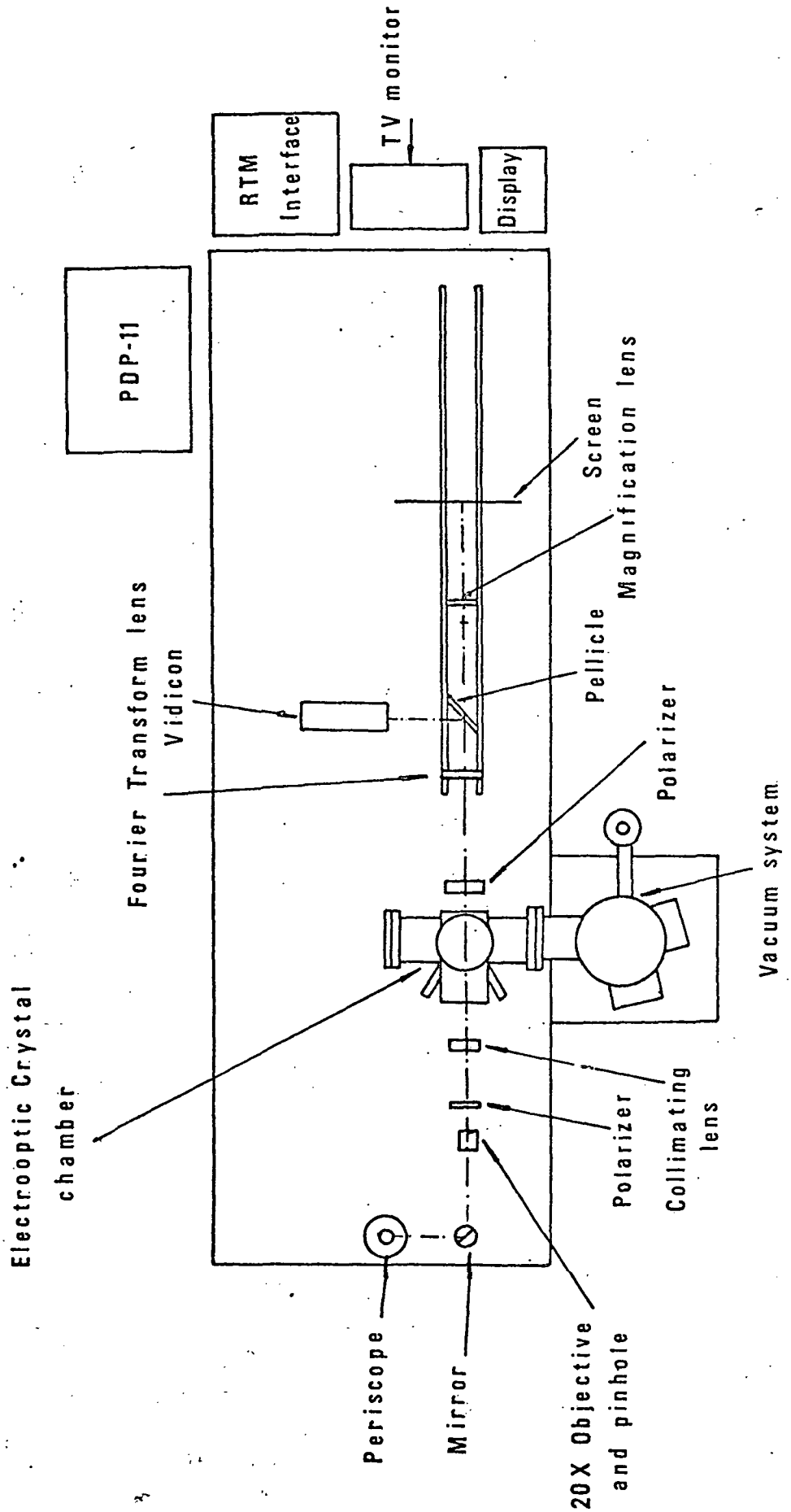


Fig. 6.2.1 Basic Optical System Arrangement

the use of the magnifying system, enlarged output plane patterns can be projected on a screen and pictures taken while the vidicon drives the computer interface and display.

6.3 Results

On line simulated radar returns for a linear array have been written on the input KD*P crystal and the corresponding output plane formats analyzed. The radar signal simulator described in paragraph 6.1 has been used throughout the experiments. The optical configuration used was shown in Fig. 3.3.1. The input collimated plane waveform is modulated by the electrical signal from the radar simulator which is written on the electro-optic crystal. With this crystal between crossed polarizers an on-line two-dimensional amplitude modulated light beam results. The optical system forms the Fourier transform of the image on the crystal and displays a magnified version of this transform on the TV monitor. The RTM computer interface then digitizes this output plane pattern on line with a variable cell size and threshold level.

All results correspond to a linear phased array of 100 elements spaced at a distance equal to one half the RF carrier wavelength. A pulsed RF signal of 20 μsec duration is used in all cases. The intermediate frequencies used are 1 MHz and 500 KHz.

Figures 6.3.1 to 6.3.8 show the results of this initial on-line processing at various points in the system and for several input targets. All of the processing and data shown are on-line.

Figure 6.3.1 shows the output plane pattern for a boresight target and a radar intermediate frequency of 1 MHz. Note that the first order diffraction peaks lie on the vertical axis. (u axis)

Figure 6.3.2 shows the output plane pattern for a target 7° off the boresight with an $f_{if}$ = 1 MHz. Note that the location of the first order diffraction

peaks are now displaced off axis along the v direction proportional to sin(7°).

Figure 6.3.3 is the RTM digitized version of Fig. 6.3.2 with suppressed D.C. term. This prevents saturation of the vidicon pick-up tube used.

Figure 6.3.4 is the output plane pattern for a target 20° off boresight with an $f_{if}$ = 1 MHz. Note that the shift in the first-order diffraction peaks is larger than before. (proportional to sin(20°)).

Figure 6.3.5 is the RTM digitized version of Fig. 6.3.4 with the D.C. term again suppressed.

Figure 6.3.6 is the output plane pattern for a target at 10° off boresight and a different radar IF frequency $f_{if}$ = 500 KHz.

Figure 6.3.7 is the RTM digitized version of Fig. 6.3.6 with the D.C. term only partially suppressed.

Finally, Fig. 6.3.8 corresponds to the same input pattern than Fig. 6.3.2 but using the phase-modulation capability of the electrooptic crystal using only an input polarizer.

These initial results prove the on-line beam forming capability of our KDP light modulator in radar processing. The validity of the input format described in the prior reports and the output plane pattern predicted by this theory were also confirmed by these tests. The on-line operation of the RTM computer interface in an on-line radar data situation has also been demonstrated. The output plane information is also available as coordinate pair locations of all principal maximums. From such data, the computer can automatically extract target angle information (from the v displacement of the spots); this data can then be used to further control the radar system or other supporting radar systems, for data storage or for display purposes as demonstrated.

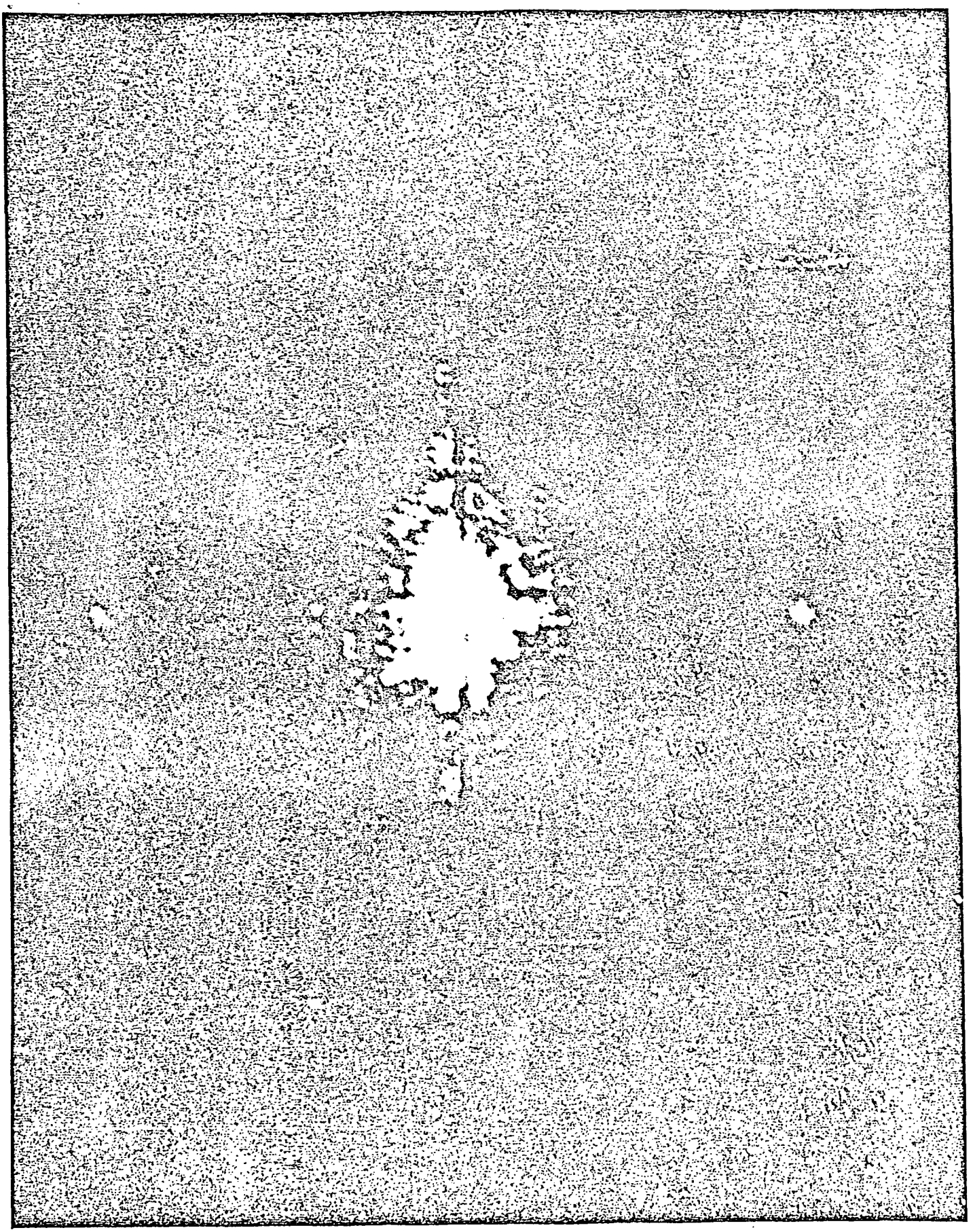

Fig. 6.3.1

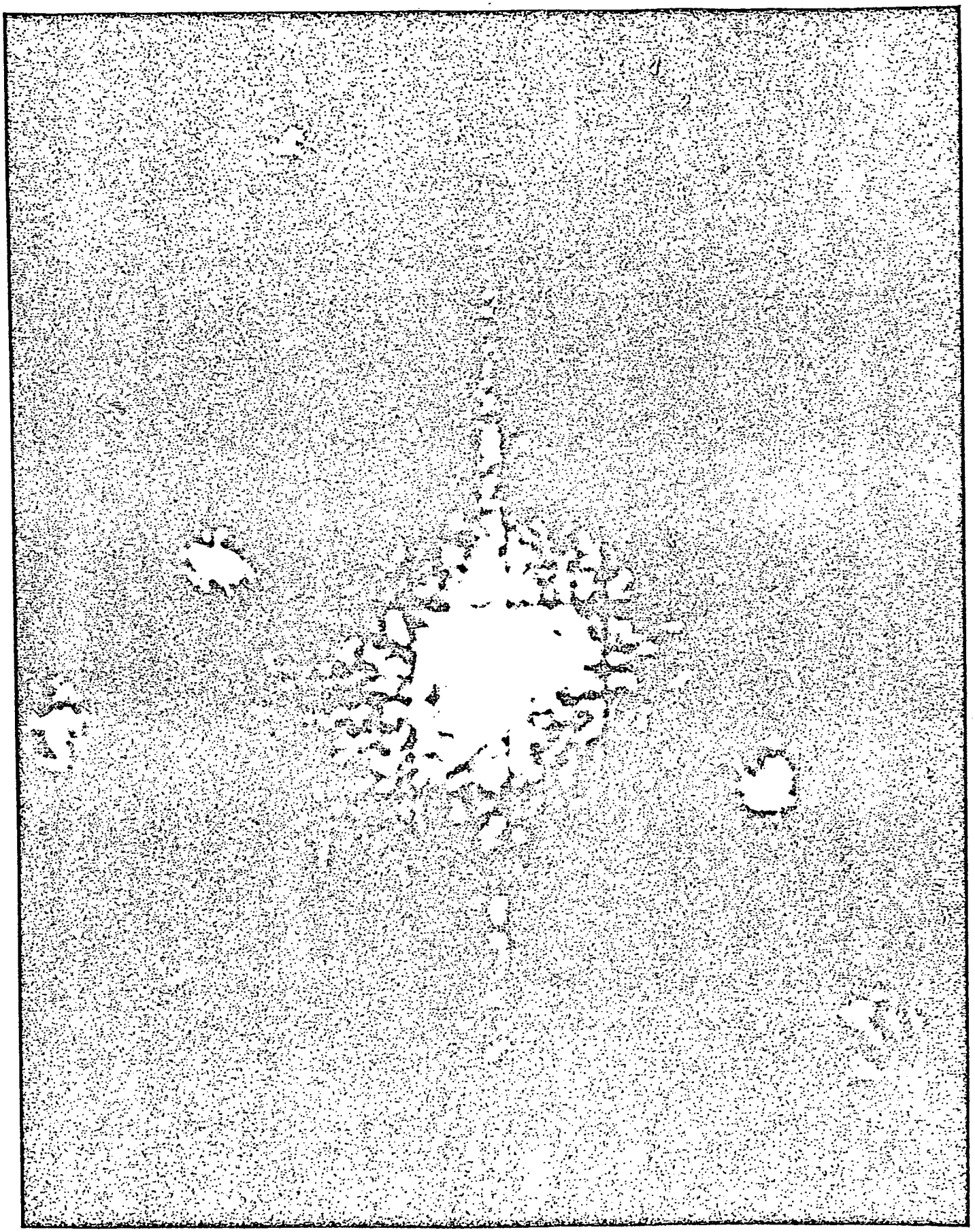

Fig. 6.3.2

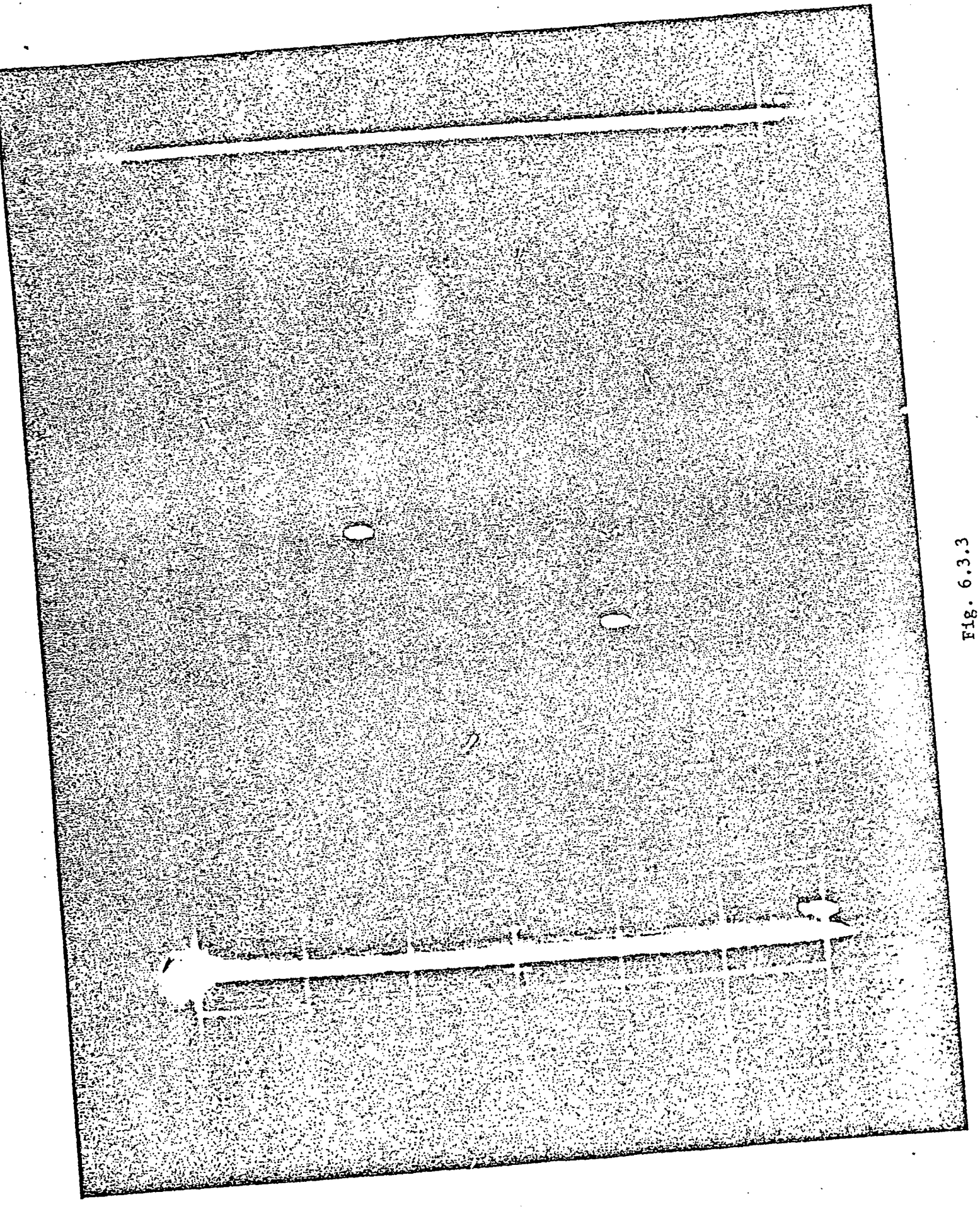

Fig. 6.3.3

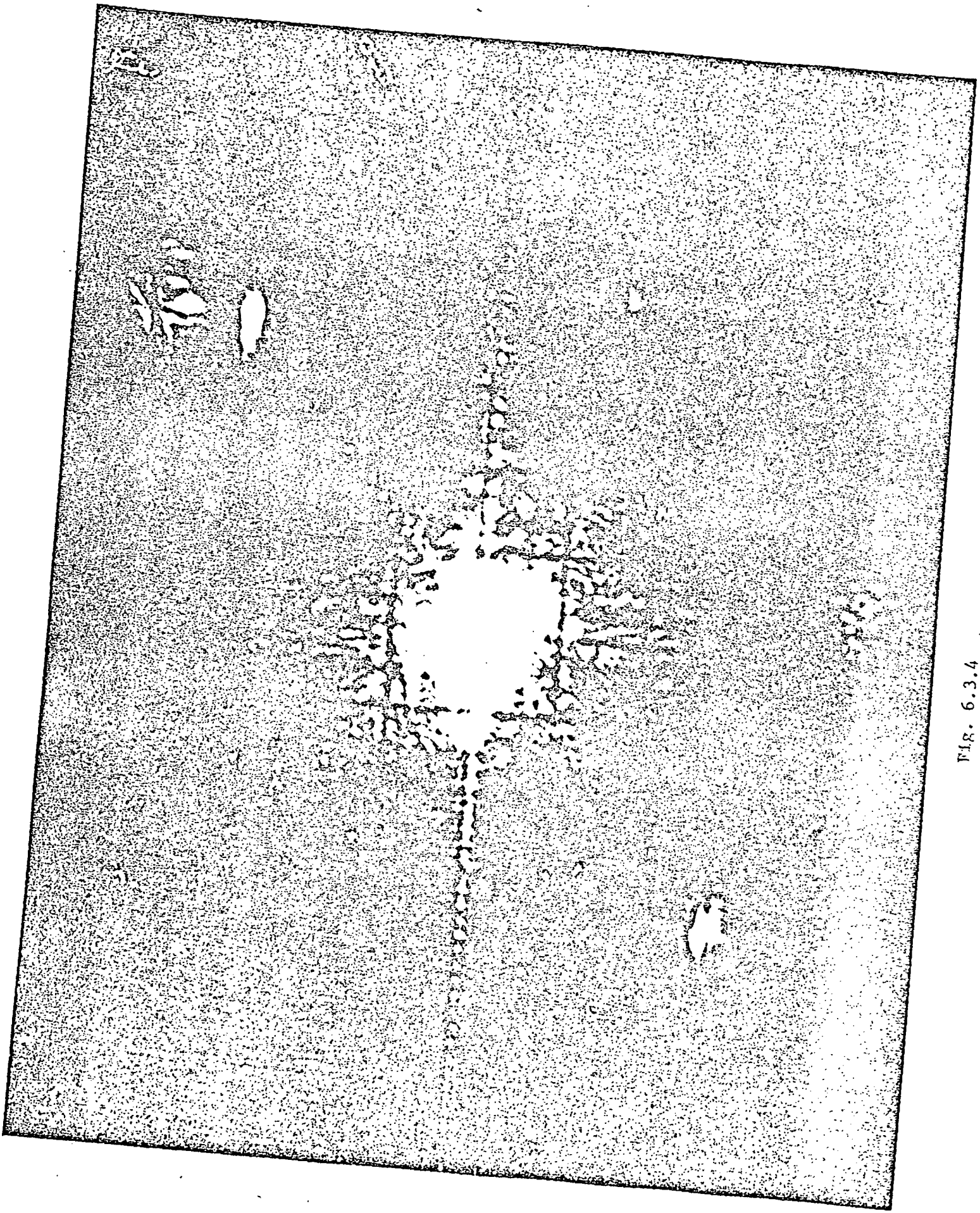

FIG. 6.3.4

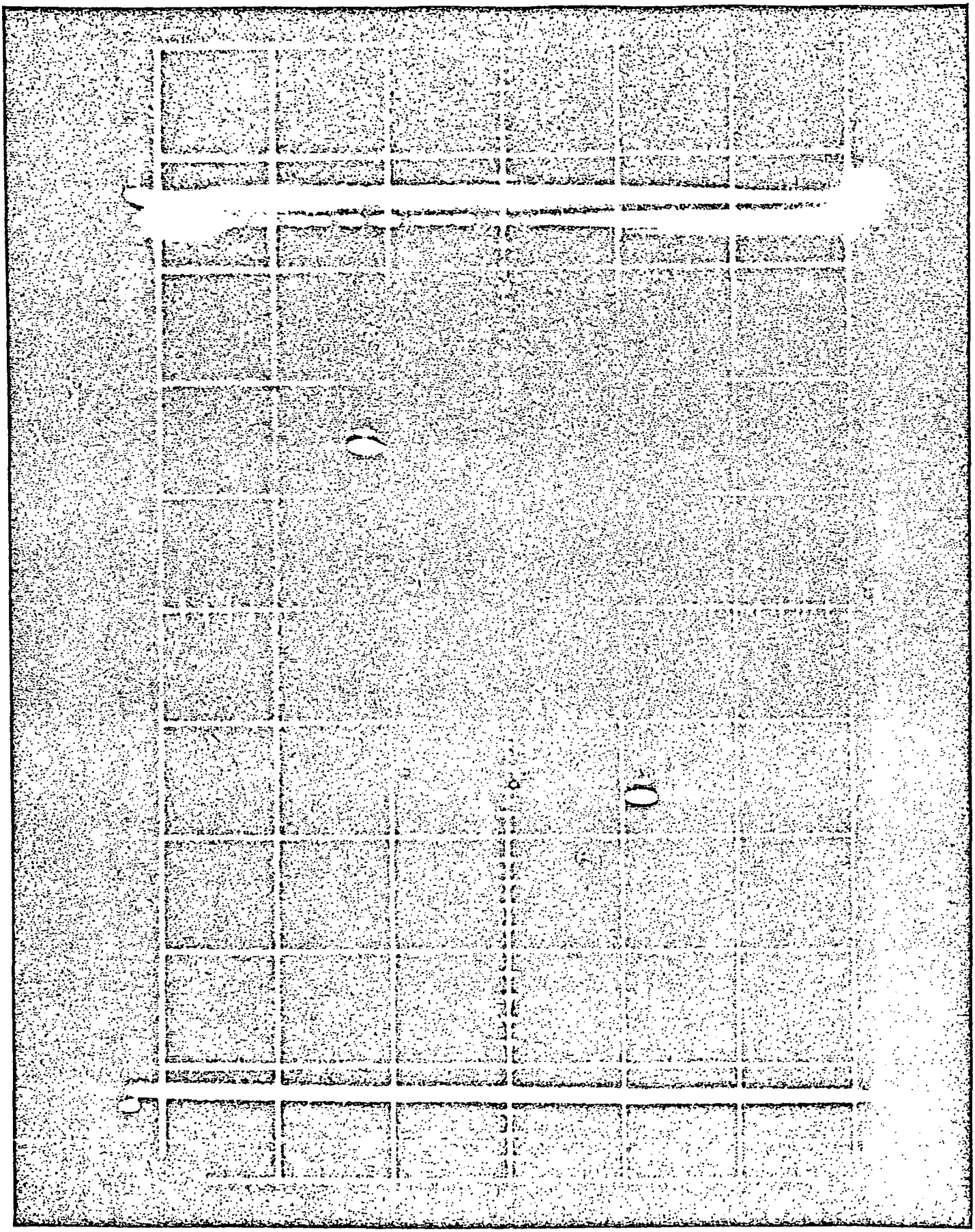

Fig. 6.3.5

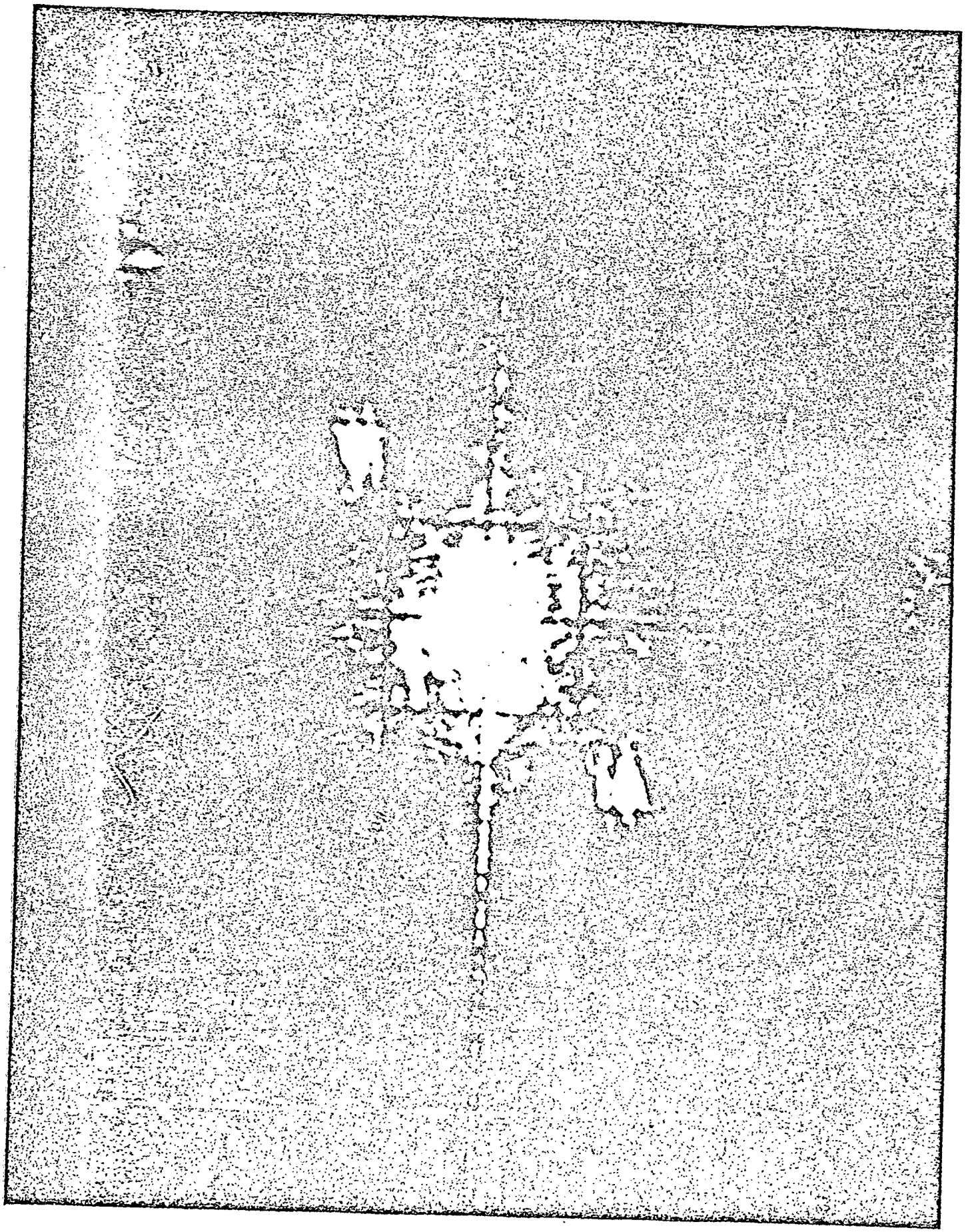

Fig. 6.3.6

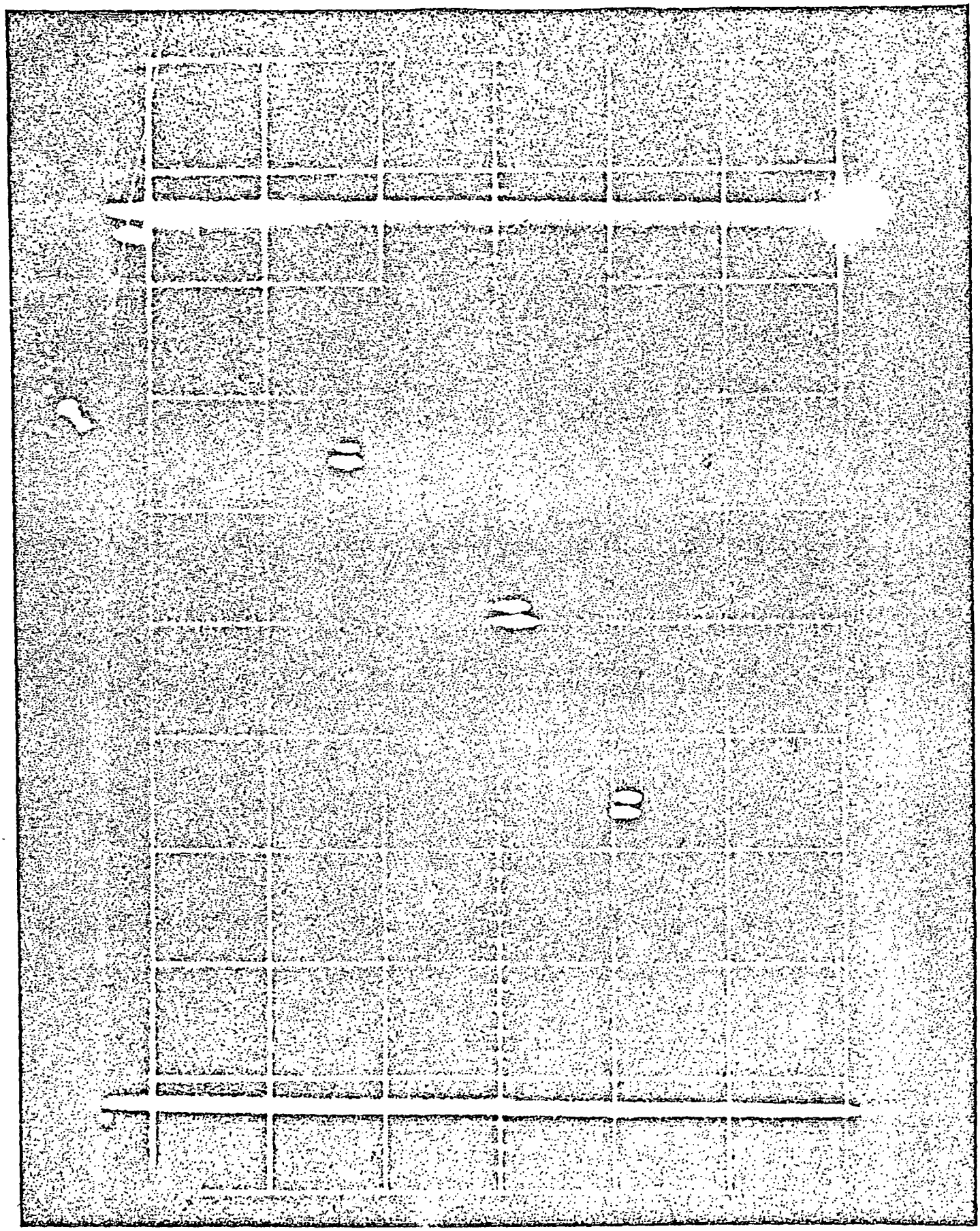

Fig. 6.3.7

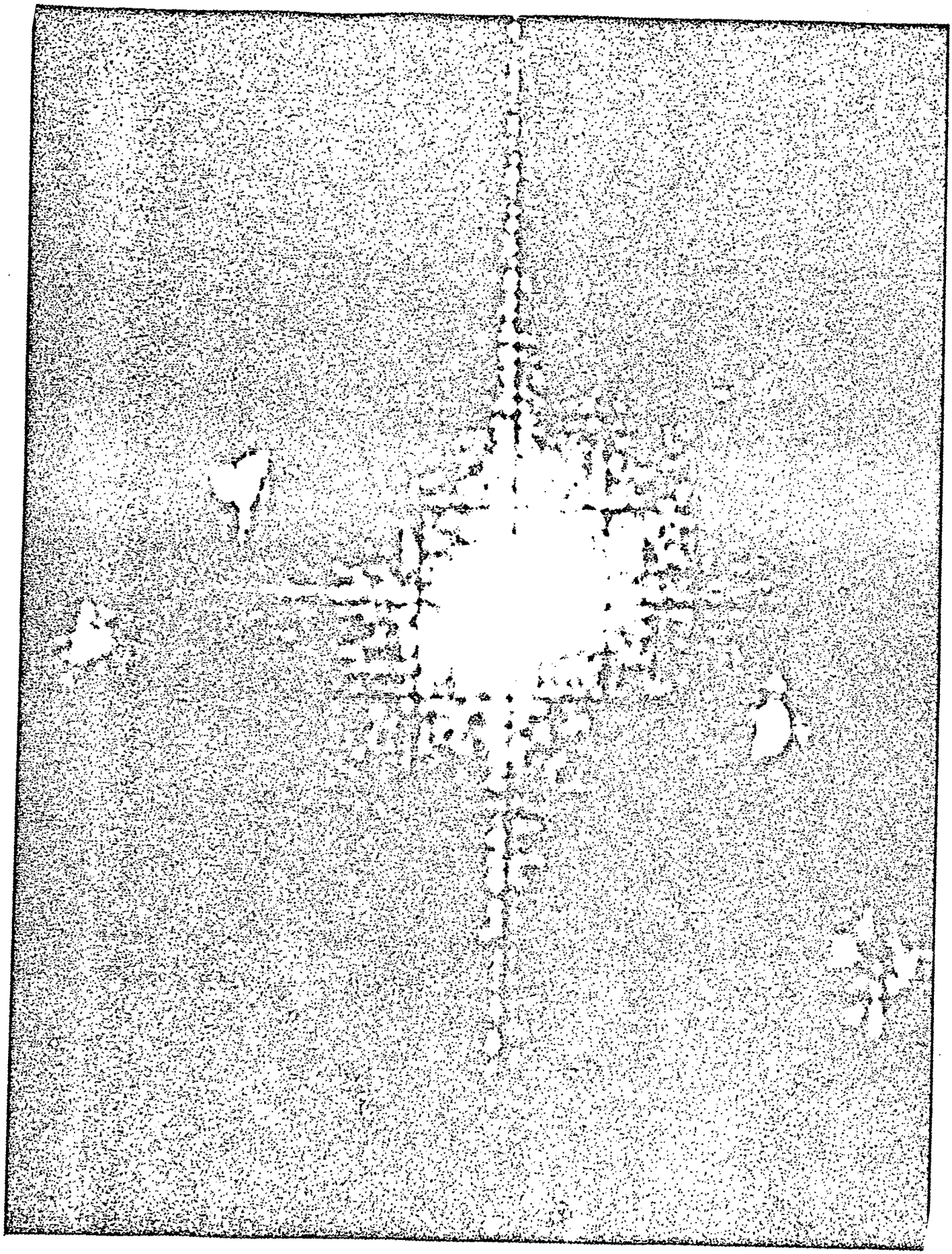

Fig. 6.3.8

CHAPTER 7

FUTURE RESEARCH

## 7.0 Introduction

In our research on radar processing using an electro-optical processor we have also considered the possibility of processing linear FM stepped, pulsed Doppler, and CW Doppler returns. The following three sections briefly outline the procedure by which the electro-optical processing techniques described in the report could be applied to this alternate radar systems.

The remaining sections of this Chapter outline more advanced processing techniques for radar data using standard optical processing techniques such as matched filtering, spatial filtering and correlation. One of the key elements in this advanced applications of optical processing to radar data involves a survey and experimental feasibility efforts in the area of on-line spatial filter materials. Section 7.5 discusses one seemingly viable material for such an adaptive on-line spatial filter. This Chapter and the aforementioned discussions will purposely be kept very brief as they are quite numerous and constitute our proposed research program in optical processing of radar data for the coming year.

## 7.1 OPTICAL PROCESSING OF PULSED-DOPPLER DATA

In pulsed Doppler systems a set of single frequency pulses is transmitted at regular time intervals. For a constant velocity target in a noise-free environment a linear phase slope will again exist across the returned echoes as it was the case in the phased array processing described in Chapters 2, 3, and 4. With a pulsed-Doppler system the target's velocity can be determined from this linear phase slope.

### 7.1.1 PULSED DOPPLER PROCESSING IN THE PRESENCE OF NOISE

In the presence of noise the phase slope across the returned echoes can be optically determined by correlating the input data with the phase slopes corresponding to all possible velocities within a given range and resolution bin. Fig. 7.1.1 shows the expected correlation peak provides information on the target velocity.

### 7.1.2 OPTICAL PROCESSOR

Using our Pockels tube modulator (Section 6.2) and the conventional optical processing configuration in Fig. 3.3.1 the returns for consecutive pulses will again be written on separate raster lines on the input crystal after being heterodyned and range gated. The two dimensional optical Fourier Transform of this input pattern as before has a first order maximum at back plane coordinates from which information on the target's velocity can be obtained.

Since N resolution cells of target velocity exist between the grating lobes of the transform it is possible to simultaneously on-line in-parallel correlate against N different velocities in real time. Multi-target velocity resolution within range bins also appears possible.

The computer interface plays a major role in such a system since one might envision a totally automated processor in which one first obtains coarse resolution by one cycle through the system. This coarse resolution information could then be used to determine the fine range spatial filter required to be inserted in the spatial filter plane. These filters may be computer generated ones which are stored in the computer memory. A more practical approach within the scope of current technology would involve storing these filters optically as multiple spatial filters (holograms). This will be expanded in Section 7.

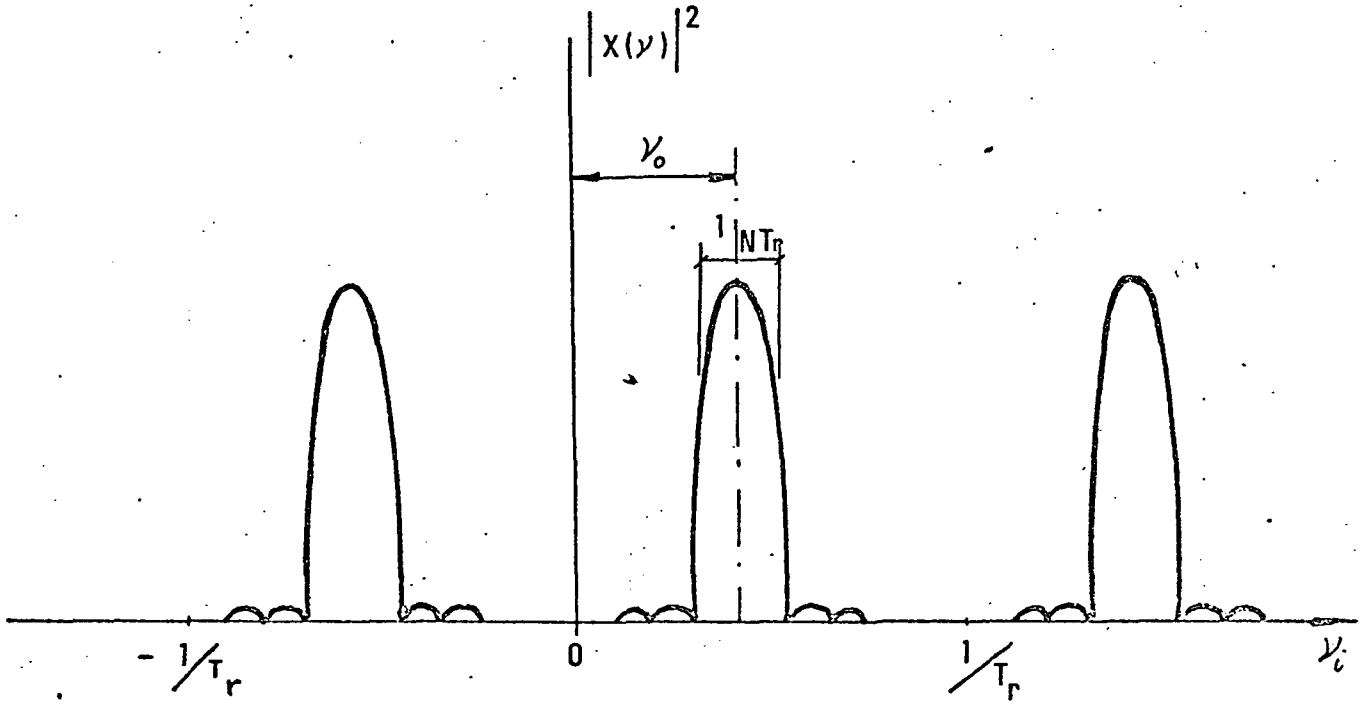


$$v_0 = \nu_i \frac{\lambda_c}{2}$$

Fig. 7.1.1 Ideal Doppler Processor Output

## 7.2 OPTICAL PROCESSING OF LINEAR-STEP FM RADAR DATA

A second type of radar signal which we considered processing was Linear stepped FM data. In this radar mode M consecutive RF pulses are transmitted at successively higher frequencies. A wide frequency spectrum is thus covered. Again a linear phase slope will exist across the returned echoes in this system for stationary targets. This slope is now a function of the target's position within a range resolution cell.

### 7.2.1 OPTICAL PROCESSOR

Using a similar optical configuration as before and a similar input format the returned echoes can again be correlated with corresponding phase slopes. The Fourier transform of the input pattern described has a first order maximum from which one can now obtain fine range resolution. With N resolution cells between continuous grating lobes, one can again perform a parallel optical correlation against filters of N ranges and thus obtain fine range resolution in any of N range resolution bins.

The correlation filters, the optical spatial filters and the role of the computer interface are various other considerations and factors in this processing that must be investigated.

## 7.3 OPTICAL PROCESSING OF CW DOPPLER DATA

Optical processing of CW doppler data directly parallels the pulsed doppler scheme. With continuous data rather than pulsed waveforms, the input processor is even simpler.

## 7.4 REAL-TIME DATA

Until actual phased array radar return data is available, efforts should be directed at the aforementioned schemes since real-time data

in these forms exists. The questions that remain to be answered are still quite numerous.

(1) The degree of preprocessing and post processing required varies with the radar type and system and must be separately evaluated for each case.

(2) The optimum optical system with special lenses etc, must be determined. This again varies with the radar system chosen.

(3) The spatial filter resolution necessary must also be determined. The processing times required will also affect the spatial filter material chosen.

(4) The resolution, speed, number of gray levels required, etc. in the output plane and the data desired from the computer interface should be determined for each radar processing made envisioned. Extension and expansion of the interface will then be possible.

## 7.5 SPATIAL FILTER MATERIALS

Many of the radar processing applications aluded to above involve spatial filtering, matched filtering, and correlations. It is possible to perform these powerful operations in parallel in an optical processor. Among the more widely researched materials for use in optical storage of information are:

1. Film
2. Photothermoplastics
3. Liquid Crystals
4. Photodichroic crystals

Film has the disadvantage of not being adaptive and of not being on-line. Photothermoplastics generally have a lifetime problem

that limits them to 10,000-100,000 cycles, liquid crystals are generally adequate for display purposes but their slow response times are not compatible with the on-line optical processing envisioned. Photothermoplastics generally require larger optical power levels but indications are that this problem can be reduced, fatigue problems overcome, etc. We are currently investigating them in an alternate application but feel they deserve attention in this specific contest of radar processing.

## 7.6 COMPUTER INTERACTIONS

In perhaps the most all encompassing project, the returned signals from a phased array, linear FM stepped, and pulsed doppler radar systems can be processed on one system with the digitized output plane, the computer interface, and the PDP-11 being used to scan the results on one radar display and store it and use the result to control a linear FM stepped radar to obtain range information, then a pulsed doppler system to obtain velocity data. The interaction of such a number of systems may be easier than at first appears. Use of the computer to store a fixed program corresponding to the returns from such a set of 2 or 3 radar systems seems reasonable. Obtaining actual radar data from 2 or 3 systems for the same target seems an unreasonable request thus simulated returns would be used. The scope of such an effort and many details are clearly rather involved--but perhaps a reasonable attempt at such a program could be made with initial results from the PDP-11 feeding our modulator expected in one year.

In a more limited and controllable situation one could use the output from the PDP-11 to control the fine and coarse range controls noted in 7.1.1. By using the digital processor to control the updatings of the spatial filters, the input data, and the stored and transmitted output data, one can

demonstrate the computer feedback control within a well defined and controllable and yet useful context.

Such a system provides a digital optical radar processor much less complex and cheaper than existing alternatives such as a dedicated large scale computer, should greatly advance the state of the art in coherent optical data processing with on-line spatial light modulators.

SUMMARY

An on-line spatial light modulator developed at CMU suitable as the input transducer for a real-time optical data processing system has been described (Chapter 1). 1000 x 1000 point resolution and on-line operation at TV frame rates is possible. The use of such a device in the analysis and processing of radar data in real time has been considered and initial results reported.

The fundamentals of signal processing for linear (Chapter 3) and planar (Chapter 4) phased array radar data as well as Pulsed Doppler and Linear-Step FM system (Chapter 7) using this input modulator have been developed. Time and space multiplexing input formats, full and thinned aperture processing, and amplitude and phase modulation schemes using the system are developed, analyzed and compared.

An interface from the optical processor to a control-digital computer has been designed, constructed, and tested. The ability to digitize the entire Fourier transform plane or the correlation plane of an optical processor in real time and input the resultant data to a digital computer for storage or for use in controlling the entire optical processor has been demonstrated. The cell resolution and size and the gray scale levels in the backplane are variable under program control.

Real-time processing of linear phased array under data has been performed for the first time by other than an acousto-optic modulator. The Pockels tube modulator offers advantages in fabrication, angular coverage and resolution, in the larger array size it is now possible to handle and in-depth of modulation etc.

The input transducer, optical system, and computer interface have all been operated in real-time with real-time radar data with the input data returns recorded on the input crystal, processed by the optical system and the output

plane pattern digitized, thresholded and outputted to a display and storage in the computer memory all in real-time synchronized to TV frame rates.

No other input modulator offers the real-time operating characteristics of the Pockels tube. Its ability to process radar data in real-time has been demonstrated. The correlation with theory and experimental results have been most encouraging. Recommended directions for future research in the area of optical processing of radar data in real-time are sketched in Chapter 7 and the proposal.

REFERENCES

1. Poppelbaum, Faiman, Casasent, Sand, "On-line Fourier Transform of Video Images," Proc. IEEE, 56(10), 1744, Oct. 1968.

2. D. Casasent, "Curie Point Operation of a Pockels Tube," IEEE Trans Electron Devices," Oct. 1973.

3. D. Casasent, "An On-line Electro-Optical Video Processing System," AEC-Coo-1469-0120, June 1969.

4. D. Casasent, J. Stephenson, "Electro-Optical Processing of Phased Array Antenna Data," Applied Optics, May 1972.

5. D. Casasent, W. Keicher, "An Electro Optical 2-D Spatial light Modulator for Real Time ODP," Proc. EOSD, Jan. 1973.

6. D. Casasent, "A Digital/Optical Computer System," IEEE Transactions Computers, Sept. 1973.

7. A. Yariv, "Introduction to Optical Electronics" (Holt, Rinehart & Winston, New York 1971).

8. R. A. Meyer, D. G. Grant, J. L. Queen, "A Digital-Optical Hybrid Correlator," Report TG 1193 A, Applied Physics Laboratory, The Johns Hopkins University, September 1972.

9. L. B. Lambert, M. Arm, A. Aimette, "Electro-Optical Signal Processors for Phased Array Antennas," in Optical and Electro-Optical Information Processing, James T. Tippet et al., Eds., (MIT Press, Cambridge, Mass. 1965).

10. R. E. Williams and K. von Bieren, "Combined Seam Forming and Cross-Correlation of Broadband Signals from a Multidimensional Array Using Coherent Optics," Applied Optics, June 1971.

11. A. W. Rihaczek, "Principles of High Resolution Radar" (McGraw-Hill, 1969).

12. C. G. Bell, J. Grason, A. Newell, "Designing Computers and Digital Systems" (Digital Press, 1972).

TABLE OF CONTENTS

# LIST OF ILLUSTRATIONS